



# Constraints on protosolar planetary disk formation from the potassium-isotope compositions of the chondritic meteorites

## Citation

Ku, Yaray. 2022. Constraints on protosolar planetary disk formation from the potassium-isotope compositions of the chondritic meteorites. Doctoral dissertation, Harvard University Graduate School of Arts and Sciences.

## Permanent link

<https://nrs.harvard.edu/URN-3:HUL.INSTREPOS:37371903>

## Terms of Use

This article was downloaded from Harvard University's DASH repository, and is made available under the terms and conditions applicable to Other Posted Material, as set forth at <http://nrs.harvard.edu/urn-3:HUL.InstRepos:dash.current.terms-of-use#LAA>

## Share Your Story

The Harvard community has made this article openly available. Please share how this access benefits you. [Submit a story](#).

[Accessibility](#)

HARVARD UNIVERSITY  
Graduate School of Arts and Sciences



DISSERTATION ACCEPTANCE CERTIFICATE

The undersigned, appointed by the  
Department of Earth and Planetary Sciences  
have examined a dissertation entitled  
“Constraints on protosolar planetary disk formation from the  
potassium-isotope compositions of the chondritic meteorites  
  
presented by Yaray Ku  
  
candidate for the degree of Doctor of Philosophy and hereby  
certify that it is worthy of acceptance.

*Signature* Stein B Jacobsen Digitally signed by Stein B  
Jacobsen  
Date: 2022.02.03 09:54:56 -05'00'

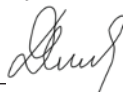
*Typed name:* Prof. Stein Jacobsen

*Signature* Jerry Mitrovica Digitally signed by Jerry Mitrovica  
Date: 2022.02.03 10:03:11 -05'00'

*Typed name:* Prof. Jerry Mitrovica

*Signature* Timothy Grove Digitally signed by Timothy Grove  
DN: cn=Timothy Grove, o=M.I.T., ou,  
email=tlgrove@mit.edu, c=US  
Date: 2022.02.07 10:57:00 -05'00'

*Typed name:* Prof. Timothy Grove

*Signature* 

*Typed name:* Prof. Dimitar Sasselov

*Signature* 

*Typed name:* Prof. Rebecca Fischer

*Date:* February 1, 2022

**Constraints on protosolar planetary disk formation from the potassium-isotope compositions of the chondritic meteorites**

A dissertation presented by

Yaray Ku

To

The department of Earth and Planetary Sciences

in partial fulfillment of the requirements  
for the degree of Doctor of Philosophy  
in the subject of Earth and Planetary Sciences

Harvard University  
Cambridge, Massachusetts  
February 2022

© – Yaray Ku

All rights reserved.

## **Constraints on protosolar planetary disk formation from the potassium-isotope compositions of the chondritic meteorites**

### **Abstract**

Potassium isotopes unveil some of the early geological activities and processes in the early solar system. Due to its relative volatile and mobile characteristics, the chemical and isotopic composition of K in chondrites, especially, provides valuable insights in figuring out the nebular thermal history in the protosolar planetary disk as well as potential effects on K from the secondary processes on their parent bodies.

The principal tool in this thesis is analyzing K-isotope ratios ( $^{41}\text{K}/^{39}\text{K}$ ) in meteorite samples. The measurement of K isotopic compositions using a Multi-Collector Inductively Coupled Plasma Mass Spectrometer (MC-ICPMS) has been significantly improved over the past five years, and the high precision analyses of K isotope were possible as a result of various innovations on MC-ICPMS, especially the use of collision cell, a technique that removes the interference of species of mass 41 ( $^{41}\text{K}$ ). Additionally, the higher detection sensitivity of the modern MC-ICPMS enables precise isotope measurements to be conducted on meteorites, many of which have traced abundances of K.

This thesis presents new constraints on major stages of the formation of our protosolar planetary disk through high-precision K isotope analyses of the bulk chondrites and their various components. The main idea which connects these studies is the high-temperature nebular processes that influence K content and isotope compositions in these oldest solar system materials. The first chapter of this thesis is the examination of the astronomical environment of the protosolar

molecular cloud via analyzing the K isotopic compositions of a total of 55 meteorite samples. This study argues that the isotopic anomalies in meteorites are inherited from a heterogeneous protosolar molecular cloud, which is likely associated with type II supernova injection before the solar system formed. Such a result implies that the survival of K isotopic heterogeneity in both undifferentiated and differentiated meteorites involves limited mixing among formation regions of the various planetary and chondrite parent bodies.

The second chapter of the thesis is estimating the formation timescale of our solar system that was associated with the collapse of protosolar molecular cloud via analyzing the K isotopic compositions of Ca-Al-rich inclusions (CAIs), the oldest materials that dates the age of solar system. The initial abundance of  $^{41}\text{Ca}$  in the solar system can be inferred from the presence of its decay product  $^{41}\text{K}$  in CAIs, and it places important constraints on the timing of the solar system's formation. This chapter reports a new initial  $^{41}\text{Ca}$  abundance that is about five times higher than the previously accepted value. This new value likely requires an injection of new stellar materials from a Wolf-Rayet or AGB star into the protosolar molecular cloud about 0.6 - 1.0 million years before the formation of the solar system.

The final chapter of this thesis is evaluating the formation environment of planetary building blocks, including small planetary bodies, in the protosolar planetary disk via analyzing the isotopic composition of K of chondrules and matrix from both carbonaceous and ordinary chondrites. This study found that a wider variation of K isotope composition in chondrules and matrix, compared to the bulk, likely reflects sample heterogeneity from the nebular environment instead of secondary processes. In addition, the lack of open-system behavior for the K isotopes suggests a near-equilibrium condition for the chondrules' formation, possibly accompanied by a high ambient gas pressure.

# Table of Contents

<b>Abstract</b>	iii
<b>Table of Contents</b>	v
<b>Acknowledgements</b>	vi
<b>Chapter 1</b> — Introduction	1
<b>Chapter 2</b> — Potassium isotope anomalies in meteorites inherited from the protosolar molecular cloud	6
<b>Chapter 3</b> — The timing of the last nucleosynthetic injection into the protosolar molecular cloud inferred from $^{41}\text{Ca}$ - $^{26}\text{Al}$ systematics of bulk CAIs	28
<b>Chapter 4</b> — Potassium isotopic composition of chondritic components from the Allende (CV3), Ochansk (H4), Saratobv (L4) and Elenovka (L5) chondrites	45
<b>Chapter 5</b> — Conclusion	83
<b>Appendix A</b> — Supporting information for Chapter 2	87
<b>Appendix B</b> — Supporting information for Chapter 3	110
<b>Appendix C</b> — Supporting information for Chapter 4	126
<b>Appendix D</b> — Supporting information for Chapter 5	138
<b>References</b>	140

## Acknowledgments

The time that I have spent at Harvard working towards my PhD has been one of the most challenging yet rewarding periods in my life. There are so many people who I must thank, who inspired me, helped me to achieve my academic goals, enriched my graduate school experience, and made this time fun and enjoyable.

I would like to start by thanking my research advisor, Stein B. Jacobsen, who I deeply admire for his passion, as well as his ability to conduct some of the most precise isotope analyses, which have led to major breakthroughs in cosmochemistry and geochemistry. The incredible patience he demonstrated while guiding me through the individual steps of each project, even including simple things like the hand-crushing of meteorites, helped me to become a careful and cautious experimentalist. With his support and encouragement, I was able to boldly try new ideas, and to keep pushing the boundary of cutting-edge science. His sheer passion for geochemistry, and his ability to positively motivate those around him, were true inspirations throughout my PhD. I would also like to thank my second advisor, Jerry X. Mitrovica, who provided endless support and helped me to achieve my academic and career goals. He is not only an amazing scientist with a great intuition for both the experimental and theoretical aspects of the field, but his drive and leadership always brought out the best in his colleagues and students. He never looked down on me for asking silly questions, and he always went out of his way to help me sort through and understand problems. His humor certainly brought joy and color to my time in graduate school, and his constant curiosity and scientific passion pushed me to become a better researcher and even a better person. I am also very grateful to my committee members, Dr. Tim Grove and Dr. Dimitar Sasselov, who supported my work throughout graduate school by providing invaluable advice. For example, I had an extremely fun and valuable experience during my oral exams, which were filled



with fruitful and encouraging discussions led by Tim and Dimitar. Such discussions helped me to thoroughly understand the impacts of my work, and to view these impacts in the broader context of the fields of astrophysics and experimental petrology.

I would also like to thank all the people in the Jacobsen and Mitrovica groups with whom I have worked directly, and who provided me with positive energy over the past few years. I would especially like to thank Michail I. Petaev, who taught me all about the basics of meteorites. While he may be the person with whom I spent the most time arguing (in a good way), many great ideas and work were accomplished through the fruitful and dynamics discussions I had with him. I am particularly thankful for the time he devoted to helping me improve my English academic vocabulary and writing style, something which has truly benefited me in every possible way. I would also like to express my gratitude toward the current and former members of the Jacobsen group: Fatemeh Sedaghatpour – the first postdoc that I worked with when I began; Eugenia Hyung, Chris Parendo, and Zack Eriksen – my colleagues who spent so many long hours in the lab with me; Robert Achert – who always encouraged me to become an astronaut; Li Zeng and Maria Peto – colleagues whose friendship continuously carried me through difficult times. Additionally, I am deeply appreciative of all the members of the Mitrovica group: Harriet Lau, Jocelyn Fuentes, Tamera Pico, Kimee Moore, Evelyn Powell, and Laura Kulowski (Bloxham group) – friends who I saw as role models when I first visited Harvard as a prospective student, and who inspired me to come to Harvard for my graduate studies; Mark Hoggard, Sophie Coulson, Marisa Borreggine, Linda Pan, Seth Olinger, Kai Morsink, Schmitty Thompson, and Alison Kim – colleagues who greatly inspired me by their passion for science and their acts of justice. The priceless relationship I had with both groups provided me with invaluable guidance and friendship throughout all the years of my PhD.

I would also like to extend my gratitude to the Harvard Origins of Life Initiative, an incredible community which helped me so much during my time at Harvard and which has always felt like a family to me. The funds and support for my research allowed me to concentrate on completing my graduate school journey, and I sincerely believe that I would not have achieved what I have without their help. I would especially like to thank Kelly Colbourn, who organized all the wonderful events and field trips for the members of the Origins of Life. Kelly has also become a great friend of mine, and her continuously upbeat, fun attitude infused my life with a variety of spices. In addition, I would like to thank Jack Szostak, who is not only extremely smart and an accomplished scientist, but is also a kind and fascinating human being. He has been my mentor in all types of things outside of academia, and he motivated me to dream big and achieve more than I could have imagined on my own. I am also very grateful to all the other wonderful members of the Origins of Life group with whom I have interacted over the years, including Yutong Shan, Travis Walton, Zoe Tod, Lydia Paziienza, Matthew Heising, JJ Dong, Matt Brennan, and Kaitlyn Loftus.

I am also immensely thankful to have spent my graduate school career at the department of Earth and Planetary Science at Harvard. It is the first place I worked after relocating from another country, and I am extremely lucky to have been a part of such an amazing community. To me, it has been like a second home. I would like to start by extending my extreme gratitude to the administration team, especially Paul Kelly, Sarah Colgan, Maryorie Garnde, Aimee Smith, Summer Smith, Marisa Reilly, Danielle da Cruz, Sabinna Cappo, and Carolyn Joones. They went above and beyond to help and support me with all my needs regarding travel expenses, school administration affairs, and technology support. I also received so much love and care from them through coffee chats and discussions about sports. I would also like to thank the EPS faculty from

whom I took classes and for whom I taught, including Charles Langmuir, Roger Fu, Rebecca Fisher, Miaki Ishii, John Shaw, Dan Shrag, Andy Knoll, and Dave Johnson. In addition, I have been incredibly lucky to have shared this experience with many other graduate students and postdocs who have become some of my closest friends over the years, including Colleen Golja, James Muller, Jess Don, Hairuo Fu, Minmin Fu, Ana González-Nayeck, Zhuo Yang, Judy Pu, Tim Clements, Ted Amdur, Mark Baum, Alec Brenner, Tia Scarpelli, Natasha Toghradjian, Aleyda Trevino, Anna Waldeck, Franklin Wolfe, Xiaotina Yang, Jiuxun Yin, Sunny Park, Simon Lock, Anna Lea Albright, and Hao Cao. I am also extremely grateful to the following people, whose friendship has meant so much to me over the years, and who have significantly added to my life during graduate school, especially my time outside of the lab: Jenny Zheng, Laura Lin, Justin Wong, Alex Ji, Alex Lascelles, Indira Pranabudi, Anqi Chen, Jun Yin, Nathaniel Yang, Siheng Chen, Kalki Kukreja, Sarah Burns, Graham Joe, and Amit and Dia Solanki. And of course, I would not have gotten to where I am today without my dearest family in Taiwan: they always supported my decisions, and they especially supported me when I decided to travel all the way across the Earth to pursue my PhD. Finally, I am eternally grateful to my wonderful husband, Matthew Nichols, whose unending support gave me the strength I needed to make it all the way through to the end of the long road that is graduate school.

# Chapter 1

## Introduction

The depletion of moderately volatile elements in many planetary bodies, compared to the CI meteorites which represents the solar system's chemical composition, is thought to result from nebular thermal processing (Cassen, 1996). Among moderately volatile and relatively abundant elements, only potassium (K) has more than one stable isotope ( $^{39}\text{K}$  and  $^{41}\text{K}$ ) and this uniquely makes it a good candidate for studying the history of volatile element depletion in the early solar system. So far, the best accessible materials to study are the undifferentiated meteorites, termed chondrites, which have not been heated to melting temperatures, and thus preserve, at least partially, chemical and isotopic records from the protosolar planetary disk. Chondrites show variable depletions in K, routinely expressed as the K/U ratios, which could be measured remotely. Remote  $\gamma$ -ray measurements also display large variations in the K/U ratios among the planetary bodies that have not been directly sampled (McCubbin et al., 2012). Therefore, understanding the mechanism that resulted in K depletion as well as in K isotopic fractionation provides important clues about the formation processes of our solar planetary disk.

The K isotopic data are usually reported as ratios of samples with respect to a standard and are shown with delta notation:  $\delta^{41}\text{K} = [(\delta^{41}\text{K}/^{39}\text{K}_{\text{sample}}) / (\delta^{41}\text{K}/^{39}\text{K}_{\text{standard}}) - 1] \times 1000$ . Precise K isotope measurements had not been reported until recently due to the difficulties of managing Ar-related interferences at and around mass 41 ( $^{41}\text{K}$ ). The earliest measurements were not precise enough to resolve the variations in K isotopes in most terrestrial and lunar materials (Humayun and Clayton, 1995). Recently, higher precision ( $\sim 0.1 \text{‰}$ ) K isotope data do show a significant K isotopic fractionation between the Earth and Moon (Wang and Jacobsen, 2016a, b) that was interpreted as a result of K loss during Moon formation. However, there is little understanding of

how K isotopes fractionate in different natural processes, and given K is a trace element in extraterrestrial materials, only a limited number of such materials, in contrast to Earth, have been analyzed so far.

The mechanisms causing the depletion of K (and other moderately volatile elements) are still debated and need to be tested by higher precision K isotope measurements. Meanwhile, stellar nucleosynthetic processes could also cause fractionation or result in nucleosynthetic isotope effects, for instance, a variation in  $^{41}\text{K}$  due to the decay of a short-lived nuclide  $^{41}\text{Ca}$ . Therefore, high-precision K isotope data will help to better understand the K fractionation among planetary bodies and to constrain the physical environments of chondrite formation in the early solar system. Determining the isotope effects and understanding the isotopic fractionation mechanism will ultimately allow for improved constraints on the processes of the formation and evolution of our solar system.

This thesis is composed of three major chapters, and presents the results of high-precision K isotope analyses from bulk chondrites, Ca-Al-rich inclusions from Allende meteorites, and other major chondritic compositions such as chondrules and matrix from both carbonaceous and ordinary chondrites. Our measurement procedures involve the use of collision gas ( $\text{H}_2$ ) to eliminate Ar-related interferences (Feldmann et al., 1999a, 1999b). All K isotope data in this thesis were collected using a *Nu* Sapphire MC-ICP-MS with a hexapole collision cell at Harvard University. The collision cell is utilized for K isotope measurement in order to eliminate  $\text{ArH}^+$ ,  $\text{Ar}^+$ , and  $\text{ArO}^+$  mass interferences, resulting in elimination of charged Ar-related species. We measured K isotope values relative to a lab standard (Suprapur  $\text{KNO}_3$  99.995% purity), and errors are reported as 2 standard error (SE). Details of methodology can be found in the Appendix, and the analytical methods have been thoroughly assessed by repeated measurements of USGS terrestrial standards

and common terrestrial materials, demonstrating consistency between our lab and others indicate that the robustness of our procedure.

## **Chapter 2: Potassium isotope anomalies in meteorites inherited from the proto-solar molecular cloud.**

This study focuses on a long-recognized inconsistency in the history of cosmochemistry. Moderately volatile elements (such as potassium) are depleted in many solar system bodies compared to their solar abundances. However, no physical process, such as thermal processing, has been able to simultaneously explain the degree of elemental depletion and isotopic fractionation—meaning the inconsistency between K isotopic variation and the degree of depletion has remain unsolved. My new data show that the variations in K isotopic compositions among solar system bodies are primarily due to pre-solar nucleosynthetic origins in earlier generation stars. A key implication of this finding is that such K isotope variations cannot be treated as tracers of volatility. Our high-precision  $^{41}\text{K}/^{39}\text{K}$  data from carefully selected meteorites are well correlated with other neutron-rich nuclides that have been interpreted to be the result of the pre-solar nucleosynthetic heterogeneity. This substantial result provides the clearest evidence to date for an isotopically heterogeneous protosolar molecular cloud, and the first evidence that such heterogeneity is also preserved in an abundant moderately volatile element.

## **Chapter 3: The Timing of the Last Nucleosynthetic Injection into the Protosolar Molecular Cloud Inferred from $^{41}\text{Ca}$ – $^{26}\text{Al}$ Systematics of Bulk CAIs.**

This study addresses a long-debated and still unsolved question in the cosmochemical and astrophysical communities on what the short-lived radionuclides (SLRs) tell us about the birth of

the solar system. Among the SLRs,  $^{41}\text{Ca}$  is of special significance due to its decay to  $^{41}\text{K}$  with half-life of only 0.1 Myr. An accurate determination of the initial  $^{41}\text{Ca}$  concentration in the solar system would place constraints on the nucleosynthetic origin of  $^{41}\text{Ca}$  and, in turn, on the birth environment of the solar system. The current estimates of the  $^{41}\text{Ca}$  concentration, based on mineral isochrons of Ca-Al-rich inclusions (CAIs) measured in-situ by an ion microprobe, are highly variable due to the large uncertainties caused by technical challenges. Such variations make constraining the origin of this nuclide difficult. My study reports, for the first time, a bulk CAI  $^{41}\text{Ca}$ - $^{41}\text{K}$  isochron obtained by the MC-ICP-MS technique and provides the most accurate determination of the  $^{41}\text{Ca}$  concentration (relative to stable  $^{40}\text{Ca}$ ) in the solar system to date, expressed as the initial  $(^{41}\text{Ca}/^{40}\text{Ca})_{\text{I}}$  ratio. The precision of our K isotope measurements is approximately two thousand times better than the precision of the ion microprobe data ( $\sim 0.030\%$  vs.  $70\%$ ). Our new  $(^{41}\text{Ca}/^{40}\text{Ca})_{\text{I}}$  ratio suggests that  $^{41}\text{Ca}$  must have been injected into the solar system from outside. In combination with the  $^{26}\text{Al}$ - $^{26}\text{Mg}$  extinct system, our data reveal that SLRs were injected into the solar system about 0.6 Myr to 1.0 Myr before its formation. This implies that the solar system formation, starting from the collapse of a parental molecular cloud, was completed in a very short time. My data provide the first reliable estimate of the  $^{41}\text{Ca}$  concentration in the solar system and strong evidence for a recent injection of  $^{41}\text{Ca}$ ,  $^{26}\text{Al}$ , and, perhaps, other SLRs from nearby stellar sources.

#### **Chapter 4: Potassium isotopic composition of chondritic components from the Allende (CV3), Ochansk (H4), Saratobv (L4) and Elenovka (L5) chondrites**

This study addresses a debate about whether chondrules, one of the major component of chondrites, have experience open-system behaviors of evaporation during heating and re-condensation during cooling events. Potassium (K), as one of the moderately volatile elements,

has great potential for resolving any mechanism behind the K isotopic fractionation among different chondritic components. Although a couple of previous studies have addressed such issues, none has carefully documented the materials being analyzed, such as for petrological characteristics. In this chapter, we present high-precision K isotope data for matrix and chondrules from both carbonaceous and ordinary chondrites, and all chondrule materials were also studied under electron microscopy before any isotope work. By doing this, we are able to connect the petrographic compositions with their K isotope data. We conclude that a wider variation of  $\delta^{41}\text{K}$  in chondrules and matrix, compared to the bulk, likely reflects the sample heterogeneity from the nebular environment rather than secondary processes. In addition, the lack of open-system behavior for K isotopes suggests that chondrule formation, the last chondrule formation event, likely occurred at a near-equilibrium environment, which might be associated with a high ambient gas pressure.



## Chapter 2

# Potassium isotope anomalies in meteorites inherited from the proto-solar molecular cloud

This chapter has been published:

Ku, Y., & Jacobsen, S. B. (2020). Potassium isotope anomalies in meteorites inherited from the protosolar molecular cloud. *Science advances*, 6(41), eabd0511.

### Abstract

Potassium (K) and other moderately volatile elements are depleted in many solar system bodies relative to CI chondrites, which closely match the composition of the Sun. Such depletions and associated isotopic fractionations were initially believed to result from thermal processing in the protoplanetary disk, but so far, no correlation between the K depletion and its isotopic composition has been found. Our new high precision K isotope data correlate with other neutron-rich nuclides (*e.g.*,  $^{64}\text{Ni}$  and  $^{54}\text{Cr}$ ), and suggest that the observed  $^{41}\text{K}$  variations have a nucleosynthetic origin. We propose that K isotope anomalies are inherited from an isotopically heterogeneous proto-solar molecular cloud, and were preserved in bulk primitive meteorites. Thus, the heterogeneous distribution of both refractory and moderately volatile elements in chondritic meteorites points to a limited radial mixing in the proto-planetary disk.

## Introduction

Thermal processing in the solar nebula is believed to have depleted solar system bodies in moderately volatile elements (MVEs) (Anders and Grevesse, 1989) and fractionated their isotopes by partial condensation of the nebular gas (Humayun and Clayton, 1995; Cassen, 1996) and/or evaporation during planetesimal collisions (Halliday and Porcelli, 2001). Among the moderately volatile and relatively abundant elements, only potassium (K) has more than one stable isotope ( $^{39}\text{K}$  and  $^{41}\text{K}$ ), with  $^{41}\text{K}$  being primarily the decay product of the short-lived  $^{41}\text{Ca}$  with  $t_{1/2} \sim 0.1\text{Myr}$  (Kutschera et al., 1992). These characteristics make K a good candidate for studying the history of nucleosynthetic components and thermal processing in the early solar system.

Many planetary bodies show variable depletions in K, often quantified by the K/U ratio. One advantage of this ratio is that it can be measured remotely by a  $\gamma$ -ray survey (McCubbin et al., 2012). For chondritic and planetary samples, Ca/K is a better indicator of K depletions because Ca is one of the refractory major elements, with well-defined and relatively constant concentrations in different solar system bodies. Early work on K isotopes in solar system bodies found no differences within an uncertainty of  $\sim 0.5\%$  (Humayun and Clayton, 1995). Recent higher precision ( $\sim 0.1\%$ ) K isotope data show K isotopic fractionation of  $\sim 0.4\%$  between the Earth and the Moon (Wang and Jacobsen, 2016b), interpreted as a result of incomplete vapor condensation during Moon formation. More recently, observed K isotope variations among planetary bodies and chondrites (Ku and Jacobsen, 2019; Tian et al., 2019; Bloom et al., 2020) were interpreted to result from potential K loss from their parent bodies. If the thermal processing (evaporation/condensation) that depleted K has also fractionated K isotopes, a correlation between K isotopic compositions and K depletions is expected. However, no clear correlation has been

found so far. Apparently, the processes that depleted K in the solar system bodies did not fractionate K isotopes to an observable degree.

Stellar nucleosynthetic processes (*e.g.*, p-, s-, and r-processes) can also result in K isotope variations, because  $^{41}\text{Ca}$ , the source of most  $^{41}\text{K}$ , is mainly produced by an s-process (Meyer and Clayton, 2000). These variations are likely preserved in chondritic meteorites because they are thought to have accreted in the accretionary disk from materials that formed in the solar nebula and/or were inherited from the pre-solar molecular cloud. Small isotopic anomalies have been found in chondrites for many neutron-rich isotopes (Trinquier et al., 2007; Qin et al., 2010; Steele et al., 2012; Dauphas, 2017; Schiller et al., 2018). While the causes of these anomalies remain uncertain, an incomplete mixing of materials from different stellar sources is a leading explanation. If the observed  $^{41}\text{K}$  variations are of nucleosynthetic origin, correlations between  $^{41}\text{K}$  and other neutron-rich nuclides in chondrites are expected.

To constrain the astrophysical environment and understand the thermal events that occurred a few million years before and after the formation of the solar system, we carried out high precision ( $\sim 30$  ppm, Appendix A, Fig. 2(A)) K isotope measurements of samples from a number of solar system objects. We studied both chondrites of different petrologic types and samples of differentiated planetary bodies, aiming to evaluate the contributions of stellar nucleosynthetic processes and mass-dependent fractionations to the observed  $^{41}\text{K}$  variations. K isotopic compositions were measured using the multi-collector ICP-MS *Nu Sapphire*, and are expressed relative to our lab standard, Merck Suprapur®:  $\delta^{41}\text{K}$  (‰) =  $((^{41}\text{K}/^{39}\text{K})_{\text{sample}} / (^{41}\text{K}/^{39}\text{K})_{\text{standard}} - 1) \times 10^3$ . Uncertainties are reported at the two-sigma level (2SE). For a convenient conversion, other commonly used standards were also measured relative to Suprapur: seawater and *NIST* SRM-3141a yielded  $\delta^{41}\text{K} = +0.215 \pm 0.024\text{‰}$  and  $+0.047 \pm 0.003\text{‰}$ ,

respectively. The  $\delta^{41}\text{K}$  notation and K isotopic standards are described in detail in section 1 of the Appendix A.

## **Materials and Methods**

We studied 15 ordinary (H, L and LL), 11 carbonaceous (CI, CM, CV, CO, and CK), and 4 enstatite chondrites (EL and EH) of different petrologic types, both finds and falls, and 12 samples of differentiated planetary bodies, including 3 Martian meteorites, 4 eucrites, and 3 terrestrial samples. Whole rock powders of 4 ordinary chondrites (Peace River-1, Bruderheim, Guareña, and Grady) were prepared by crushing and powdering > 50 g of each meteorite. An additional 0.12 g powder aliquot of Peace River from a different source (Peace River-2 prepared from > 5 g) was also analyzed to compare with a larger sample to test the sample representativeness of ordinary chondrites. Samples of other chondrites were prepared from > 2 g rocks, which is sufficient to represent the bulk composition, with very few exceptions of carbonaceous chondrites. Samples weighing < 5 g were crushed gently using high-purity aluminum oxide mortars and pestles to minimize possible metal contamination.

Samples of some meteorites were obtained from multiple sources in order to test homogeneity of these meteorites by repeated measurements; they are distinguished by Arabic numerals (*e.g.*, Allende-1, Allende-2, *etc.*). Additionally, we have tested the homogeneity of the sample powder by dissolving multiple aliquots of many samples. The separately dissolved aliquots of the same powdered sample have also passed through different columns to test the reproducibility of our column processing; such aliquots are marked by characters a, b, (*e.g.*, Allende-1-a, Allende-1-b, *etc.*) in Table 1.

Aliquots (50-150 mg) of the whole-rock powders were dissolved in multiple steps using mixtures of HF, HCl and HNO<sub>3</sub>. Samples were heated to 210°C in a CEM MARS 6 microwave

digestion system repeatedly. After complete digestion, aliquots were re-dissolved in 0.5N HNO<sub>3</sub> for K ion exchange column chemistry. The solutions were loaded on the 13 mL Bio-Rad AG50W-X8 cation-exchange resin (100-200 mesh) chromatography columns and processed with our established procedure (Wang and Jacobsen, 2016a), except less sample was loaded (~ 10 mg whole rock). Solutions were passed through the columns twice to purify the K-cuts (> 99% yield) and re-dissolved in dilute HNO<sub>3</sub> (~0.32N) for inductively coupled plasma mass spectrometry (ICP-MS) analysis.

The K isotopes were measured at Harvard University with the multi-collector ICP-MS *Nu Sapphire* (serial # SP001). We used the low-energy ion path and a hexapole collision cell to eliminate mass interferences from Ar-bearing ions such as ArH<sup>+</sup>, Ar<sup>+</sup>, and ArO<sup>+</sup>. Solutions containing ~250 ppb of K yield ~4 nA <sup>39</sup>K signal. Samples and standard were matched for <sup>39</sup>K intensity within 1%. A single analytical sample-standard bracketing run (~5 repeats) consumes ~4 ml of the solution, equivalent to ~1 µg of K. We reported the measured K isotope values relative to our lab standard Merck Suprapur® KNO<sub>3</sub> of 99.995% purity. Because K analytical solutions could be contaminated with small amounts of Ca, we also measured mass 40 (for Ca) to monitor the possible formation of <sup>40</sup>CaH<sup>+</sup> (mass 41 interferes with <sup>41</sup>K) in both analytical samples and standards. The contribution of <sup>40</sup>CaH<sup>+</sup> to the mass 41 peak was calculated from the analysis of K standard solution spiked with Ca. The δ<sup>41</sup>K values of all samples of a particular run were corrected for <sup>40</sup>CaH<sup>+</sup> interference, typically less than 0.02‰. Additionally, we monitored the quality of each analytical run by analyzing an extra standard solution with up to 20% concentration mismatch. Runs were considered acceptable only when the δ<sup>41</sup>K difference between the ‘normal’ and ‘mismatching’ standard is less than 0.05‰ (an example is shown in the Appendix A, Fig. 1).

High precision isotope ratio measurements require repeated measurements to evaluate the uncertainty of a sample's mean value. The uncertainty was calculated and reported as doubled standard error (SE) of the mean ( $2\sigma_{SE}$ ). Error estimates need to be verified by comparing external reproducibility and internal uncertainty. Therefore, we have taken into account (1) within-run uncertainties, (2) instrument day-to-day variability, and (3) column chemistry and dissolution uncertainties. The first quantity is the internal uncertainty while the second and third quantities are defined here as external reproducibility.

The within-run uncertainty is the calculated standard error of a sample that was repeatedly measured within an analytical run, given by

$$2 \cdot \sigma_{SE} = 2 \cdot \frac{\sigma_{SD}}{\sqrt{n}},$$

where  $n$  is the bracketing repeats for a sample within a run (typically  $n = 5$ ). The standard deviation (SD) could be estimated by the self-bracketing on a standard within an analytical run (typically  $2SD = 65$  ppm). The internal uncertainty ( $2SE$ ) was, thus, calculated as 30 ppm for a sample (Appendix A, Fig. 2(A)). Uncertainties reported in Table 1 were replaced with 30 ppm if less than that value.

The external reproducibility takes into account the instrumental day-to-day variability, and uncertainties of column processing and sample dissolution. The instrumental day-to-day variability was estimated by measuring one aliquot repeatedly on different days. We calculated the variations ( $2SD$ ) of  $\delta^{41}K$  values of a single aliquot, BHVO-2, which was measured for nine days, to be 27 ppm. We reported this as our external reproducibility for a single measurement (Appendix A, Fig. 2(B)). The consistency between internal (within-run) uncertainty (30 ppm) and external reproducibility (27 ppm) implies there is no additional variability added to the data.

Figure 2(C) in the Appendix A shows that the uncertainties of column chemistry and dissolution processes are negligible, even if the uncertainties from dissolution processes for meteorites may be larger than typical terrestrial samples due to materials (SiC, graphite, *etc.*) that are hard to dissolve. We compare the mean  $\delta^{41}\text{K}$  values for two aliquots (a and b) from the same samples that were dissolved independently and analyzed on multiple days.

The group mean and the corresponding 2SE are calculated based on different meteorites. That is to say, if a meteorite was analyzed more than once, we first calculated the mean of these two or more analyses, and then considered the calculated value as a single data point for the calculation of the group mean.

Most of the samples in this study were acquired from different sources, and some of them were dissolved and analyzed more than once. For instance, Allende was obtained from 2 different sources (Allende-1 and -2), and Allende-1 was dissolved twice independently. The CV group mean should, however, consider Allende and Vigarano meteorites equally. We first calculate the mean  $\delta^{41}\text{K}$  for Allende by averaging [mean (Allende-1a, Allende-1b), Allende-2]. Then, we calculate the mean for Vigarano-1 from averaging Vigarano-1a and Vigarano-1b. Finally, the group mean for CV chondrites is the mean value of Allende (both -1 and -2) and Vigarano-1, which is  $-0.184\%$ .

## Results

We found well-resolved  $\delta^{41}\text{K}$  differences among different planetary bodies, including Mars, Earth and Vesta, as well as between ordinary, enstatite, and carbonaceous chondrites (Fig.1 and Table 1). The samples of the same chondritic meteorites from different sources yield similar  $\delta^{41}\text{K}$  values, suggesting the homogeneity of the samples and robustness of the measurements.

Two individual pieces of CI chondrite analyzed in this work, Orgueil-2 and Orgueil-3, were obtained from different sources to establish the  $\delta^{41}\text{K}$  value of CI meteorites, which are considered the best representation of the starting material in the solar system. The mean  $\delta^{41}\text{K}$  values of  $-0.133\text{‰}$  for the CI group is calculated based on these two samples. The original  $\delta^{41}\text{K}$  value for CI chondrites that was published in (Wang and Jacobsen, 2016b) and that has been widely used in the literature (*e.g.*, Bloom et al., 2020) is indistinguishable from the bulk silicate earth (Wang and Jacobsen, 2016a). In this study, we analyzed the same material from (Wang and Jacobsen, 2016b), and found that this sample contains nearly 8 wt% Earth crustal materials, based on major and trace element compositions. This implies that most of its K is terrestrial, not meteoritic. This issue is discussed in detail in the Appendix A.

The group mean  $\delta^{41}\text{K}$  and the corresponding 2SE are calculated based on different meteorites. The mean  $\delta^{41}\text{K}$  value is  $-0.054\text{‰}$  for CM chondrites,  $-0.070\text{‰}$  for CO chondrites,  $-0.184\text{‰}$  for CV chondrites,  $-0.255\text{‰}$  for one CK chondrite,  $-0.264\text{‰}$  for EH chondrites, and  $-0.696\text{‰}$  for the main cluster of the ordinary chondrites (H, L and LL). The ordinary chondrites have the lightest  $\delta^{41}\text{K}$  among all samples analyzed. The H and L chondrite  $\delta^{41}\text{K}$  values form a single cluster in the  $\delta^{41}\text{K} - \text{Ca/K}$  ratio diagram (Fig. 1), but one LL chondrite, Parnallee, has a significantly lighter  $\delta^{41}\text{K}$  value of  $-0.917\text{‰}$  (Table 1). We have analyzed interior materials (Holbrook-1) and the fusion crust (Holbrook-1(c)) of the same meteorite and found indistinguishable  $\delta^{41}\text{K}$  values. There are small variations of  $\delta^{41}\text{K}$  in carbonaceous chondrites, but the mean  $\delta^{41}\text{K}$  value (CM, CO, and CV) is indistinguishable from CI chondrites. Enstatite chondrites (EH), which are enriched in K, have a lighter  $\delta^{41}\text{K}$  value relative to CI chondrites. The mean of EL chondrites is not included because the two samples analyzed have very different  $\delta^{41}\text{K}$  values (Table 1).



The samples of differentiated planetary bodies show differences in K isotopic compositions, with the mean  $\delta^{41}\text{K}$  values being  $-0.177\text{‰}$  for Mars and  $+0.422\text{‰}$  for the eucrite parent body, which generally agree with (Tian et al., 2019). Mars might possess a unique bulk composition in the inner solar system, intermediate between carbonaceous chondrites and Earth. The eucrite parent body, Vesta, is strongly volatile depleted and shows an enrichment in  $^{41}\text{K}$  compared to other meteorites and Earth. The bulk mean Earth, which is depleted in K relative to both carbonaceous and ordinary chondrites, has an intermediate  $\delta^{41}\text{K}$  value of  $-0.414\text{‰}$ . The mean value is determined based on three samples, BCR-2, BHVO-2 and CHEPR (mid-ocean ridge basalt) in order to be consistent with the previous work (Wang and Jacobsen, 2016a).

Our results are generally consistent with previously published  $\delta^{41}\text{K}$  values after correcting for different standards, except for one CI  $\delta^{41}\text{K}$  derived from a contaminated sample (Wang and Jacobsen, 2016b; Bloom et al., 2020). Some inconsistencies and larger  $\delta^{41}\text{K}$  variations observed in previous studies (Zhao et al., 2019; Bloom et al., 2020) are likely due to the use of non-representative samples ( $\sim 0.1$  gram), and the significant use of meteorite finds. Samples studied here, on the other hand, were mostly meteorite falls powdered from more than 2 grams of whole rock (up to 200 grams). In addition, many meteorites were obtained from multiple sources to overcome the possible heterogeneity of individual pieces. Despite a general agreement in the mean  $\delta^{41}\text{K}$  values for each meteorite group between this study and (Bloom et al., 2020), we favor discussion and interpretation of the data based on samples studied here (see Appendix A).

**Table 1.** K isotopic composition of each sample in this study

Group	Sample	Find/ Fall	Type	$\delta^{41}\text{K}$ Suprapur (‰)	$\pm$ 2SE *	N	n	Group Mean	$\pm$ 2SE	Crushed powder (g)	Sources	$\delta^{41}\text{K}$ SRM-3141a (‰)
CI	Orgueil-2a	Fall	CI1	-0.125	0.030	5	2 1	-0.133**	0.051	0.11	SAO (JW)	-0.172
	Orgueil-2b			-0.192	0.030	5	2 6					-0.239
	Orgueil-3	Fall	CI1	-0.107	0.038	3	1 4					-0.154
CM	Murray-1a	Fall	CM2	0.205	0.033	4	1 9	-0.054	0.285	0.29	SAO (JW)	0.158
	Murray-1b			0.241	0.046	2	9					0.194
	Mighei-1a	Fall	CM2	-0.255	0.046	2	1 0			1.94	SAO (JW)	-0.302
	Mighei-1b	Fall	CM2	-0.246	0.046	2	9			10.00	SAO (UM)	-0.293
	Murchison-1a			-0.112	0.030	10	5 0					-0.159
Murchison-1b	-0.155	0.065	1	5	-0.202							
CO	Ornans-1	Fall	CO3.4	-0.012	0.029	5	2 4	-0.070	0.157	0.88	SAO (JW)	-0.059
	Ornans-2	Fall	CO3.4	-0.057	0.038	3	1 4					6.45
	DaG 749	Find	CO3	-0.216	0.038	3	1 7			1.75	ASU	-0.263
	NWA7916	Find	CO3	0.136	0.033	4	2 1			1.60	ASU	0.089
	Kainsaz	Fall	CO3.2	-0.165	0.038	3	1 4			1.70	NEMS	-0.212
CV	Allende-1a	Fall	CV3	-0.187	0.030	10	5 0	-0.184	0.140	34	SAO (UM)	-0.234
	Allende-1b			-0.197	0.030	9	4 6					-0.244
	Allende-2	Fall	CV3	-0.035	0.033	4	1 9			4000	USNM3529	-0.082
	Vigarano-1a	Fall	CV3	-0.237	0.033	4	1 9			0.67	SAO (JW)	-0.284
	Vigarano-1b	-0.270	0.046	2	9	-0.317						
CK	NWA6254	Find	CK4	-0.255	0.046	2	1 2			2.22	ASU	-0.302
EH	Abee-1a	Fall	EH4	-0.293	0.025	7	3 6	-0.264	0.056	1.00	NEMS	-0.340
	Abee-1b			-0.292	0.046	2	9					-0.339
	Indarch-1a	Fall	EH4	-0.119	0.038	3	1 5			1.82	NEMS	-0.166
	Indarch-1b	-0.160	0.033	4	2 2	-0.207						
	Indarch-2	Fall	EH4	-0.333	0.038	3	1 5			0.23	HMNH	-0.380
EL	MacHill 88481	Find	EL3	-0.556	0.038	3	1 5			0.44	ANSMET	-0.603
	Eagle	Fall	EL6	0.082	0.046	2	9			0.69	NEMS	0.035
LL	Tuxuac-1a	Fall	LL5	-0.609	0.046	2	1 1	-0.740	0.141	2.46	NEMS	-0.656
	Tuxuac-1b			-0.543	0.038	3	1 4					-0.590
	Parnallee	Fall	LL3	-0.917	0.038	3	1 7			1.34	ASU	-0.964
	Vicencia	Fall	LL3	-0.759	0.038	3	1 7			1.32	ASU	-0.806
	Chainpur	Fall	LL3.4	-0.708	0.046	2	1 0			0.99	SAO (JW)	-0.755
L	Marion Iowa	Fall	L6	-0.679	0.030	5	2 2			2.00	HMNH	-0.726
	Homestead	Fall	L5	-0.725	0.030	6	2 9			2.00	HMNH	-0.772

	Bruderheim	Fall	L6	-0.672	0.038	3	1			70	SAO (UM)	-0.719
	Peace River-1	Fall	L6	-0.632	0.038	3	1			190	SAO (UM)	-0.679
	Peace River-2	Fall	L6	-0.672	0.033	4	2			0.12	Caltech (JW)	-0.719
	Holbrook-1	Fall	L6	-0.636	0.038	3	2			0.93	SAO(JW)	-0.683
	Holbrook-1 (c)	Fall		-0.621	0.038	3	2			0.60		-0.668
	Holbrook-2	Fall	L6	-0.658	0.046	2	1	-0.675	0.028	3.07	HMNH	-0.705
							0					
H	Kernouve	Fall	H6	-0.628	0.030	5	2			2.00	HMNH	-0.675
	Dresden	Fall	H6	-0.681	0.030	5	2			2.00	HMNH	-0.728
	Forest City	Fall	H5	-0.724	0.030	6	2			2.00	HMNH	-0.771
	Grady	Find	H3	-0.710	0.038	3	1			70	Caltech (JW)	-0.757
	Guareña	Fall	H6	-0.681	0.038	3	1			53.40	Caltech (JW)	-0.728
	Estacado	Find	H6	-0.609	0.038	3	1	-0.672	0.037	2.80	NEMS	-0.656
							5					
Mars	Nakhla-1	Fall	Nakhla	-0.193	0.029	5	2			0.25	SAO(JW)	-0.240
	Nakhla-2	Fall	Nakhla	-0.164	0.029	5	2			0.23	SAO(JW)	-0.211
	QUE94201.55	Find	Shergottite	-0.152	0.038	3	1			0.10	ANSMET	-0.199
	Zagami-1	Fall	Shergottite	-0.279	0.038	3	1			0.11	NEMS	-0.326
	Zagami-2	Fall	Shergottite	-0.120	0.038	3	1	-0.177	0.027	0.94	ASU	-0.167
							4					
Vesta	Stannern	Fall	Eucrite	0.503	0.038	3	9			0.26	SAO(JW)	0.456
	Bouvante	Find	Eucrite	0.270	0.038	3	1			0.13	SAO(JW)	0.223
							2					
	Sioux. County	Fall	Eucrite	0.202	0.038	3	1			0.20	SAO(JW)	0.155
	Juvinas	Fall	Eucrite	0.712	0.046	2	1	0.422	0.232	0.14	SAO(JW)	0.665
							0					
Earth	BHVO-2		Basalt	-0.333	0.030	9	4				USGS	-0.380
	BCR-2		Basalt	-0.370	0.030	9	4				USGS	-0.417
	CHEPR		Basalt	-0.538	0.033	4	1	-0.414	0.126		Harvard (CL)	-0.585
							8					

Internal uncertainty = 30ppm

The interior portion and fusion crust of Holbrook-1 were powdered independently; the fusion crust, Holbrook-1 (c) is not included in calculating the group mean.

NIST SRM-3141-a was measured with respect to Suprapur =  $+0.047 \pm 0.003\%$ .

The group mean and the corresponding 2SE are calculated based on different meteorites. Details in Materials and Methods.

\* The uncertainty (2SE) is  $2SD (65 \text{ ppm})/\sqrt{N}$  and was replaced with 30 ppm if less than 30 ppm. Additional uncertainty is negligible when converting Suprapur to SRM-3141a.

*N*: numbers of independent analytical runs.

*n*: total number of the bracketed  $\delta^{41}\text{K}$  values from *N* days.

\*\* The meteorite group means and 2SE are based on small numbers (numbers of different meteorites); CI group is based on two chunks of one meteorite, Orgueil.

Abbreviated sample sources:

**ANSMET**: Antarctica Meteorite Collection, NASA; **ASU**: Center for Meteorite Studies, Arizona State University; **Caltech (JW)**: Caltech Jerry Wasserburg; **HMNH**: Harvard Museum of Natural History; **Harvard (CL)**: Harvard University (Charlie Langmuir); **MNH**: Museum national d'Histoire naturelle; **NEMS**: New England Meteoritical Services; **SAO (JW)**: Smithsonian Astrophysical Observatory (John Wood); **SAO (UM)**: Smithsonian Astrophysical Observatory (Ursula Marcin); **USNM3529**: Smithsonian USNM3529, 4kg Allende powder.

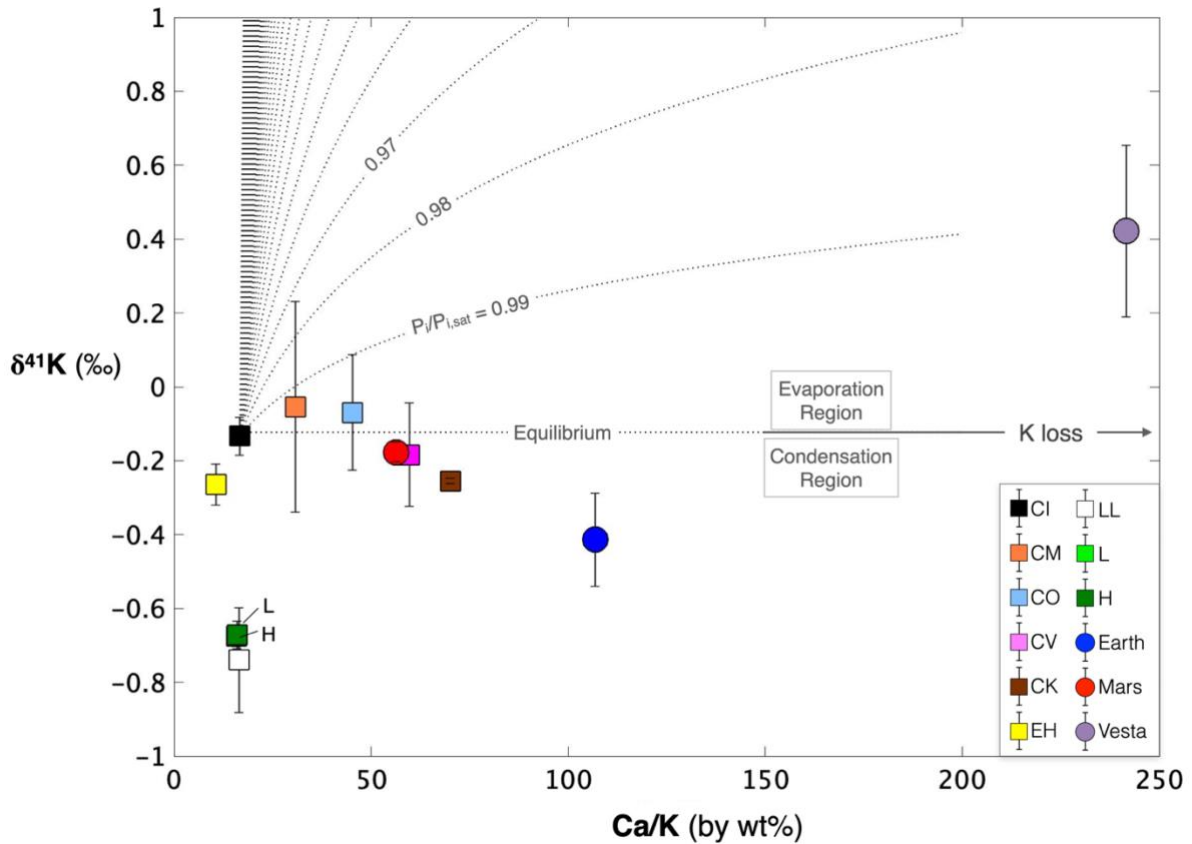


**Figure 1. Chemical and isotopic variations of K among chondrites and planetary bodies.** Each data point is the group mean calculated using available samples within each group. The corresponding uncertainties on the group means are larger than the analytical uncertainty because of the heterogeneity among samples within groups (details in table 1). Note that evaporation/condensation cannot explain our K isotopic data. The K and Ca concentrations in each group are taken from the literature (McDonough, 2003; Taylor, 2013; Alexander, 2019a, b). The group mean and uncertainties (2SE) for the CI group in this study are based on Orgueil.

## Discussions

### Mass-dependent fractionation of K isotopes during evaporation/condensation

Variations in  $\delta^{41}\text{K}$  are often explained by evaporation/condensation processes which could occur under kinetic or equilibrium conditions. In the case of equilibrium ( $P_i/P_{i,\text{sat}} = 1$ , where  $P_{i,\text{sat}}$  is the saturation pressure for species  $i$ ), the isotopic composition of the condensed phase must be heavier than the bulk system, but the magnitude of fractionation (the horizontal dotted line in Fig. 1) is expected to be smaller than the current analytical uncertainty. Under  $P_i/P_{i,\text{sat}} < 1$ , evaporation of K from a condensed phase would enrich the residue in  $^{41}\text{K}$ . The magnitude of fractionation increases from a near-equilibrium value to 22‰ (Richter et al., 2011) as the  $P_i/P_{i,\text{sat}}$  ratio decreases to  $\sim 0$  (Fig. 1; Appendix A discussion). If  $P_i/P_{i,\text{sat}} > 1$ , the condensate is expected to be depleted in  $^{41}\text{K}$ , with the magnitude of fractionation decreasing to  $\sim 0$ ‰ as condensation continues in a closed system. Thus, if CI chondrites were the starting material for the solar nebula, then the observed magnitude of K isotopic fractionation in K-depleted samples cannot be explained by the loss of K during evaporation or condensation. Therefore, single-stage nebular thermal processing cannot account for the observed nebula-wide  $\delta^{41}\text{K}$  variations.

While other MVEs such as Zn and Cu (Lodders, 2003) also show depletion in planetary bodies, K behaves very differently from them. For example, Zn and Cu are more easily fractionated during impact vaporization (Moynier et al., 2009, 2010), but no K isotopic fractionation was found in tektites (Jiang et al., 2019). A lack of correlations between  $\delta^{41}\text{K}$  and  $\delta^{66}\text{Zn}$  and  $\delta^{65}\text{Cu}$  (Appendix A, Fig. 6) further suggests incoherent behaviors among MVEs during nebula thermal processes and planetary formation (Wood et al., 2006). We have also considered parent body processes (*i.e.*, aqueous alteration), and conclude that such processes cannot explain the overall K isotope variations in chondrites. A constant K-Rb ratio has been found for different meteorite groups

studied here and the bulk Earth (Appendix A, Fig. 7). In addition, we found that  $\delta^{41}\text{K}$  vs Al/K, Cr/K, Fe/K and Ni/K in different chondrite groups and Earth show the same pattern, regardless of whether the element that K is compared to, is mobile or immobile. The observed  $\delta^{41}\text{K}$  variations could be due to a heterogeneous distribution of either anomalous pre-solar grains or local aqueous alteration products. We have minimized such effects by using large samples (up to 200 grams) whenever possible, and using group means for each meteorite class based on multiple samples. Thus, we argue that the mean  $\delta^{41}\text{K}$  of each group should minimize these effects of small-scale sample heterogeneity.

### **Evidence supporting the Type-II supernova injection**

Alternatively, the observed variations of  $\delta^{41}\text{K}$  in meteorites may reflect a heterogeneous distribution of  $^{41}\text{Ca}$  in the solar nebula. The presence of extinct  $^{41}\text{Ca}$  (now  $^{41}\text{K}$ ) found in Ca-Al-rich inclusions (CAIs) (Goswami, 1998) could result from either *in situ* irradiation, through the  $^{42}\text{Ca}(p, pn)^{41}\text{Ca}$  reaction, or injection by a recent supernova explosion. Thus, the observed  $^{41}\text{K}$  variations could potentially reflect varying proportions of Ca-rich (CAIs) and Ca-poor (chondrules and matrix) components of chondrites. Using available literature data and mass-balance calculations, we found that the contribution of  $^{41}\text{K}$  from CAIs to the total  $^{41}\text{K}$  balance is not sufficient to explain the observed K isotope variations in meteorites (details can be found in the Appendix A discussion).

Therefore,  $^{41}\text{K}$  (decay product of  $^{41}\text{Ca}$ ) must have been heterogeneously distributed in the proto-solar molecular cloud; such heterogeneity was preserved in the solar nebula and recorded in the primitive meteorites. The inhomogeneous distribution of  $^{41}\text{K}$  could be caused by one or more injections of  $^{41}\text{K}$  from a nearby stellar source into the pre-solar molecular cloud.  $^{41}\text{Ca}$  is primarily formed via neutron capture from abundant and stable  $^{40}\text{Ca}$ , and may be continuously ejected from

massive stars during their Wolf-Rayet phase, or ejected by final explosions of supernovae (Clayton, 2003; Liu et al., 2012). The main sources of pre-solar  $^{41}\text{K}$  ( $^{41}\text{Ca}$ ) are still debated, but it is almost certain that when a massive star explodes in a supernova, neutron-rich isotopes are ejected into the molecular cloud, which become part of the solar nebula materials (Prantzos et al., 1986; Timmes et al., 1995). Neutron-capture extinct radionuclides (*e.g.*,  $^{41}\text{Ca}$ ,  $^{129}\text{I}$ ) and neutron-rich isotopes, especially the ones in the Fe peak (*e.g.*,  $^{48}\text{Ca}$ ,  $^{50}\text{Ti}$ ,  $^{54}\text{Cr}$ , and  $^{64}\text{Ni}$ ), are likely formed by nuclear reactions in stars shortly before the solar system formation (Lugaro et al., 2014). Because most  $^{41}\text{Ca}$  has decayed to  $^{41}\text{K}$  due to its half-life of  $\sim 0.1\text{Myr}$ , massive stellar winds and supernova ejecta would add abundant  $^{41}\text{K}$  and little  $^{41}\text{Ca}$  to the solar nebula materials.

To evaluate whether K isotopic variations could result from an injection of  $^{41}\text{K}$ , we compare  $\delta^{41}\text{K}$  to  $\varepsilon^{64}\text{Ni}$  and  $\varepsilon^{54}\text{Cr}$  (Fig. 2). The mass-independent anomalies in  $^{64}\text{Ni}$  and  $^{54}\text{Cr}$  (expressed in  $\varepsilon$ -notation) are generally thought to reflect the heterogeneous distribution of distinct nucleosynthetic components in the solar system (Trinquier et al., 2007; Qin et al., 2010; Steele et al., 2012). We found positive correlations between  $^{41}\text{K}$ ,  $^{64}\text{Ni}$  and  $^{54}\text{Cr}$  suggesting that  $^{41}\text{Ca}$  (the precursor of  $^{41}\text{K}$ ) was probably produced in a Type-II supernova shell (Steele et al., 2012). This implies that the observed K isotopic variations reflect the heterogeneous distribution of pre-solar nuclides in the solar system. Earth, which is usually an end member in many nucleosynthetic isotope anomaly plots, such as  $\mu^{142}\text{Nd}^*$  and  $\varepsilon^{92}\text{Mo}$  (Appendix A, Fig. 9), has an intermediate value between the carbonaceous and ordinary chondrites in  $\delta^{41}\text{K}$ ,  $\varepsilon^{64}\text{Ni}$  and  $\varepsilon^{54}\text{Cr}$ . The varying sequence of objects in each diagram suggests that the correlations of  $\delta^{41}\text{K}$  with other isotopes cannot simply be due to a mixing between two end members, CM (or CI) and ordinary chondrites. Instead, possibly more than two nucleosynthetic components were present to explain the overall solar system anomalies observed in neutron-rich isotopes.

## Testing a multi-component mixing model

The chemical and isotopic compositions of chondrites result from mixing several components formed under different physicochemical conditions. For example, (Alexander, 2019a) used a four-component mixing model to successfully reproduce the K concentrations in six carbonaceous chondrite groups. These components are: (1) CAIs, (2) matrix of the CI composition, (3) chondrules compositionally similar to the volatile-depleted CI chondrites, and (4) H<sub>2</sub>O-rich ices. Bloom et al. (2020) used a similar model to explain the  $\delta^{41}\text{K}$  variations observed in carbonaceous chondrites by the mixing of chondrules and matrix. The matrix  $\delta^{41}\text{K}$  was approximated by the bulk CI  $\delta^{41}\text{K}$  value of  $-0.53\text{‰}$ , while the chondrule  $\delta^{41}\text{K}$  value ranging from  $-0.28\text{‰}$  to  $2.08\text{‰}$  was calculated assuming fractional evaporative K loss (1-10%) from initial CI composition described by the Rayleigh fractionation law. However, since the initial CI  $\delta^{41}\text{K}$  value of  $-0.53\text{‰}$  measured in the contaminated Orgueil sample is incorrect, both modeled  $\delta^{41}\text{K}$  values are also incorrect. Once the wrong initial CI  $\delta^{41}\text{K}$  value of  $-0.53\text{‰}$  is replaced with the correct one of  $-0.133\text{‰}$ , the mixing model fails to account for the observed  $\delta^{41}\text{K}$  variations in both carbonaceous and ordinary chondrites. Thus, mixing of different components that experienced various degrees of thermal processing in the solar nebula is an unlikely explanation for the overall K isotope variations found in chondrites.

Let's now evaluate whether the four-component mixing model of (Alexander, 2019a) can reproduce the observed  $\delta^{41}\text{K}-\epsilon^{64}\text{Ni}$  and  $\delta^{41}\text{K}-\epsilon^{54}\text{Cr}$  correlations. Since ices are supposed to contain no K, Ni, and Cr, such a model reduces to three components with unknown  $\delta^{41}\text{K}$  values. Following (Alexander, 2019a), we approximate matrix with the bulk CI  $\delta^{41}\text{K}$  value of  $-0.133\text{‰}$ . The limited data on individual chondrules from Hamlet, a LL4 brecciated chondrite (Koefoed et al., 2019), show a very wide  $\delta^{41}\text{K}$  range, with the most chondrules having lighter  $\delta^{41}\text{K}$  than the



bulk CI chondrites. This result is inconsistent with the fractional evaporative loss of K assumed by Bloom et al. (2020), but is in line with the observed addition of SiO<sub>2</sub> to crystallizing chondrule melts from the ambient gas (Krot et al., 2004; Chaussidon et al., 2008; Libourel and Portail, 2018). Since no reliable  $\delta^{41}\text{K}$  value for chondrules is currently available, we approximate it by the  $\delta^{41}\text{K}$  value of  $-0.692\%$  from the bulk ordinary chondrites, which are known to contain up to 80 vol % chondrules (Scott and Krot, 2003). The  $\delta^{41}\text{K}$  value of  $0.249\%$  for CAIs is calculated based on the assumption that all  $^{41}\text{K}$  is the product of  $^{41}\text{Ca}$  decay (Appendix A discussion), and the  $\epsilon^{64}\text{Ni}$  and  $\epsilon^{54}\text{Cr}$  values are from (Birck and Lugmair, 1988; Trinquier et al., 2007). The results of a three-component mixing are shown in Fig. 2. Because of the large positive anomalies of  $\epsilon^{64}\text{Ni}$  and  $\epsilon^{54}\text{Cr}$  in CAIs, the calculated mixing region is enriched in these nuclides and shifts away from the observed arrays, regardless of the  $\delta^{41}\text{K}$  values in CAIs. Hence, our data cannot be explained by the mixing of major chondrite components.

The most likely interpretation for the correlations of  $\delta^{41}\text{K}$  with  $\epsilon^{64}\text{Ni}$  and  $\epsilon^{54}\text{Cr}$  in bulk chondrites is pre-solar anomalies. As  $^{41}\text{Ca}$  could also be partially produced by s-processes, the  $^{41}\text{K}$  anomalies could arise from a combination of s-processes in other stars and a Type-II supernova explosion (consistent with  $^{64}\text{Ni}$ ). There is, however, not much evidence, so far, supporting a s-process origin, and our data thus preferentially suggest the Type-II supernova as the main source of pre-solar  $^{41}\text{K}$  heterogeneity.

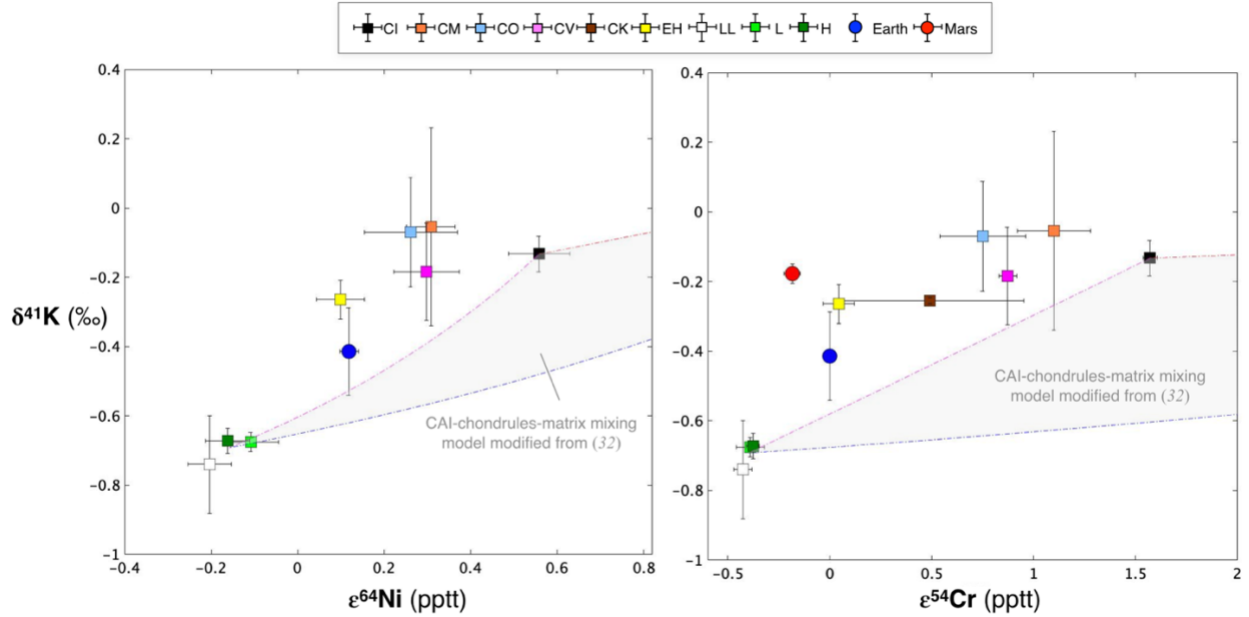


**Figure 2. Variations of  $\delta^{41}\text{K}$ ,  $\varepsilon^{54}\text{Cr}$ , and  $\varepsilon^{64}\text{Ni}$  in bulk samples.** The concentrations of each element are from (Alexander, 2019a, b), and mean  $\varepsilon^{54}\text{Cr}$  and  $\varepsilon^{64}\text{Ni}$  data for each group are from (Dauphas, 2017) (see Appendix A, Fig. 8 for complete references). The gray regions show the three-component mixing model (modified from Alexander, 2019a) of chondrules, matrix and CAIs. The chondrule and matrix components are estimated by the average ordinary and CI chondrites, respectively. The correlations between  $\delta^{41}\text{K}$ ,  $\varepsilon^{54}\text{Cr}$ , and  $\varepsilon^{64}\text{Ni}$  suggest that these anomalies are primarily caused by nucleosynthetic processes, and cannot be generated by a multi-components mixing model between major chondrite components. The correlations also cannot be explained by the mixing of two isotopically distinct reservoirs, such as CM (or CI) and ordinary chondrites. This is because mixing between two endmembers would yield straight lines in  $\delta^{41}\text{K}$ –Ca/K plots (Fig. 1, and similar plots of the Appendix A, Fig. 7(B)), which is not observed. In addition, mixing the two end-members’ compositions is unlikely to reproduce both volatile-depleted Earth and volatile-enriched enstatite chondrites that both have intermediate values of  $\delta^{41}\text{K}$ ,  $\varepsilon^{64}\text{Ni}$  and  $\varepsilon^{54}\text{Cr}$ .

## Implications for an isotopically heterogeneous molecular cloud

Out of many scenarios regarding the formation of an isotopically heterogeneous protoplanetary disk, three are illustrated in Fig. 3. The first scenario assumes that isotopically homogeneous materials infalling from the molecular cloud experienced nebula-wide thermal processing, resulting in the formation of an isotopically heterogeneous inner disk depleted in MVEs (Fig. 3A). The partial evaporation of thermally unstable phases would fractionate nuclides of different origins to the same degree (*e.g.*,  $^{46}\text{Ti}$  and  $^{50}\text{Ti}$ ) (Trinquier et al., 2009). If so, the isotopic composition of an element should correlate with its MVEs depletion, which is not observed for K (Fig. 1). We thus rule out this model.

In the second scenario (Fig. 3B), the degree of heterogeneity is time-dependent and reflects mixing between isotopically different materials from the inner and outer disk. Like in the first scenario, the proto-solar disk forms from a homogeneous molecular cloud, but only the inner disk becomes depleted in neutron-rich isotopes during thermal processing. As the inner disk gradually mixes with the outer disk, the degree of isotopic heterogeneity changes with time. A special case of this scenario (Schiller et al., 2018) predicts that larger, later-formed bodies like Earth would have heavier  $\mu^{48}\text{Ca}$  than smaller, earlier-formed ones such as Mars and Vesta due to continuous admixing of isotopically heavier materials from the outer disk (*i.e.*, carbonaceous chondrites). However, this case cannot explain the fact that Earth has lighter  $\delta^{41}\text{K}$  than Mars. The lack of correlation between K depletion and  $\delta^{41}\text{K}$  rules out thermal processing as the main cause for the inner-outer isotopic differences.

In the third scenario (Fig. 3C), isotopic heterogeneity in the proto-solar disk was inherited from an isotopically heterogeneous molecular cloud. If so, the isotopic heterogeneity of both moderately volatile ( $^{41}\text{K}$ ) and refractory ( $^{54}\text{Cr}$  and  $^{64}\text{Ni}$ ) nuclides preserved in meteorites can only

be explained by a limited mixing of nucleosynthetic materials. The depletion in MVEs, caused by thermal processing, does not need to correlate with the isotopic composition as long as mixing in the disk occurs only on a local scale. It also implies that the feeding zones of planetesimals and planets are relatively narrow, and do not mix with one another. The correlations between  $\delta^{41}\text{K}$  and other neutron-rich refractory nuclide ( $\epsilon^{64}\text{Ni}$ ,  $\epsilon^{54}\text{Cr}$ ) anomalies can be preserved in this scenario. Thus, such a model is favored by our K data.

The survival of K isotopic heterogeneity implies a limited mixing among formation regions of the various planetary and chondrite parent bodies. Perhaps, any gaps in the proto-planetary disk (Kruijer et al., 2017; Pinte et al., 2018; Teague et al., 2018) can further segregate the pre-solar (pre-CAI formation) isotopically distinct reservoirs, and serve as barriers against radial mixing. Such local isotopic heterogeneity can, in fact, survive through later disk-wide disturbances – *the Grand Tack* (Walsh et al., 2011), and would be preserved in the compositionally diverse asteroid belt where the most primitive meteorites might have come from (DeMeo and Carry, 2014). The isotopic anomalies, now, observed for both refractory and moderately volatile elements in primitive meteorites are inherited from the heterogeneous proto-solar molecular cloud, which is likely associated with Type-II supernova injection before the solar system formed.

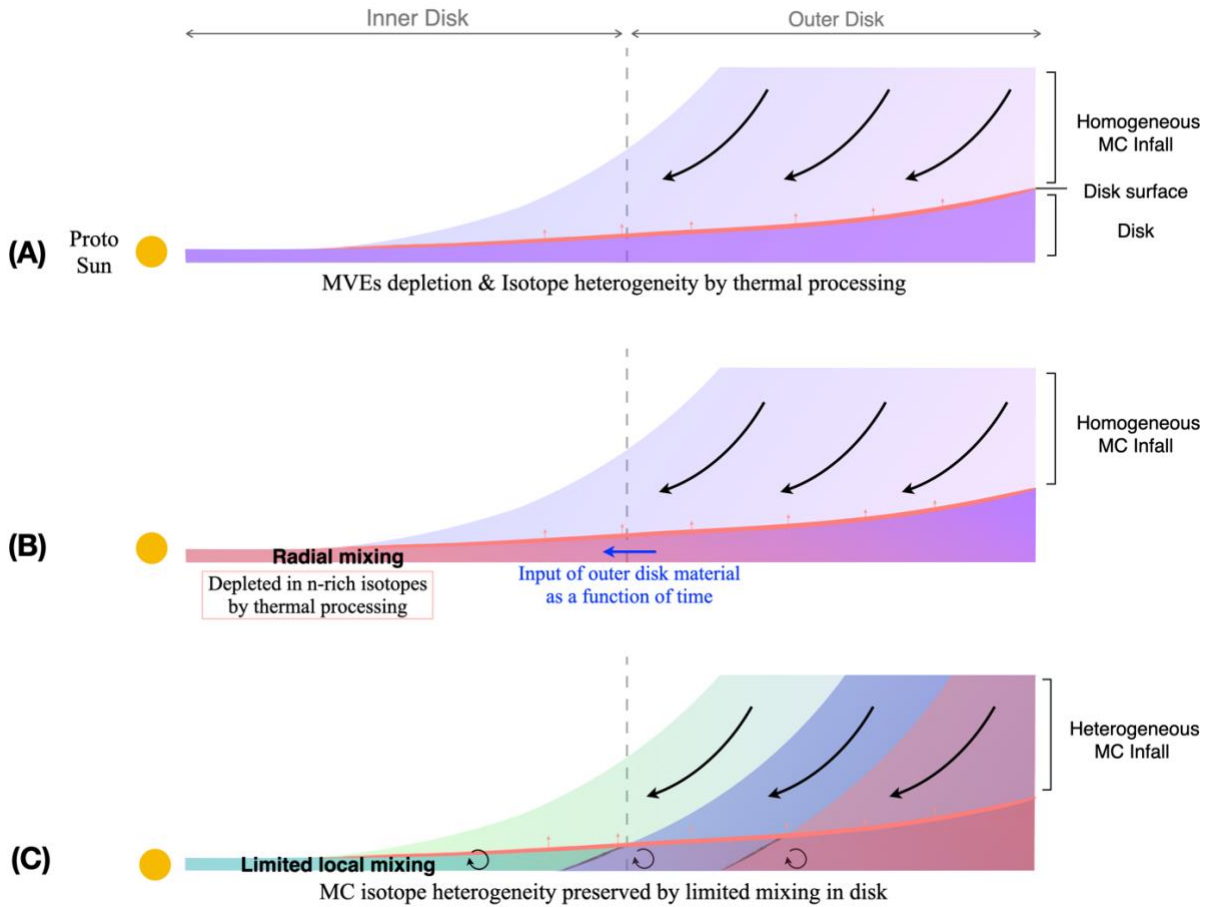


**Figure 3. Models explaining the observed isotopic heterogeneity and MVEs depletions in the solar protoplanetary disk.** (A) A nebular thermal processing of infalling, isotopically homogeneous material from the molecular cloud results in both isotopic heterogeneity (for  $\epsilon^{46}\text{Ti}$  and  $\epsilon^{50}\text{Ti}$ ) and variable depletions in MVEs in the disk (Trinquier et al., 2009). An expected correlation between isotope compositions and depletion of MVEs is not observed for K, ruling out this model. (B) Isotopic heterogeneity (for  $\mu^{48}\text{Ca}$  and others) in the inner disk (depleted in n-rich isotopes) results from thermal processing of a homogeneous molecular cloud material. The inner disk gradually mixes with materials from the outer disk, making the isotopic composition of solid bodies in the inner solar system a function of time (increasing n-rich isotopes with time) (Schiller et al., 2018). This would produce correlations among isotope compositions, MVEs depletions, and

sizes of planetary bodies in the inner solar system, which is not observed for K, ruling out this model too. (C) Isotopic heterogeneity inherited from an isotopically heterogeneous molecular cloud. Thermal processing in the disk produces the MVEs depletions in the solid objects of the inner disk. No correlation between isotope compositions and MVE depletions is expected as long as mixing in the disk occurs on a local scale only, but the correlation between MVEs ( $\delta^{41}\text{K}$ ) and other n-rich refractory nuclides ( $\epsilon^{64}\text{Ni}$ ,  $\epsilon^{54}\text{Cr}$ ) can be preserved. This is the model favored by our K isotope data.

## Chapter 3

### **The Timing of the Last Nucleosynthetic Injection into the Protosolar Molecular Cloud Inferred from $^{41}\text{Ca}$ – $^{26}\text{Al}$ Systematics of Bulk CAIs**

This chapter is currently under review at the *Astrophysical Journal Letters*.

#### **Abstract**

Short-lived radionuclides (SLRs) provide important information about the chronology of the early solar system. Among them,  $^{41}\text{Ca}$ , due to its decay to  $^{41}\text{K}$  with half-life of only 0.1 Ma (Jörg et al., 2012), is particularly valuable in constraining the timescales and origins of both SLRs and formation of the oldest solar system materials, the Ca-Al-rich inclusions (CAIs). The initial abundance of  $^{41}\text{Ca}$  in the solar system, expressed as the  $(^{41}\text{Ca}/^{40}\text{Ca})_{\text{I}}$  ratio, is the key to unveiling the origin of this nuclide. Here, we report a new solar system  $(^{41}\text{Ca}/^{40}\text{Ca})_{\text{I}}$  ratio of  $2.22 \times 10^{-8}$  derived from the K isotope compositions of two CAIs. This new ratio is 5 times higher than the previous value inferred from a mineral isochron (Liu, 2017). Such a high  $(^{41}\text{Ca}/^{40}\text{Ca})_{\text{I}}$  ratio in the CAIs exceeds that expected for the protosolar molecular cloud by  $\sim 1000\times$ , implying very late injection of the  $^{41}\text{Ca}$  (and possibly other SLRs) into the protosolar molecular cloud. The correlated enrichments of  $^{41}\text{Ca}$  and  $^{26}\text{Al}$  in the bulk CAI samples hint for a common stellar origin of both SLRs. The injection time estimated from our new data depends on the stellar source – it ranges from 0.6 Ma for a Wolf-Rayet wind to 1.0 Ma for a TP-AGB star ejecta.

## Introduction

Short-lived radionuclides (SLRs, half-lives of  $\sim 0.1$  to 100 Ma) that were present in the early solar system are now considered extinct because they have decayed below the detection level (Dauphas and Chaussidon, 2011). They provide important constraints on the chronology of the earliest solar system events including formation of CAIs, chondrules, and accretion of early planetesimals as well as their chemical differentiation and thermal evolution. Extinct nuclides also trace their nucleosynthetic sources and place constraints on the birth environment of the solar system. Many SLRs are believed to be products of the long-term chemical galactic evolution, while those with half-lives  $< 1$  Ma require late addition to the protosolar molecular cloud. Such an addition could be caused by either an injection from young stellar sources or in-situ production by irradiation of local materials in the protosolar molecular cloud or the solar nebula itself. For example, an explosion of a nearby star, which triggered the collapse of the protosolar molecular cloud and the formation of the solar system, might have injected SLRs into it. Another possible source is the wind from a Wolf-Rayet star, an idea that is supported by new data (Dwarkadas et al., 2017). Thus, constraining the origin of SLRs may elucidate how the forming solar system was influenced by the ambient astrophysical environment (Adams, 2010). Among the SLRs,  $^{41}\text{Ca}$ , with an extremely short half-life of 0.0994 Ma (Jörg et al., 2012), is perhaps the most important nuclide to study the processes that produced SLRs and to constrain the timescale of molecular cloud collapse and the eventual formation of a young stellar object like our Sun.

Previously, the abundance of  $^{41}\text{Ca}$  was inferred from the detection of radiogenic  $^{41}\text{K}$  excesses ( $\delta^{41}\text{K}^*$ ) in the oldest solar system materials, Ca–Al-rich Inclusions (CAIs) in carbonaceous chondrites (Srinivasan et al., 1994, 1996; Goswami, 1998). CAIs are the first solids formed in the solar nebula. The absolute U–Pb age of CAIs defines the age of our solar system



(Amelin et al., 2010). Because of their early formation, CAIs provide insights into the sources of the SLRs in the solar system. Given their high Ca and very low K concentrations, CAIs are also perfect for studying the origin of  $^{41}\text{Ca}$ . The abundance of  $^{41}\text{Ca}$  expressed as the  $(^{41}\text{Ca}/^{40}\text{Ca})_{\text{I}}$  isotope ratio of  $1.41 \times 10^{-8}$  (Srinivasan et al., 1996) has historically been inferred from  $^{41}\text{Ca}$ – $^{41}\text{K}$  isochrons by in-situ secondary ion mass spectrometry (SIMS or ion microprobe) measurements of  $^{41}\text{K}$ , the decay product of  $^{41}\text{Ca}$ , expressed as  $^{41}\text{K}/^{39}\text{K}$  isotope ratios. Recently (Liu, 2017) reported a much lower  $(^{41}\text{Ca}/^{40}\text{Ca})_{\text{I}}$  ratio of  $4.6 \times 10^{-9}$  than that of previous studies (Srinivasan et al., 1994, 1996; Goswami, 1998), resulting in a re-evaluation of the significance of  $^{41}\text{Ca}$  in the earliest solar system models, as well as the origins of  $^{41}\text{Ca}$ . This revision is the result of interference corrections in the mass spectrometric measurements that was not done in the earlier studies.

Here, we report a new  $(^{41}\text{Ca}/^{40}\text{Ca})_{\text{I}}$  ratio for the solar system inferred from a bulk CAI isochron established by multi-collector inductively coupled plasma mass spectrometry (MC-ICP-MS). The key advantage of MC-ICP-MS is its ability to eliminate the severe matrix interferences characteristic of the ion microprobe technique. As a result, the MC-ICP-MS allows, for the first time, a precise  $^{41}\text{Ca}$ – $^{41}\text{K}$  chronometry of bulk CAIs with uncertainties of  $^{41}\text{K}/^{39}\text{K}$  isotope ratios as small as 0.030%.

## Results

We studied 4 CAI samples (3 chips of SJ101 and the whole CH007 inclusion), 1 matrix sample (Mx), and 1 chondrule sample (CH001) from the Allende CV3 chondrite, described in detail in the Appendix B. The bulk concentrations of major and trace elements (Appendix B, Fig. 1) were measured in small aliquots by a quadrupole ICP-MS; the remainders were passed through ion-exchange columns for K separation, and the isotope analyses were performed using the *Nu Sapphire* (#SP001) MC-ICP-MS equipped with a collision cell. Potassium isotope compositions

are expressed relative to our laboratory standard, Merck Suprapur:  $\delta^{41}\text{K}$  (‰) =  $[(^{41}\text{K}/^{39}\text{K})_{\text{sample}}/(^{41}\text{K}/^{39}\text{K})_{\text{standard}} - 1] \times 10^3$ . Uncertainties are reported at the two-sigma level, and an overall sample reproducibility of 0.030‰ is applied to all samples here (details in the Appendix B).

Three SJ101 pieces (A, B and C) show enrichment in  $^{41}\text{K}$  compared to the CH007 CAI ( $\delta^{41}\text{K} = -0.294\text{‰}$ ). SJ101-A has a  $\delta^{41}\text{K}$  value of  $-0.036\text{‰}$ , while SJ101-B and -C yield more positive values of  $+0.226\text{‰}$  and  $+0.236\text{‰}$ , respectively. The CH001 chondrule has a  $\delta^{41}\text{K}$  value similar to CH007, while the matrix (Mx) has the most negative  $\delta^{41}\text{K}$  value among all analyzed samples (Table 1). The K isotopic compositions of CAIs, plotted along with  $^{40}\text{Ca}/^{39}\text{K}$  ratios in figure 1, yield a  $^{41}\text{Ca}$ - $^{41}\text{K}$  isochron with the  $(^{41}\text{Ca}/^{40}\text{Ca})_{\text{I}}$  ratio of  $(2.22 \pm 0.18) \times 10^{-8}$ . By analogy with the initial  $(^{26}\text{Al}/^{27}\text{Al})_{\text{I}}$  ratio of the bulk CAI isochron, we interpret this value as the initial ratio for the solar system. The addition of the matrix sample (Mx) to the CAI isochron would slightly lower the  $(^{41}\text{Ca}/^{40}\text{Ca})_{\text{I}}$  ratio down to  $(1.87 \pm 0.11) \times 10^{-8}$  (more discussion of isochron fitting in Appendix B, A.3-A.4). However, since other chondritic components such as chondrule (CH001) and whole rock Allende (Allende-1) lie significantly above the initial  $\delta^{41}\text{K}$  of the CAI isochron (Appendix B, Fig. 4), it is unclear whether the addition of matrix to the CAI isochron is justified. Therefore, we consider the bulk CAI isochron and the inferred  $(^{41}\text{Ca}/^{40}\text{Ca})_{\text{I}}$  ratio of  $2.22 \times 10^{-8}$  to be more robust. We also note that the goodness of the fits for these isochrons is far from perfect, as discussed in the Appendix B and Table 2. In order to get perfectly fit isochrons, the errors for our data points should be about four times larger than the analytical uncertainty we are reporting, and that is highly unlikely. Therefore, we consider our estimate of  $(^{41}\text{Ca}/^{40}\text{Ca})_{\text{I}} = 2.22 \times 10^{-8}$  to be the average value for the time interval of formation of CAIs which have experienced multiple

melting events recorded in their texture and mineralogy before the accretion of the CV parent body. The  $\pm 0.18 \times 10^{-8}$  is the  $2\sigma_m$  uncertainty for this estimate.

The previously reported  $\delta^{41}\text{K}$  values of 3 CAIs (Jiang et al., 2021), also measured by MC-ICP-MS, are indistinguishable from the bulk Allende. Given the lack of petrographic description of these CAIs and unreasonably high concentrations of FeO, Na<sub>2</sub>O, and K<sub>2</sub>O in them, suggestive of contamination, we prefer not to add these data to our isochron.

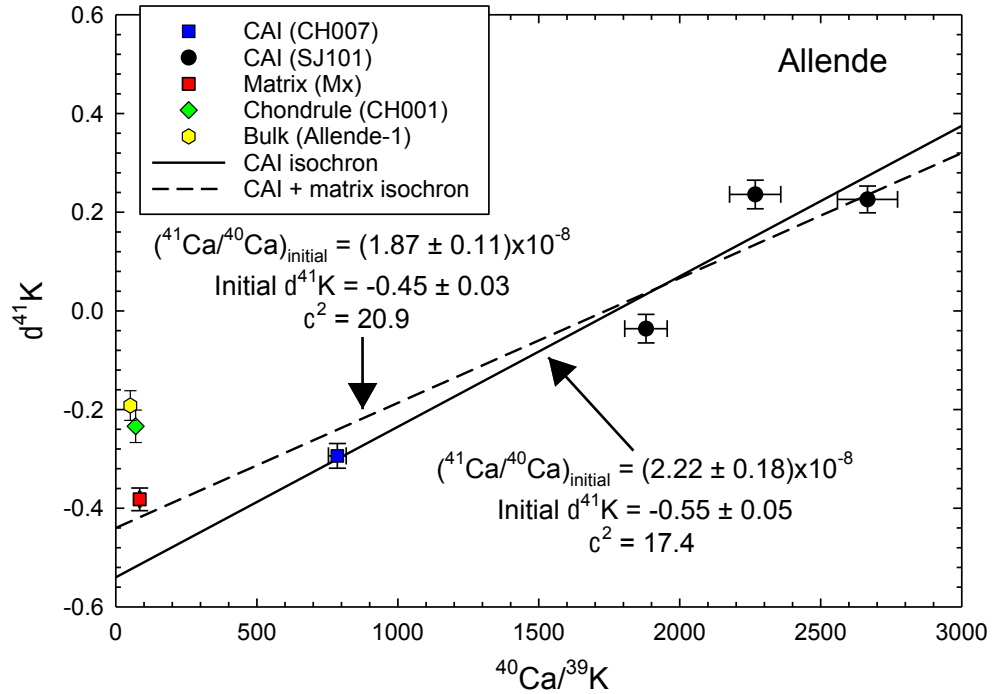


**Figure 1.  $^{41}\text{Ca}$ – $^{41}\text{K}$  fossil isochron diagram.** Four CAI fragments form a linear array that is interpreted as a fossil isochron (solid line). The solar  $(^{41}\text{Ca}/^{40}\text{Ca})_{\text{i}}$  ratio and  $\delta^{41}\text{K}$  values with two-sigma level (2SEM), uncertainties of this CAI isochron are calculated using the weighted least-squares method (Williamson, 1968). The dotted line shows a similar fit to the CAIs and matrix. The isochron provides the new estimate of the solar system  $(^{41}\text{Ca}/^{40}\text{Ca})_{\text{i}}$  ratio that is about a factor of five higher than the previous value (Liu, 2017). The chondrule and the whole rock samples plot substantially above the initial  $\delta^{41}\text{K}$  of the CAI isochron, demonstrating internal K isotope heterogeneity of the Allende meteorite. The goodness of fit is indicated by the  $\chi^2$ -value (for details see Appendix B, table 1).

**Table 1.**

K isotope composition for Allende whole rock, matrix, chondrule and 4 CAI samples.

Sample Name	Material	Weight (mg) <sup>†</sup>	K ppm <sup>‡</sup>	Ca ppm <sup>‡</sup>	<sup>40</sup> Ca/ <sup>39</sup> K <sup>§</sup>	2 $\sigma$ - <sup>40</sup> Ca/ <sup>39</sup> K	$\delta^{41}\text{K}$ (‰)	2 $\sigma$ - $\delta^{41}\text{K}$ <sup>¶</sup>	<i>N</i>	<i>n</i>
Allende-1	Bulk	172.0	337	17070	51.3	2.1	-0.192	0.030	19	116
Mx	Matrix	39.0	166	13771	84.3	3.4	-0.382	0.030	8	46
CH001	Chondrule	4.4	949	65445	69.9	2.8	-0.234	0.033	4	20
CH007	CAI	17.3	252	195201	785	31	-0.294	0.030	7	27
SJ101-A	CAI	27.1	64	118419	1880	75	-0.036	0.030	5	29
SJ101-B	CAI	29.7	49	129746	2666	107	0.226	0.030	6	24
SJ101-C	CAI	30.1	60	133475	2268	91	0.236	0.030	5	27

*N*: analytical runs on different days; *n*: total sample-standard bracket measurements from *N* days.

The  $\delta^{41}\text{K}$ -values of seawater and NIST SRM-314 standards measured relative to Suprapur are  $+0.215 \pm 0.024\text{‰}$  and  $+0.047 \pm 0.003\text{‰}$ , respectively (Ku and Jacobsen, 2020).

\*The bulk Allende-1 is based on analyses of 2 separate aliquots (Allende-1a and Allende-1b) of the Allende whole rock powder (Ku and Jacobsen, 2020).

<sup>†</sup>Weight of the dissolved sample powder.

<sup>‡</sup>Concentrations of Ca and K were measured by quadrupole ICP-MS.

<sup>§</sup>The atomic <sup>40</sup>Ca/<sup>39</sup>K ratio was calculated using IUPAC values (Meija et al., 2016a, b) for atomic weights (Ca = 40.078; K = 39.0983) and isotopic compositions (<sup>39</sup>K/<sup>total</sup>K = 0.932581 and <sup>40</sup>Ca/<sup>total</sup>Ca = 0.96941).

<sup>¶</sup>Analytical uncertainty of  $\delta^{41}\text{K}$  (2 $\sigma$ <sub>m</sub>) (relative to the Merck Suprapur KNO<sub>3</sub>; see Ku and Jacobsen, 2020) for each sample is either the calculated standard error (2SEM) or the external reproducibility, 0.030‰, whichever is larger.

## Validity of the Bulk CAI $^{41}\text{Ca}$ – $^{41}\text{K}$ Isochron

Lack of Si and Mg isotope fractionation in SJ101 (Jacobsen et al., 2008; Petaev and Jacobsen, 2009) provides clear evidence that neither SJ101 as a whole nor its precursors have experienced non-equilibrium processing involving kinetic isotope fractionation of these elements. Indeed, K, as a more volatile element than Mg and Si, could have been lost, at least partially. However, at such high temperatures the near-equilibrium isotopic fractionation of K, if it has occurred, is very small and likely negligible (more discussion in Appendix B). The melilite mantles in Type B1 CAIs like CH007 are typically interpreted as evidence of evaporative loss of Si and Mg during earlier stages of CAI crystallization before the mantles seal off the interiors. Such a loss is expected to induce kinetic isotope fractionation, which has not been found in two CAIs studied in detail by Bullock et al. (2013). Even if such kinetic evaporation occurred, it would make the K isotope composition of CH007 heavier than that of SJ101. However, CH007 is lighter than SJ101 so this effectively rules out derivation of the K isotopic composition of CH007 from that of SBJ101. Theoretically, heavier K isotopic composition of SBJ101 can be explained by a non-equilibrium evaporative loss of K from CH007, but the depletion of SBJ101 in refractory Ca, Al and Ti along with the enrichment in moderately volatile Mg and Si relative to CH007 rules out such a formation scenario. Therefore, the overall positive correlation between  $\delta^{41}\text{K}$  and  $^{40}\text{Ca}/^{39}\text{K}$  ratios is unlikely to be a result of a mass-dependent K isotope fractionation.

A two-component mixing model between matrix and CAIs (Fig. 2) also fails to reproduce the linear  $\delta^{41}\text{K}$ –Ca/K correlation. For instance, the matrix as an end member of the  $\delta^{41}\text{K}$ –Ca/K array (Fig. 1) deviates strongly from the mixing arrays in the  $\delta^{41}\text{K}$ –Mn/K and  $\delta^{41}\text{K}$ –Cr/K plots. Moreover, the detailed and thorough investigation of SJ101 (Petaev and Jacobsen, 2009) shows only miniscule patches of matrix attached to its exterior and a lack of such material inside. This

effectively rules out matrix contamination of the SJ101 interior fragments used in this study. The images of CH007 (Appendix B, Fig. 3) do show some matrix loosely attached to the inclusion. It is unclear how much matrix has left after fragmentation and sonication of the sample, but its contribution to the dissolved sample can be accessed from the concentrations of highly volatile elements (*e.g.*, Pb and Tl), which are enriched in the matrix by factors of  $\sim 28$  and  $\sim 27$ , respectively. Assuming all Pb and Tl in CH007 are from matrix (Appendix B, table 2), the maximum contribution from matrix is only 3.7 wt%. Since the matrix-free samples of SJ101 also contain Pb and Tl at  $\sim 0.5 \times$  CH007 levels, the matrix contribution to CH007 must be  $\sim 2$  wt% or less. The effect of such a small addition of matrix on either the K isotopic composition or the K/Ca ratio of the CH007 CAI is less than the analytical uncertainty.

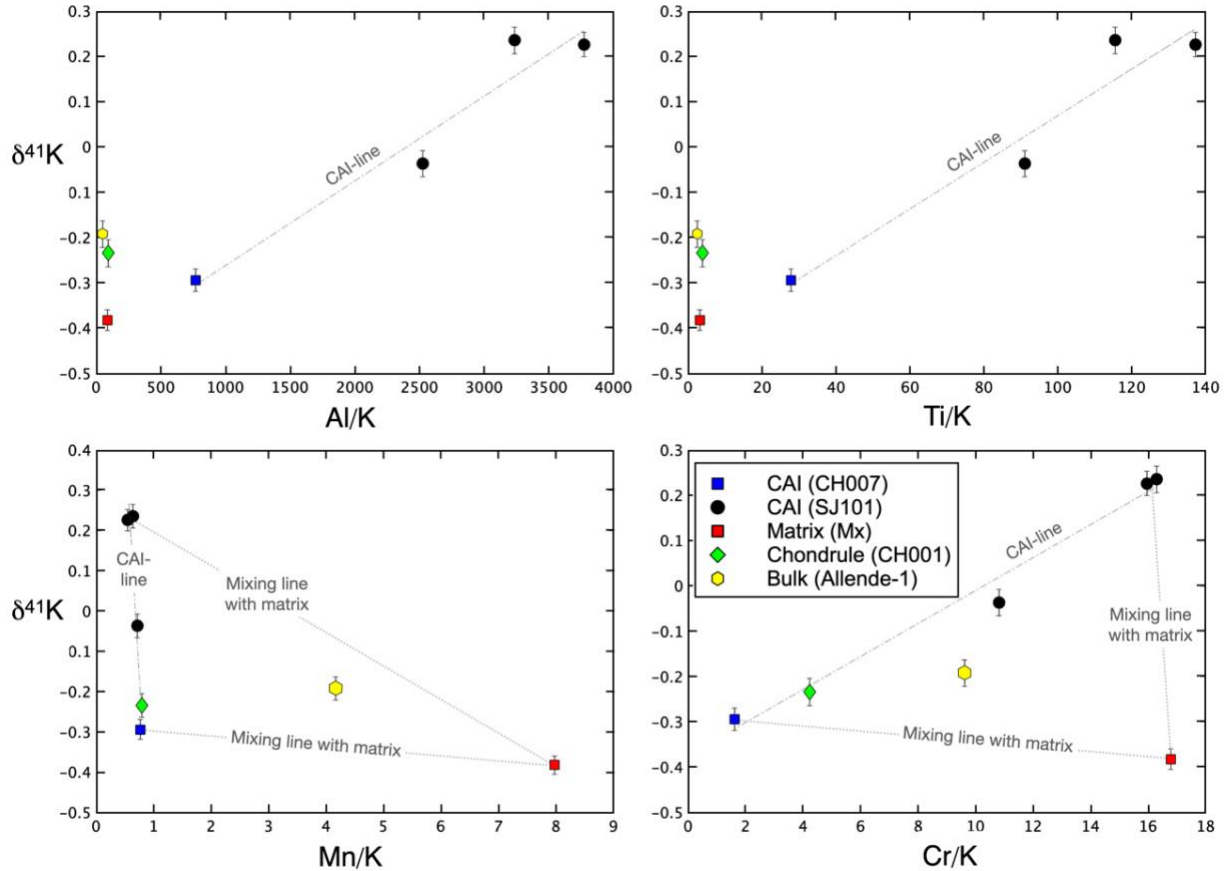


**Figure 2. Matrix-CAI mixing relationships.** Two-component mixing yields straight lines in these diagrams. Aluminum (Al) and Ti are refractory elements, and Mn and Cr are moderately volatile elements, but slightly more refractory than K. The plots of  $\delta^{41}\text{K}$  versus ratios of refractory elements to K show similar patterns to that of  $\delta^{41}\text{K}$ – Ca/K isochron (Fig. 1), meaning that all refractory elements (Ca, Al, and Ti) behave coherently. In contrast, the plots of  $\delta^{41}\text{K}$  versus ratios of moderately volatile elements (Mn and Cr) to K show different patterns, implying that the linear relationship in the isochron diagram between matrix and CAIs cannot be the result of a simple 2-component mixing of matrix and CAIs. Therefore, the linear correlation between  $\delta^{41}\text{K}$  and  $^{40}\text{Ca}/^{39}\text{K}$  suggests that the excesses in  $^{41}\text{K}$  in the samples studied are due to  $^{41}\text{Ca}$  decay, so the observed correlation is an isochron. Concentrations listed in Appendix B, table 2.



Another process that could have affected both the K isotopic compositions and the K/Ca ratios of the samples studied is the interaction of these objects with each other via an aqueous fluid circulated on the CV chondrite parent body. The recent study of secondary aqueous alteration of Allende CAIs (*e.g.*, Krot et al. 2021) shows that during the alteration Si, Na, Cl, K, Fe, S, and Ni could be added to, while Ca, Mg, and some Al could be removed from the host inclusions to a various degree. Such an alteration typically affects only melilite and anorthite; it is highly localized and never extends to a whole inclusion. Our detailed study of SJ101 (Petaev and Jacobsen, 2009) detected only a few grains of melilite partially replaced by grossular, monticellite, and rare wollastonite. Minute euhedral grains of andradite were observed in voids. The lack of Na-rich phases among alteration products implies that no Na, and, most likely, no K were added. Additionally, Sr, a very mobile elements during aqueous alteration, show coherent concentrations with other refractory elements across all SJ101 chips. The lack of Sr concentration anomalies demonstrates that aqueous alteration could only have a minor effect in these samples (Appendix B, Fig. 4). However, both CH001 and CH007 (Appendix B, Fig. 2-3) provide clear mineralogical evidence of metasomatic reactions of their peripheral portions with an aqueous fluid containing Na, Cl, K, Si, Fe, Mg, Mn, Ca and, perhaps, other chemical elements. Among them, K, Ca, Na and Cl are of particular interest because the first two elements directly affect the  $\delta^{41}\text{K}-^{40}\text{Ca}/^{39}\text{K}$  correlation while Na and Cl are excellent tracers of the extent of alteration. Si, Na, and Cl have been added to and Ca removed from both CH001 and CH007, resulting in substitution of anorthite (CH001) and melilite (CH007) by sodalite and nepheline. The fate of K is different – its concentration is markedly increased in the altered areas of CH001 where some nepheline grains contain up to ~1.5 wt% K<sub>2</sub>O, but the K distribution in the K<sub>K $\alpha$</sub>  X-ray map of CH007 is homogenous throughout the whole sample, regardless of the Na and Cl distributions. Also, the EDS point

analyses of alteration phases in CH007 do not detect K. The bulk Na/K ratio in CH007 (~26) is markedly higher than that in other samples (ranges from 15 to 18), suggesting that the aqueous alteration did not add much K to CH007. Thus, it appears that most of the K in CH007 is indigenous.

We interpret the scatter of data points along the isochron as a result of initial sample heterogeneity that is perhaps not surprising for a nuclide ( $^{41}\text{Ca}$ ) with such a short half-life. Since neither thermal and chemical processing nor two-component mixing can account for the observed linear relationship between the  $\delta^{41}\text{K}$  excesses and  $^{40}\text{Ca}/^{39}\text{K}$  ratios, we prefer to interpret this linear correlation as an isochron due to  $^{41}\text{Ca}$  decay.

Our  $(^{41}\text{Ca}/^{40}\text{Ca})_{\text{I}}$  ratio for the solar system of  $2.22 \times 10^{-8}$  is about 5 times higher than the previous value of  $4.6 \times 10^{-9}$  inferred from SIMS measurements (Liu, 2017). The latter study was able to analyze samples with an extremely wide range of Ca/K ratios ( $10^3$  to  $10^6$ ) on a micro-scale. However, since the precision of the SIMS measurements was low (uncertainties exceeding 70%), isobaric interferences with other species could result in a false correlation in a fossil isochron diagram (such an example for the  $^{60}\text{Fe}$ – $^{60}\text{Ni}$  system is discussed by Trappitsch et al. (2018)). In addition, the resultant  $^{41}\text{K}/^{39}\text{K}$ – $^{40}\text{Ca}/^{39}\text{K}$  correlation and its slope heavily rely on very few points with extremely low K. Such analytical challenges are likely the main cause of the large variations in the  $(^{41}\text{Ca}/^{40}\text{Ca})_{\text{I}}$  ratios (from  $1.4 \times 10^{-8}$  to  $4.2 \times 10^{-9}$ ) among published mineral isochrons (Srinivasan et al., 1996; Sahijpal et al., 2000; Ito et al., 2006; Liu et al., 2012; Liu, 2017). Moreover, the mineral isochrons themselves could also reflect resetting by the multiple events in many CAIs. On the other hand, the MC-ICP-MS technique removes such isobaric interferences by analyzing chemically separated high purity K solutions. The precision of such isotope ratio measurements is very high (0.030‰). However, the MC-ICP-MS technique requires larger

samples, and measurements are very challenging for bulk samples with extremely high Ca and low K concentrations ( $^{40}\text{Ca}/^{39}\text{K} > 5000$ ).

### **CAI Processing Interval**

Previously, the  $(^{41}\text{Ca}/^{40}\text{Ca})_I$  ratio for the solar system was established by SIMS analyses of a few CAIs (Appendix B, table 4). The discrepancy of  $(^{41}\text{Ca}/^{40}\text{Ca})_I$  ratios between the SIMS and our MC-ICP-MS studies likely results from the differences between the bulk and mineral isochrons, which date the initial closure of the  $^{41}\text{Ca}$ – $^{41}\text{K}$  system of a whole CAI and subsequent disturbances, respectively. The mineral isochrons for the Type B1 E65 and Type A NWA 3118 1N-b CAIs are different, with both having lower  $^{41}\text{Ca}/^{40}\text{Ca}$  ratios (Liu et al., 2012; Liu, 2017) than our bulk Type B CAI isochron. The existence of two distinct  $^{41}\text{Ca}$  reservoirs for type-A and type-B CAIs is inconsistent with the  $\delta^{26}\text{Mg}$  isotope data (MacPherson et al., 2017) revealing no temporal evolutionary sequence among CAIs of different types. This means that the younger ages with lower  $(^{41}\text{Ca}/^{40}\text{Ca})_I$  ratios inferred from mineral isochrons, which date the last mineral re-equilibration events, probably reflect nebular processing of CAIs. Specifically, the mineral  $^{41}\text{Ca}$ – $^{41}\text{K}$  isochrons of (Liu et al., 2012; Liu, 2017) are  $\sim 0.4$  Ma younger than our bulk CAI isochron; this time difference likely corresponds to an interval of CAI processing after the  $^{41}\text{Ca}$ – $^{41}\text{K}$  closure age determined by the bulk CAI isochron.

A similar CAI processing interval of 0.2 Ma was used by MacPherson et al. (2017) to explain the variations of  $(^{26}\text{Al}/^{27}\text{Al})_I$  ratios among 25 CAI mineral isochrons relative to the bulk CAI isochron. A combination of  $^{41}\text{Ca}$ – $^{41}\text{K}$  and  $^{26}\text{Al}$ – $^{26}\text{Mg}$  extinct systems extends the CAI processing interval (Fig. 3) to  $\sim 0.26$  Ma when considering the large uncertainty of the E65  $(^{26}\text{Al}/^{27}\text{Al})_I$  ratio.

### **Origin and Nucleosynthetic Injection of $^{41}\text{Ca}$**

The SJ101 mineral  $^{26}\text{Al}$ - $^{26}\text{Mg}$  isochron (MacPherson et al., 2017) yields an age and a  $(^{26}\text{Al}/^{27}\text{Al})_{\text{I}}$  ratio indistinguishable from the bulk  $^{26}\text{Al}$ - $^{26}\text{Mg}$  Allende CAI isochron (Jacobsen et al., 2008), implying that SJ101 experienced very little or no mineral disturbances after its initial formation. This suggests that the inferred  $(^{41}\text{Ca}/^{40}\text{Ca})_{\text{I}}$  and  $(^{26}\text{Al}/^{27}\text{Al})_{\text{I}}$  ratios of SJ101 currently provide the best estimate of the initial abundances of  $^{41}\text{Ca}$  and  $^{26}\text{Al}$  in the solar system.

The  $^{41}\text{Ca}$  in the solar system could have been produced by *in-situ* irradiation in the early solar nebula or could have been delivered by stellar nucleosynthetic injections from outside the solar nebula. The former, involving nuclear reactions with energetic protons and alpha particles, could result in local  $^{41}\text{Ca}$  heterogeneity in the solar nebula (Lee et al., 1998), as is the case of  $^{10}\text{Be}$ . However, the calculated production rates of  $^{41}\text{Ca}$  and  $^{10}\text{Be}$  by irradiation have failed to match the relative abundances of both nuclides (Liu et al., 2012; Liu, 2017). On the other hand, higher  $(^{41}\text{Ca}/^{40}\text{Ca})_{\text{I}}$  and  $(^{26}\text{Al}/^{27}\text{Al})_{\text{I}}$  ratios in CAIs inferred from the bulk  $^{41}\text{Ca}$ - $^{41}\text{K}$  and  $^{26}\text{Al}$ - $^{26}\text{Mg}$  isochrons likely point to a similar origin of  $^{41}\text{Ca}$  and  $^{26}\text{Al}$ , perhaps by a stellar s-process.

Pollution of the protosolar molecular cloud by freshly produced nuclides injected by shock waves from supernova explosions, AGB or Wolf-Rayet star winds, is the main working hypothesis, which is used to explain the higher abundances of the shortest-lived extinct nuclides in the solar system relative to the galactic background (Appendix B, table 5). For example, the  $(^{26}\text{Al}/^{27}\text{Al})_{\text{I}}$  ratio of  $(5.23 \pm 0.13) \times 10^{-5}$  for the solar system is more than three orders of magnitude higher than that of the protosolar molecular cloud ( $1.1 \times 10^{-8}$ , Appendix B, table 6). The new solar system  $(^{41}\text{Ca}/^{40}\text{Ca})_{\text{I}}$  of  $(2.22 \pm 0.18) \times 10^{-8}$  is also about three orders of magnitude higher than that of the molecular cloud ( $4 \times 10^{-11}$ , Appendix B, table 6). Clearly, the inferred concentrations of both  $^{41}\text{Ca}$  and  $^{26}\text{Al}$  in CAIs require late injection(s) from outside the protosolar molecular cloud.

The constraints on timing of such injections are dependent on the initial solar system abundances and nucleosynthetic sources of injections. As discussed above, the initial  $(^{41}\text{Ca}/^{40}\text{Ca})_i$  and  $(^{26}\text{Al}/^{27}\text{Al})_i$  ratios of the solar system are defined by the bulk CAI (not mineral) isochrons. Then, by tracing the closed-system evolution of both isotope systems back in time and comparing the calculated values with those modeled for TP-AGB stars, Type II supernova (Wasserburg et al., 2006), and Wolf-Rayet stars (Young, 2014) one can estimate the time of injection for each nucleosynthetic source (Fig. 3b). This time ranges from 0.60 Ma for a 60 solar mass ( $M_\odot$ ) Wolf-Rayet star to 0.85–1.05 Ma for a low mass ( $1.5 M_\odot$ – $2 M_\odot$ ) AGB star or  $\sim 1.45$  Ma for a  $15 M_\odot$  Type II supernova.

Theoretical predictions and astrophysical observations demonstrate the plausibility of the triggered formation of the solar system, known as a rapid collapse of the protosolar molecular cloud (Hartmann et al., 2012; Dale, 2015). If the majority of both  $^{41}\text{Ca}$  and  $^{26}\text{Al}$  is due to a late injection, then the well-determined initial abundance of both nuclides places an upper limit on the time span between the collapse of the protosolar molecular cloud and the formation of the solar system. Among the three possible sources mentioned above, a supernova injection is currently inconsistent with the low abundance of  $^{60}\text{Fe}$  in solar system materials (Trappitsch et al., 2018). Thus, the event that might have triggered the collapse of the parental molecular cloud would have taken place between 0.6 and 1.0 Ma before CAI formation, implying a very short timescale of formation for our Sun.

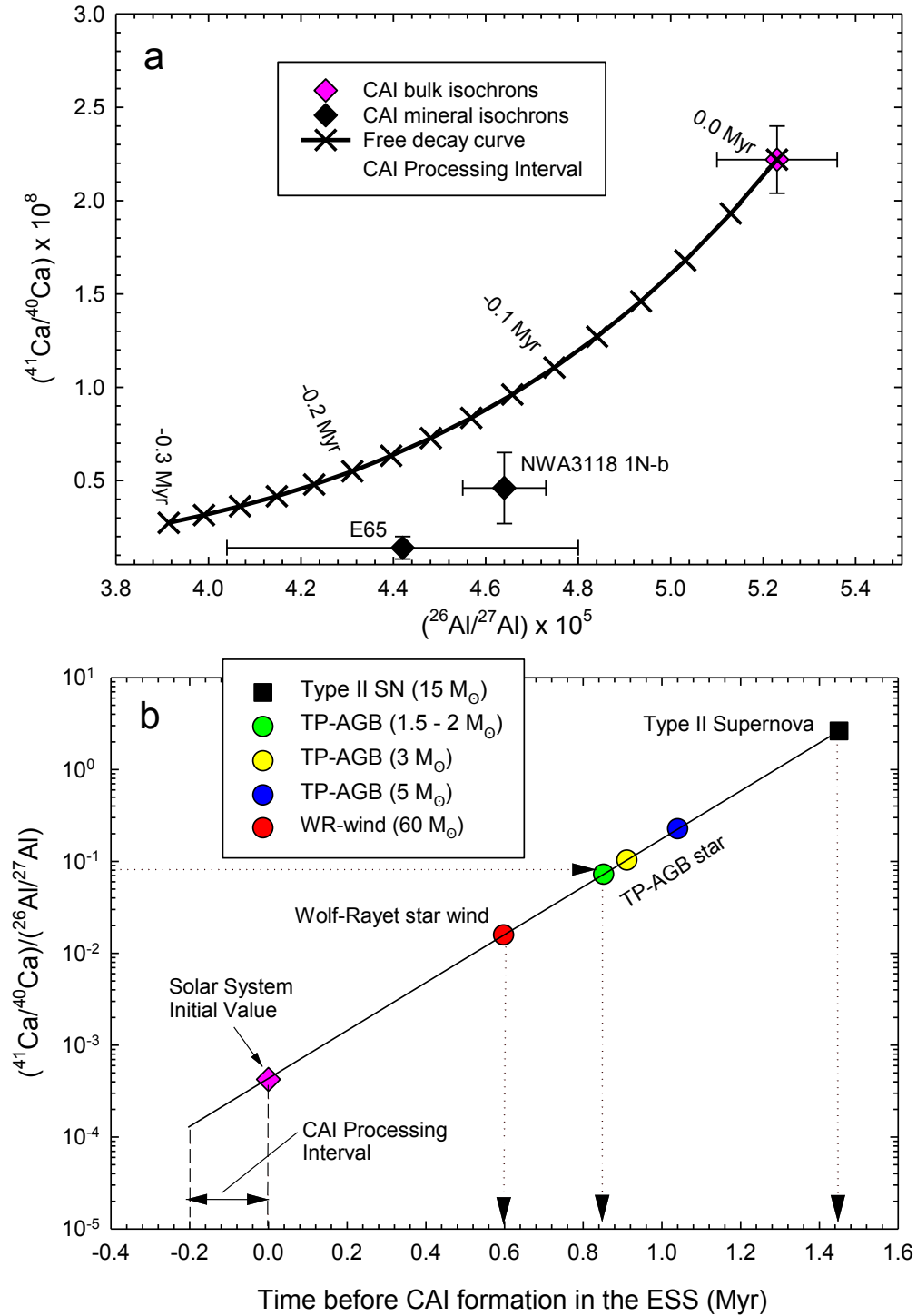


**Figure 3.**  $^{41}\text{Ca}$  and  $^{26}\text{Al}$  constraints on early solar system chronology. (a) Comparison of  $^{41}\text{Ca}/^{40}\text{Ca}$  and  $^{26}\text{Al}/^{27}\text{Al}$  bulk CAI (this study), and mineral isochrons. The mineral isochrons are from E65 (Efremovka) (Liu et al., 2012; Srinivasan and Chaussidon, 2013), and NWA 3118 #1Nb

(MacPherson et al., 2013; Liu, 2017). Our new estimate of  $(^{41}\text{Ca}/^{40}\text{Ca})_i$  is consistent with the  $(^{26}\text{Al}/^{27}\text{Al})_i$  results (Jacobsen et al., 2008), with both showing higher initial values of bulk CAI isochrons than those of mineral isochrons. The age difference between the bulk CAI and mineral isochrons is likely caused by CAI processing after their formation. Combining two extinct isochrons yields  $\sim 0.26$  Ma interval as the best estimate of CAI processing time for these 3 samples. This interval is consistent with the total 0.2 Ma timespan inferred from the  $^{26}\text{Al}$ – $^{26}\text{Mg}$  mineral isochrons of 25 CAI samples. Note, that time runs backward, *i.e.* younger events are negative while the older events, pre-dating CAI formation, are positive relative to the  $t_0$ , the CAI formation time represented by the bulk CAI isochrons. (b) Evolution of the  $(^{41}\text{Ca}/^{40}\text{Ca})/(^{26}\text{Al}/^{27}\text{Al})$  ratio with time before CAI formation. The slope of the line is defined by the mean lives of  $^{41}\text{Ca}$  (0.1434 Ma) and  $^{26}\text{Al}$  (1.035 Ma), while its position is tied to the solar system initial values reported here and in the literature (Jacobsen et al., 2008). The  $(^{41}\text{Ca}/^{40}\text{Ca})/(^{26}\text{Al}/^{27}\text{Al})$  values for different stellar sources – AGB stars, Type II supernovae (Wasserburg et al., 2006) and Wolf-Rayet stars (Young, 2014). The dashed arrowed lines show the times of injection into the protosolar molecular cloud. The numbers before  $M_\odot$  symbols are stellar masses relative to the Sun’s mass. The estimated injection times range from 0.6 Ma for  $60 M_\odot$  Wolf-Rayet stars, 0.85 to 1.04 Ma for  $1.5 - 5 M_\odot$  TP-AGB stars to 1.45 Ma for a  $15 M_\odot$  Type II supernova. Data and references are listed in Appendix B, tables 4-5.

## Chapter 4

### **Potassium isotopic composition of chondritic components from the Allende (CV3), Ochansk (H4), Saratobv (L4) and Elenovka (L5) chondrites**

This chapter will be submitted to the *Geochimica et Cosmochimica Acta*.

#### **Abstract**

Chondrules, formerly silicate melt droplets, are believed to have experienced a certain degree of heat processing during their formation. Nevertheless, their volatile depletion pattern of chemical fractionation is not accompanied by the large isotopic fractionation expected of low-pressure nebular environments. A notable example of this behavior occurs for the moderately volatile element, potassium (K). However, measurements of the K isotopic composition for each of the major silicate chondritic components are currently very limited. Here, we report high precision K isotope data for various types and sizes of the major chondrite components, matrix and chondrules, from the Allende (CV3), Ochansk (H4), Saratobv (L4) and Elenovka (L5) chondrites. During the course of this investigation, the individual chondrules were carefully examined and imaged using SEM/EPMA techniques before dissolution processes was performed for chemical and isotopic analysis. While previous studies attributed the observed  $\delta^{41}\text{K}$  variations of chondrules to parent body alteration, the current measurements allow us to further constrain the processes which affected K isotope fractionation within the different chondritic components in both the solar nebula and meteorite parent body environments. The measured  $\delta^{41}\text{K}$  values range from  $-0.113\%$  to  $-0.355\%$  (2SE =  $0.030\%$ ) in Allende chondrules, with the exception of one chondrule, and they range from  $-0.382\%$  to  $-0.330\%$  in Allende matrix. No systematic trend was observed in the  $\delta^{41}\text{K}$



values between the aqueous altered and unaltered chondrules, implying that aqueous alteration does not affect  $\delta^{41}\text{K}$  to any significant degree in Allende meteorites. The  $\delta^{41}\text{K}$  values in the three ordinary chondrites range from  $-0.356\text{‰}$  to  $-0.722\text{‰}$  and  $-0.433\text{‰}$  to  $-0.960\text{‰}$  for chondrules and matrix, respectively. While no direct correlation between  $\delta^{41}\text{K}$  and the degree of metamorphism (petrologic type) can be drawn, impact brecciation seems to be the most likely explanation for the nearly  $\sim 0.5\text{‰}$  magnitude of fractionation in the dark components of an impact breccia sample, Ochansk. Overall, we find no direct relationship between the  $\delta^{41}\text{K}$  values in chondrules and the chondrule size or type. Nor do we observe any correlation between  $\delta^{41}\text{K}$  and K depletion. Importantly, while parent bodies processes may cause a minor degree of scatter in the K isotope composition, none of these processes show systematic trends or direct, observable effects in the  $\delta^{41}\text{K}$  values, suggesting that the variation in  $\delta^{41}\text{K}$  from various chondritic components mostly likely reflects the heterogeneity of the samples.

## **Introduction**

Chondritic meteorites are the key to understanding the evolution of the early solar nebula and the formation of the building blocks of the terrestrial planets. The chondrites are composed of four major components: metallic Fe-Ni, chondrules, matrix, and refractory inclusions. Some of the latter are named CAIs: Ca-Al rich inclusions. Matrix is a fine-grained material consisting of everything which cements the other components together. Minor components of Fe oxides and sulfides, carbonates, sulfates, or even organic matter are also often found in some matrix. Chondrules are sub-millimeter- to centimeter-sized silicate spherules with different textures, indicative of the dis-equilibrium crystallization of silicate melts. They comprise roughly 30 to 80 vol.% of chondrites, with the exception of CI chondrites (Lauretta et al., 2006). The texture and mineralogy of chondrules, as well as their isotope composition, provide constraints on the

conditions of their formation during the earliest transit heating events in the nebula. While the elemental and isotopic compositions of matrix and chondrules from various types of chondrites have been investigated previously (Jones, 2012), both the chondrule formation mechanisms and the relationship between chondrules and matrix are still not well understood and remain highly debated. One of the major unresolved issues is why the observed volatility-based pattern of chemical fractionation is not accompanied by the large isotopic fractionation which is expected for superheated molten silicate droplets suspended in the nebular gas at low pressures. Furthermore, the question of whether chondrules experienced evaporation during heating and subsequent re-condensation during cooling, and whether such evaporation and condensation processes (or thermal processes in general) occurred under equilibrium or dis-equilibrium conditions, remains uncertain.

To identify the possible formation mechanisms and conditions for the chondrules, precise measurements of both the chemical concentration and isotopic compositions of potassium (K) are essential. This is because of potassium's volatility at high temperatures and its mobility within low temperature environments: from the isotopic ratios of the two K isotopes,  $^{41}\text{K}$  and  $^{39}\text{K}$ , one can potentially discern thermal events that fractionated the K isotopes under dis-equilibrium conditions (*i.e.*, vaporization and condensation), as well as parent body alteration. Previous analyses of K isotopes for individual chondrules from the Semarkona LL3.0 chondrite by in situ SIMS (secondary-ionization mass spectrometry) showed a wide range of  $\delta^{41}\text{K}$  values from  $-10\%$  to  $18\%$  (Alexander and Grossman, 2005), which was found to be unrelated to Rayleigh-type loss of K. Recent higher precision studies of the K isotopic compositions of chondrules and matrices from the ordinary chondrite Hamlet (LL4) (Koefoed et al., 2020) and the carbonaceous chondrite Allende (CV3) (Jiang et al., 2021), which were performed using multi-collector inductively

coupled plasma mass spectrometry (MC-ICP-MS), found rather narrow ranges of K isotope variations. Such behavior is also inconsistent with Rayleigh-type loss of K. Instead, it was suggested that these variations are due to secondary parent body alteration. However, no petrographic or chemical evidence was provided to support the claims of aqueous alteration. Because the reported  $\delta^{41}\text{K}$  values were based on just single measurements, given the very low concentration of K in some chondrules and the small sample sizes utilized in those studies, the wide range of  $\delta^{41}\text{K}$  variations previously observed in chondrules may reflect inadequate reproducibility of the isotope analyses. Additionally, a new study reported both K and Rb isotope data in the bulk carbonaceous meteorites, and it claims that the correlation between  $\delta^{41}\text{K}$  and  $\delta^{87}\text{Rb}$  is best explained by a binary mixing between CI-like matrix and chondrule components (Nie et al., 2021). However, such models are based on theoretical calculations and no individual chondrules nor matrix was analyzed for the  $\delta^{41}\text{K}$  and  $\delta^{87}\text{Rb}$  values. Therefore, it is very important to further constrain the K isotopic compositions of chondrules and matrix in both carbonaceous and ordinary chondrites, and re-evaluate the existing models.

Here, we report mineralogical compositions, chemical compositions, and K isotope data for the major chondrite components in order to investigate if there are K isotopic fractionations between components. Furthermore, we examine whether such fractionations are correlated with elemental fractionations caused by thermal processing during their formation or during secondary parent-body processes such as aqueous alteration or impact events.

## **Samples**

We analyzed 9 chondrules (CH001-010) and 3 matrix samples (SF001-003) with different grain sizes from Allende (CV3<sub>ox</sub>); 1 matrix sample (Mur-Mx) from Murchison (CM2); 7 chondrules (ch#1-4, ch#11-13) and 2 matrix samples with (N1826-Mx1) and without (N1826-

Mx2) tiny chondrules from Elenovka (L5); 2 chondrules (ch#5-6) and a homogeneous matrix sample (N311-Mx) from Saratov (L4); 4 chondrules (ch#7-10) and 2 matrix samples of dark (N75-Mx) and light (N76-Mx) lithologies from Ochansk (H4). All chondrule samples were studied by SEM/EPMA techniques to classify them and evaluate K concentrations before the isotope work. The large chondrules were cast into epoxy resin and then sliced off-center; smaller and larger parts were used for SEM/EPMA and isotope studies, respectively. Smaller chondrules or their fragments, formed by gentle crushing, were mounted on a glass slide using thick carbon paint for SEM/EDS studies and later, after a thorough cleaning, dissolved for isotope studies. The sample numbers and weights as well as chondrule types are listed in tables 1 and 2; the trace element concentrations are reported in the Appendix C.

### **Carbonaceous chondrites**

*Allende:* The samples of the Allende matrix were prepared by sequential sieving of the 43 g sample fragmented by the SELFRAG Company. The matrix grain sizes range from 44 to 150  $\mu\text{m}$ . The Allende chondrules were collected over years from different samples by the late Dr. Ursula B. Marvin who transferred them to one of us upon her retirement. Three large chondrules (CH001, CH002, and CH003) were sliced, with the CH001 slice having been polished. Other chondrules or their fragments were studied as chunks.

*Murchison:* ~ 2 g bulk specimen was received from the Field Museum, Chicago. After gentle crushing of the specimen, several chondrules intergrown with matrix were selected as potential samples for K isotope studies, but the SEM/EDS studies revealed very low total amounts of K insufficient for precise isotope analyses. Therefore, only a matrix sample without visible chondrules was selected for the K isotope work.

### **Ordinary chondrites**

All samples of ordinary chondrites were separated from large specimens and macroscopically and microscopically (Ochansk) described at the Vernadsky Institute and then further processed at Harvard.

*Elenovka*: The two matrix samples were collected from the specimen #1826. The sample #1826-Mx1 consists of small matrix chunks intergrown with tiny chondrules. The sample N1826-Mx2 is a well-averaged mixture of matrix silicate grains of <100 microns in size. All 7 chondrules were picked up from the specimen N1836. Four large chondrules (ch#1-4) were sliced, others were studied intact (Fig. 2).

*Saratov*: The matrix sample (#311-Mx) consists of small matrix chips devoid of large chondrules. Two chondrules (ch#5-6) were sliced, with the ch#5 slice having being polished to reveal its fine texture (Fig. 2).

*Ochansk*: While the samples of this meteorite were subject of several recent studies (*e.g.*, Osadchii et al., 2017; Bakhtin et al., 2017; Stenzel et al., 2017), its petrographic description is rather scarce and sketchy (Zavaritskiy and Kvasha, 1952; Yudin and Smyshlyaev, 1963; Horejsi, 2012). All authors point to its brecciated texture defined by intermixed fragments of dark and light lithologies and the presence of macroscopic smooth surfaces reminiscent of slippage plains, but there is no description of petrologic difference between the two lithologies. In several thin sections examined by us, the boundaries between the light and dark clasts are typically irregular and sharp (Fig. 3); only in one thin section the light and dark lithologies are separated by a clear fracture, which can be interpreted as a slippage plane. The main difference between the two lithologies is the distribution of opaque minerals and the degree of shock metamorphism experienced by silicate minerals. In the dark lithology, numerous tiny grains of troilite and Fe-Ni metal are homogeneously distributed in the matrix, and olivine grains exhibit weak mosaic extinction, and

planar fractures consistent with the shock stage S2-3 (mainly S2). In the light lithology, olivine grains show sharp extinction and lack planar features, indicative of the shock stage S1; troilite and Fe-Ni metal occur as relatively large grains in the matrix. Other petrographic characteristics of two lithologies such as size distribution of chondrules and mineral fragments, chondrule types, *etc.* seem to be identical and typical of H chondrites.

The samples representing the dark (#75-Mx, ch#7 and ch#9) and light (#76-Mx, ch#8 and ch#10) lithologies were selected from the specimens #75 and #76, respectively. All chondrules are rather small and were studied intact (Fig. 2).

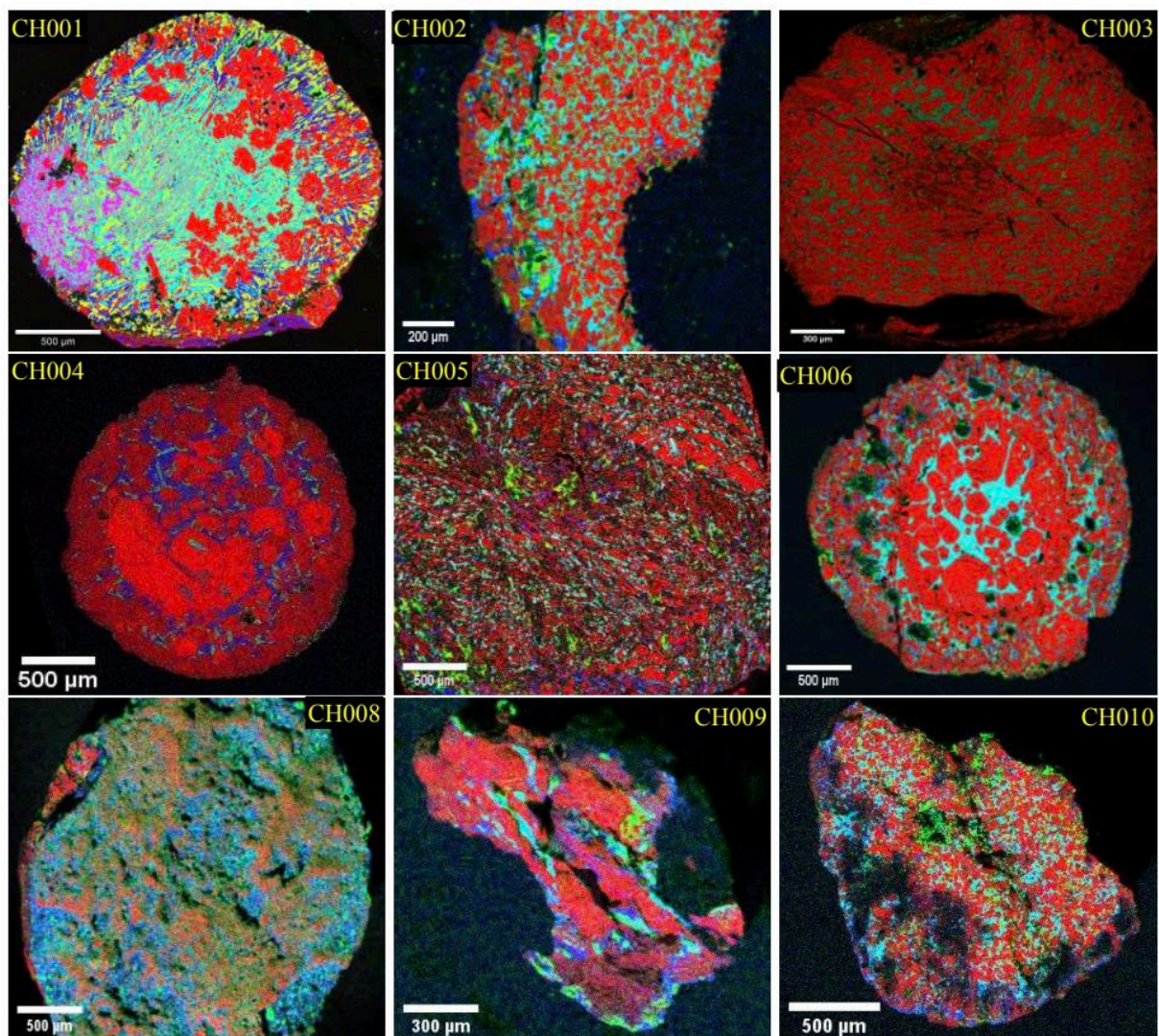
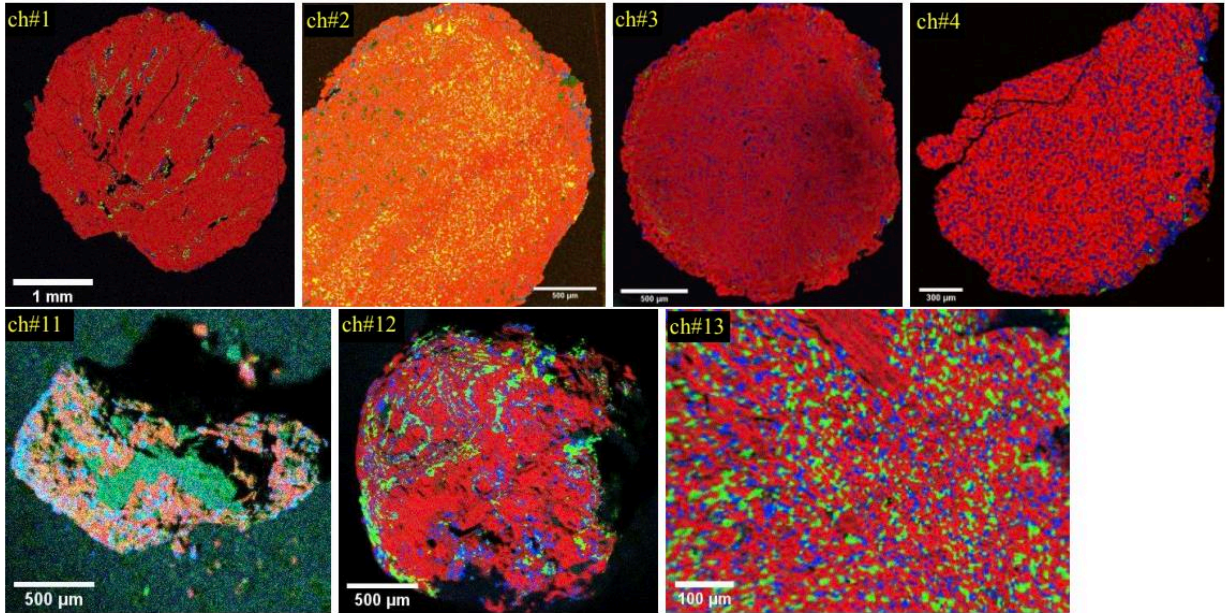


Figure 1. The combined elemental maps of Allende chondrules, Mg (red), Ca (green), and Al (blue)  $K_{\alpha}$  X-rays.





**Figure 2.** The combined elemental maps of Ordinary chondrules of Elenovka, Mg (red), Ca (green), and Al (blue)  $K_{\alpha}$  X-rays.



**Figure 3.** Thin section of an ordinary chondrite, Ochansk. A sharp irregular boundary between light and dark lithologies in transmitted light. The section size is 25 × 45 mm.



## **Analytical Methods**

### **SEM/EPMA Studies**

The chondrule chunks and slices were imaged and analyzed by the SEM/EPMA techniques using the JXA-8230 electron microprobe at Harvard University equipped with four WDS and one EDS spectrometers. All samples were lightly carbon-coated. The samples with uneven surfaces (chunks) were imaged and analyzed by the EDS system controlled by the PC-SEM software, while the slices, both polished and unpolished, were studied by the combined EDS/WDS spectrometry controlled by the PC-EPMA. The accelerating voltage and beam current varied from 10 to 25 kV and 5 to 100 nA, respectively. The mineral compositions were measured by either standardless EDS or standardized WDS techniques, both applying the ZAF correction procedures. The WDS analyses were calibrated using well-known mineral standards used in this laboratory (Petaev and Jacobsen, 2009). In the case of standardless EDS, the mineral stoichiometry was used as a measure of the analysis quality. The EDS and WDS analyses of the same mineral grains in polished samples (CH001 and ch#5) yielded nearly identical results.

### **Sample Dissolution**

Chondrule, matrix and CAI separates were gently crushed using a sapphire ( $\text{Al}_2\text{O}_3$ ) mortar and pestle. Aliquots of sample powders were weighed (Table 1), and transferred to 30 mL Savillex PFA beakers. After addition of acid mixtures (0.5 mL HF + 2 mL  $\text{HNO}_3$  + 1 mL HCl), the capped beakers were heated at 160°C on a hotplate for a day. The resulting solutions were dried down, and a mixture of 2 mL  $\text{HNO}_3$ , 6 mL HCl, and 1 mL  $\text{H}_2\text{O}$  was added to each sample for the second dissolution step. Then the beakers were placed into Teflon coated EasyPrep vessels for high-temperature and high-pressure applications in a CEM MARS 6 microwave digestion system. The

samples were heated repeatedly to 210°C for 30 minutes until the samples were completely dissolved. After dry-down, the samples were re-dissolved in 0.5 N HNO<sub>3</sub>.

Concentrations of both major and trace elements in aliquots of each sample were measured by a Thermo Scientific quadrupole ICP-MS (iCAP TQ). The remaining solutions were passed through Quartz-glass ion-exchange chromatography columns filled with Bio-Rad AG50-X8 (100-200 mesh) ion-exchange resin to separate K. This step was repeated up to three times to ensure that the K cuts are purified (>99%). The collected K solutions were dried down and re-dissolved in dilute 0.32 Normality HNO<sub>3</sub> for K isotope analyses.

### **Potassium Isotope Analyses**

The K isotopes were measured at Harvard University by the multi-collector ICP-MS *Nu Sapphire* equipped with a dual (high- or low-energy) ion path. In this work, we used the low-energy path and a hexapole collision cell to eliminate mass interferences from the Ar-bearing ions, ArH<sup>+</sup>, Ar<sup>+</sup>, and ArO<sup>+</sup> (technical details can be found in Moynier et al., 2021). An Elemental Scientific Apex Omega desolvating nebulizer was used as a sample introductory system for dry plasma usage. Additional details of instrumental setup and operation are provided in the previous study (Ku and Jacobsen, 2020).

The potassium isotope ratios were determined by the standard-sample bracketing method, and were measured relative to a lab standard prepared from a batch of Merck KgaA high-purity KNO<sub>3</sub> (labeled “Suprapur”). Data are reported in delta notation relative to this standard:

$$\delta^{41}\text{K} = \left( \frac{(^{41}\text{K}/^{39}\text{K})_{\text{sample}}}{(^{41}\text{K}/^{39}\text{K})_{\text{Suprapur}}} - 1 \right) \times 10^3,$$

with the conversion of the  $\delta$  values between our lab standard ( $\delta^{41}\text{K}_{\text{Suprapur}}$ ) and NIST-SRM-3141a ( $\delta^{41}\text{K}_{\text{NIST-3141a}}$ ) being expressed as:

$$\delta^{41}\text{K}_{\text{Suprapur}} = \delta^{41}\text{K}_{\text{NIST-3141a}} + 0.047 \quad (\text{Ku and Jacobsen, 2020}).$$

To minimize the interference arising from small amounts of Ca, a Ca-spiked standard solution was also analyzed during each analytical run. We measured mass 40 of Ca to monitor the presence of a Ca-hydride,  $^{41}(\text{CaH}^+)$ , which interferes with  $^{41}\text{K}$  in both sample and standard solutions. Such interferences can be estimated independently for each analytical run from the  $\delta^{41}\text{K}$  values obtained from the Ca-spiked standard relative to the unspiked standard. We then applied small corrections to samples that were analyzed during the same analytical run to account for such interferences.

### **Analytical Uncertainty and Reproducibility**

The within-run uncertainty of 0.03‰ is the calculated standard error (SE) obtained from repeated measurements of a standard solution that was not processed through column chemistry. The external reproducibility of 0.027‰ is the calculated variation (2SD) of  $\delta^{41}\text{K}$  values obtained from the USGS rock standard BHVO-2 measured repeatedly over 9 days. The consistency between the internal (within-run) uncertainty (0.03‰) and the external reproducibility (0.027‰) implies that there are no additional uncertainties introduced during sample dissolution or chromatographic column chemistry. Details of uncertainty estimation are described by Ku and Jacobsen (2020).

### **Results**

All samples were analyzed for their chemical composition of 48 elements using quadrupole ICP-MS. None of the chondrule or matrix samples analyzed show terrestrial contamination, as

suggested by the flat and unfractionated Rare Earth Elements (REE) patterns relative to the CI composition (Appendix C, Figs. 1-8).

### Allende matrix

Five separated fractions of Allende fine materials (labeled as SF) were originally identified as matrix because of their fine grain size. The two coarse fractions, SF004 and SF005, have a grain size larger than 75 nm, indicating the potential presence of tiny chondrules or even the possible existence of materials which are an assemblage of broken fragments of Allende rock. In fact, the trace and major element concentrations in these two samples show elemental patterns (and isotopic compositions, discussed later) similar to those of the average Allende chondrules and the whole rock sample (Appendix C, Fig. 4-5), respectively. In addition, SF004 and SF005 both have very low concentrations of Pb and Tl, just like the Allende chondrules, which sits in contrast with the two fine-grained Allende matrix samples.

While the other three fractions (SF001-003) were fine-grained and were carefully examined under a binocular microscope, very tiny broken chondrules that are difficult to separate by hand may still be present. The SF003 fraction, in particular, likely contains tiny chondrule fragments based on its relatively low concentrations of Pb and Tl (Appendix C, table 1) compared to SF001 and SF002. A mass balance calculation which uses the Pb concentrations in the most Pb-rich sample, SF002, and the average Allende chondrules as end-members suggests that SF003 may contain up to ~90% chondrules. However, the Pb concentration alone cannot be the only indicator which determines the nature of this sample, as Pb is a fairly heterogeneous element which comes in different proportions in Allende matrix samples.

Therefore, due to the nearly identical major and trace element patterns (Appendix C, Fig. 8) among SF001-003, which indicates the purity of the separated matrix materials, we believe that

SF001(Mx), SF002(Mx), and SF003(Mx), with their finer grain size, should be considered as Allende matrix in our study. Further, we consider SF004(Ch) and SF005(f) as containing assemblages of tiny broken chondrules and Allende rock fragments (mixtures of major components), a result of the initial separation processes.

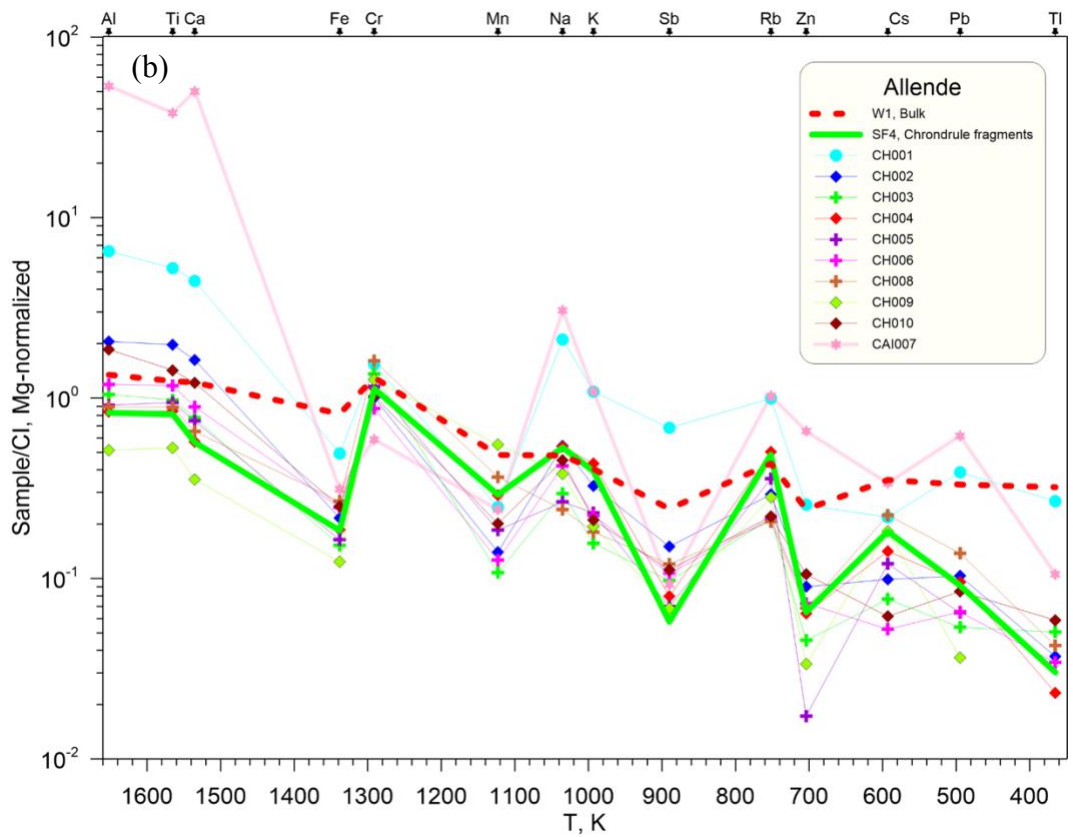
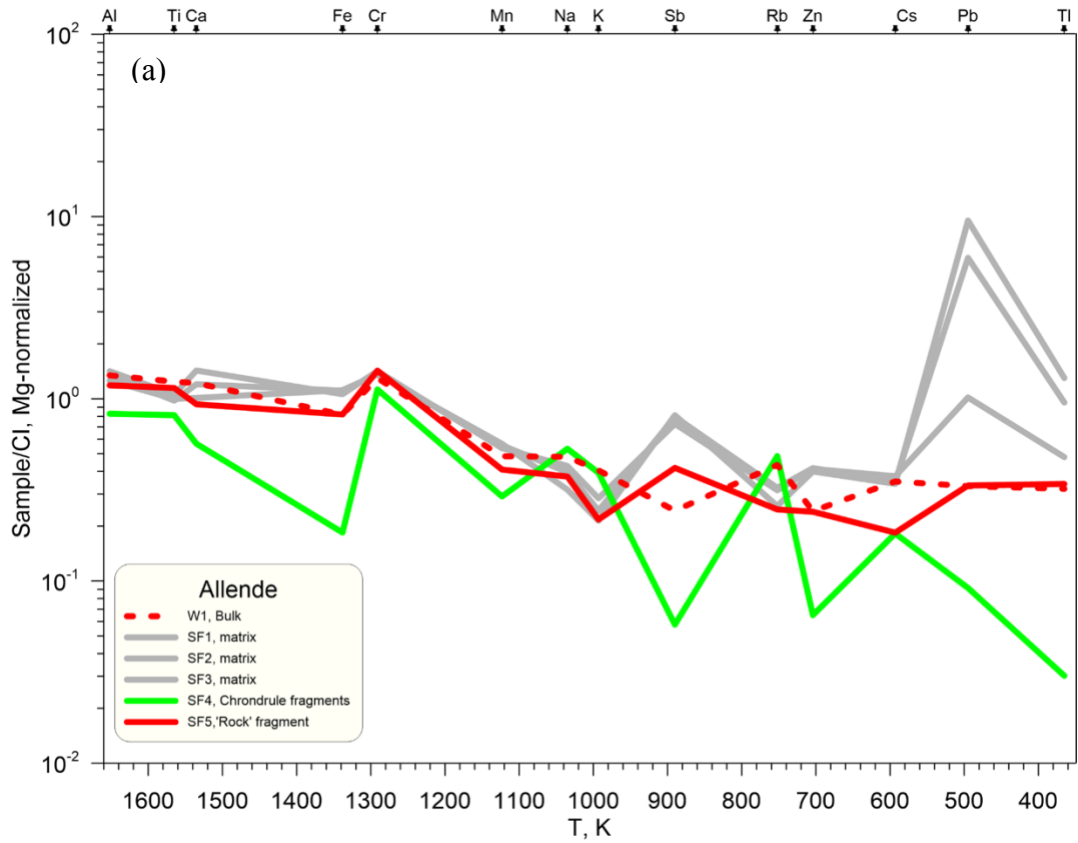
### **Depletion patterns of chondrule and matrix samples**

Concentrations of selected elements in the samples studied, normalized to CI chondrites (McDonough and Sun, 1995) and Mg (Fig. 4), show typical volatility-based depletion patterns with no systematic variations among different chondrule types. The depletion patterns are slightly different between Allende matrix (Fig. 4a) and Allende chondrites (Fig. 4b), and we also plot the Allende CAI samples for comparison, where a clear enrichment of refractory elements is shown. The nearly identical depletion patterns between the SF004(Ch) and the average Allende chondrules further support our conclusion that this fraction is merely an assemblage of tiny, broken chondrules. The sample SF005(f) also shows a similar pattern to the Allende bulk sample, which again supports our previous conclusion that this sample is merely an assemble of Allende rock fragments.

We also compared our results to the current literature on K isotope data reported for Allende matrix (Jiang et al., 2021). There, two Allende matrices were found to have nearly identical depletion patterns to the five Allende bulk samples that were reported (Appendix C, Fig. 9). However, each of the bulk samples used in that study actually weighed < 0.1 gram and are therefore not necessarily representative samples. In contrast, the Allende whole rock sample published in one of our previous works (Ku and Jacobsen, 2020) came from a 34-gram source powder. Because the Allende whole rock data from Jiang et al. (2021) are likely non-representative, and because the elemental patterns between their Allende fragments and their

matrix samples match, this implies that the samples which they claim to be matrix may be similar to our SF005(f) separation. That is, it seems that the samples which they consider to be matrix actually consist of fractions of Allende fragments. Additionally, we note here that the 3 CAI samples from Jiang et al. (2021) show a ~100 times enrichment in volatile elements for Na, K, Sb, and only one sample was plotted in the CAI field of a Glen's diagram (Appendix C, Fig. 10). Therefore, any comparison of the Allende matrix or chondrules that is made between the current study and that of Jiang et al. (2021) needs to take into account the deficits found in the latter work.

The depletion patterns of matrix samples from three ordinary chondrites studied here are rather similar despite their different chemical and petrologic types. The ordinary matrix samples (Fig. 4c) may be slightly enriched in volatile elements relative to the corresponding chondrules (Fig. 4d), but the differences are very minor. Compared to Allende, the three ordinary chondrites do show a 'steeper' depletion toward the highly volatile elements. The bulk ordinary chondrites also show a range of concentration that is similar to the ordinary matrix and chondrules, despite some variations in the highly volatile elements. In summary, any correlations between the depletion patterns with different chondritic components were not observed, but Allende chondrules, matrix and CAIs show slightly different depletion patterns, while the ordinary chondrites seem to have identical patterns across all components.



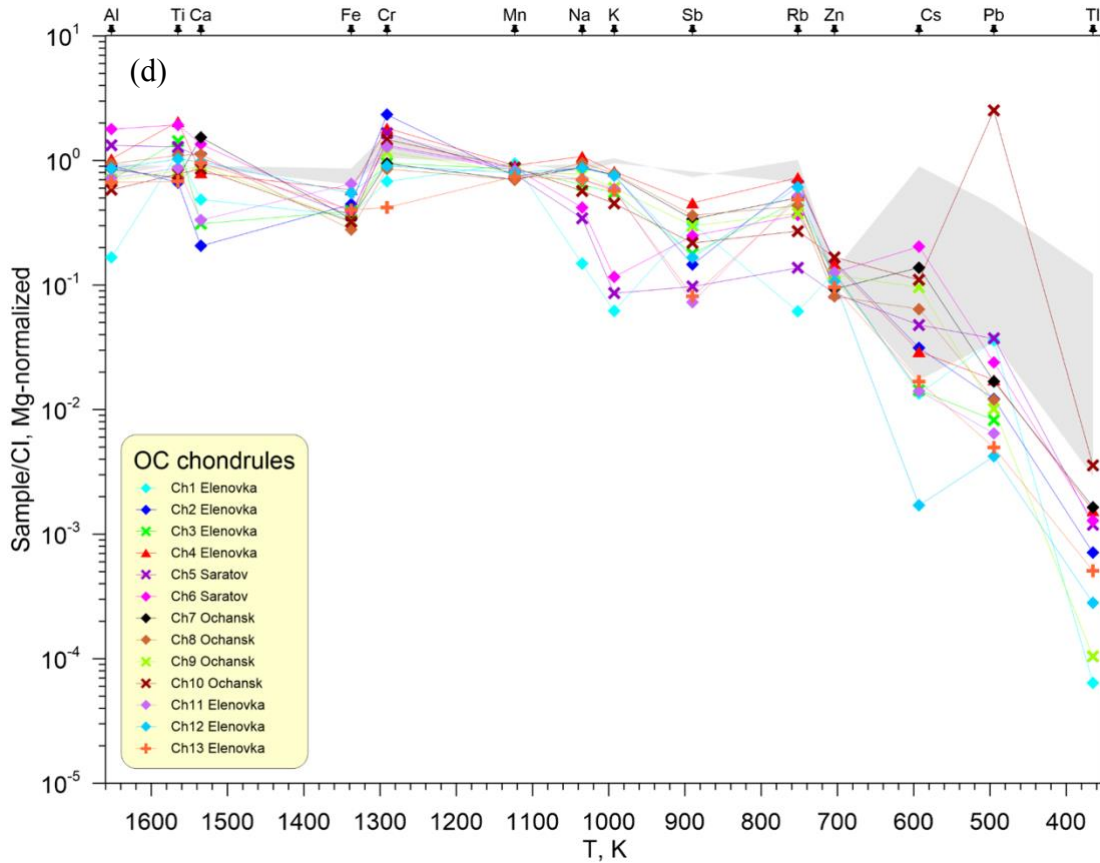
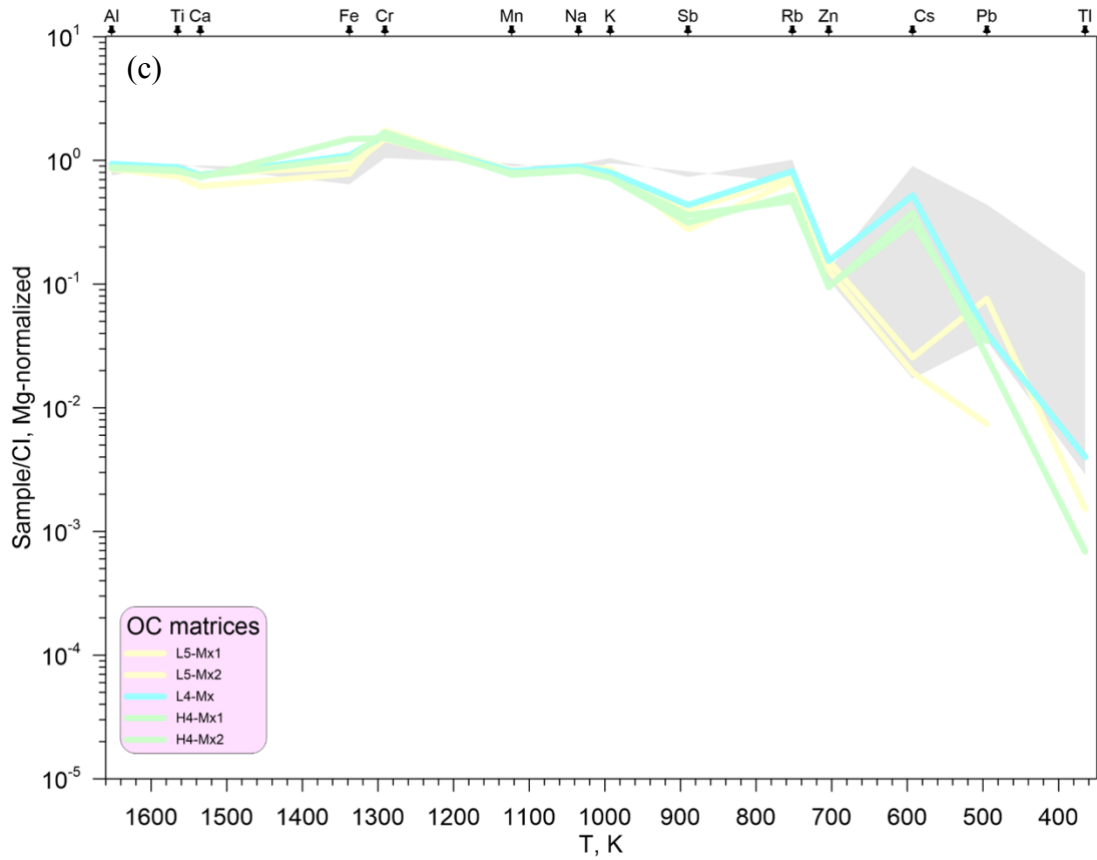




**Figure 4. Elemental depletion patterns of samples from Allende matrix (4a), Allende chondrules and CAIs (4b), matrix for 3 ordinary chondrites (4c), and chondrules for 3 ordinary chondrites (4d).** Concentration for each element is normalized to the CI composition (McDonough and Sun, 1995) and to Mg concentration. The depletion pattern is of the sequence in the order of the condensation temperatures. The bulk concentration for Allende and selected ordinary chondrites (Ku and Jacobsen, 2020) of massive powder source (>10 g) are also shown here for comparison and reference.

**Potassium isotope composition of matrix, chondrules, and CAIs from Allende (CV3) and Murchison (CM2)**

The  $\delta^{41}\text{K}$  values among the Allende samples analyzed range from  $-0.113\text{‰}$  to  $-0.382\text{‰}$ , except for one chondrule (CH009), which has a very low  $\delta^{41}\text{K}$  value of  $-1.967\text{‰}$ . These results show no apparent correlation with either chondrule type (*e.g.*, Type-I, Type-II) or alteration degree. For instance, the Type-II chondrule CH008 has a  $\delta^{41}\text{K}$  value which is essentially identical to the Type-I chondrule CH010. The unaltered chondrule CH004 has a  $\delta^{41}\text{K}$  value that is similar to the altered chondrule CH002, which has an obvious aqueous altered rind (Fig. 7-8). The Ca-rich chondrule CH001 has a  $\delta^{41}\text{K}$  value similar to the major cluster of Allende chondrules, likely due to its aqueously altered history. The finest matrix, SF001, yields a  $\delta^{41}\text{K}$  value of  $-0.382\text{‰}$ , which we consider to be the best estimate of  $\delta^{41}\text{K}$  for the Allende matrix. The other slightly coarser sample, SF002, has a somewhat heavier K isotope composition compared to SF001, and the SF003 sample – a possible mixture of chondrule and matrix – has a similar  $\delta^{41}\text{K}$  value to the Allende matrix samples. The SF004 (Ch) and SF005(f) samples, on the other hand, show  $\delta^{41}\text{K}$  values similar to those of the average chondrules and the Allende whole rock.

The mean  $\delta^{41}\text{K}$  value of Allende chondrules generally agrees with that of Jiang et al. (2021) after excluding the outliers and after considering the analytical uncertainties of both studies, although we observe a systematic shift towards heavier  $\delta^{41}\text{K}$  values compared to that previous work. This could potentially arise from the different techniques that were utilized in the two studies for isotope measurements. Specifically, Jiang et al. (2021) conducted isotope measurements using a cold-plasma, whereas here we have used collision-cell techniques. Given the good agreement between the  $\delta^{41}\text{K}$  values of a USGS standard, BHVO-2, for Jiang et al. (2021) and Ku and Jacobsen (2020), however, the minor differences in  $\delta^{41}\text{K}$  values of Allende samples between Jiang et al.,

2021 and the current work most likely reflect the sample heterogeneity between the samples used in the two studies.

In general, all Allende chondrule and matrix samples show a limited range of  $\delta^{41}\text{K}$  values, and such small differences among each component most likely reflects the heterogeneity of the Allende meteorite. The overall variations, excluding one outlier (CH009), range from  $-0.113\text{‰}$  to  $-0.360\text{‰}$ , and from  $-0.330\text{‰}$  to  $-0.382\text{‰}$  for Allende chondrule and matrix samples, respectively. The matrix sample of the CM2 chondrite Murchison yielded a  $\delta^{41}\text{K}$  value of  $-0.197\text{‰}$ , which is slightly lighter than the two previous values ( $-0.112\text{‰}$  and  $-0.155\text{‰}$ ) of the bulk Murchison meteorite (Ku and Jacobsen, 2020). Overall, the matrix samples of the carbonaceous chondrites analyzed here have lighter K isotope compositions compared to the bulk, but the difference is very small.

#### **Potassium isotope composition of matrix and chondrules from ordinary chondrites**

In Elenovka (L5), two matrix samples (with and without chondrules) have identical  $\delta^{41}\text{K}$  values, similar to those of the main cluster of six chondrules. One Elenovka chondrule (#1) has a lighter  $\delta^{41}\text{K}$  value than other chondrules, but the difference of  $\sim 0.15\text{‰}$  is relatively small. All separates from Elenovka are enriched in the heavier isotope relative to the bulk L chondrite (Ku and Jacobsen, 2020). Two Saratov (L4) chondrules have similar  $\delta^{41}\text{K}$  values closely resembling the bulk L chondrites. The matrix of Saratov is lighter than both chondrules and the bulk. Again, the difference of  $0.13\text{‰}$  in  $\delta^{41}\text{K}$  between the Saratov chondrule and matrix samples is similar to the variation among Elenovka samples, and most likely reflects sample heterogeneity. The matrices of the dark and light lithologies from the Ochansk (H4) chondrite have similar  $\delta^{41}\text{K}$  values, but the chondrules from the dark lithology are enriched in heavier K isotopes compared to

those from the light lithology. The magnitude of fractionation between chondrules and matrix is much larger in the dark lithology (Fig. 6).

The overall ranges of  $\delta^{41}\text{K}$  variations in the three ordinary chondrites studied here are  $-0.356\text{‰}$  to  $-0.722\text{‰}$  and  $-0.433\text{‰}$  to  $-0.960\text{‰}$  for chondrules and matrices, respectively. These ranges are larger than those of the bulk H and L chondrites, but they are relatively small compared to the scatter of the chondrule and matrix data from the Hamlet (LL4) chondrite (Koefoed et al., 2020). Similar to the carbonaceous chondrites, no significant K isotopic fractionation is observed between ordinary matrices and chondrules. In addition, no correlations are found between the values of  $\delta^{41}\text{K}$  and chondrule type.

**Table 1.**  
K isotope composition of carbonaceous chondrites.

Sample Name	Component	Classification	Weight (mg) <sup>†</sup>	K [ppm] <sup>‡</sup>	$\delta^{41}\text{K}$ (‰)	2SE <sup>§</sup>	<i>N</i>	<i>n</i>
<i>USGS Terrestrial standard</i>								
GSP-2	Whole Rock	N/A			-0.382	0.030	5	23
RGM-1	Whole Rock	N/A			-0.308	0.030	5	26
W-2	Whole Rock	N/A			-0.428	0.046	2	9
<i>Allende (CV3)</i>								
Allende-1*	Whole rock	N/A	34000	337	-0.192	0.030	19	116
SF001(Mx)	Matrix	gr < 37 $\mu\text{m}$	39.0	166	-0.382	0.030	8	46
SF002(Mx)	Matrix	37 < gr < 44 $\mu\text{m}$	597.6	176	-0.309	0.030	9	47
SF003(Mx)	Matrix	44 < gr < 75 $\mu\text{m}$	7059.7	233	-0.330	0.030	8	46
SF004(Ch)	Chondrule fragments	75 < gr < 150 $\mu\text{m}$	3091.4	243	-0.224	0.033	4	19
SF005(f)	Rock fragment	150 $\mu\text{m}$ < gr	10480.0	204	-0.223	0.030	10	48
CH001 [f]	Chondrule	Ca-Al-rich (type-I)	8.8	949	-0.234	0.033	4	20
CH002 [f]	Chondrule	PO_1+altRim	9.0	414	-0.275	0.030	5	24
CH003 [f]	Chondrule	BO_2	12.9	255	-0.163	0.030	7	30
CH004	Chondrule	PO_1+igRim	53	663	-0.172	0.030	11	47
CH005	Chondrule	BO_1	25.7	324	-0.181	0.030	7	29
CH006	Chondrule	PO_1+igRim2	25.3	406	-0.113	0.030	7	29
CH008	Chondrule	BO_2+melt	18.8	259	-0.360	0.030	6	28
CH009	Chondrule	POP_1	17.4	293	-1.967	0.030	6	27
CH010	Chondrule	PO_1	14.8	269	-0.355	0.030	6	27
CH007	CAI	Type-B1	19.1	252	-0.294	0.030	7	29
SBJ101-A	CAI	Type-B	27.1	64	-0.036	0.030	5	24
SBJ101-B	CAI	Type-B	29.7	49	0.226	0.030	6	27
SBJ101-C	CAI	Type-B	30.1	60	0.236	0.030	5	24
<i>Murchison (CM2)</i>								
Murchison-1*	Whole rock	N/A	10000	525	-0.134	0.030		
Mur-Mx	Matrix	N/A	2000	130	-0.197	0.030	6	28

\* Whole rock samples are described in Ku and Jacobsen (2020).

<sup>†</sup> Source powder weight for the whole rock and matrices component. Individual chondrule studied and dissolved.

<sup>‡</sup> Concentrations of Ca and K were measured by quadrupole ICP-MS.

<sup>§</sup> Analytical uncertainty of  $\delta^{41}\text{K}$  ( $2\sigma$ ) for each sample is either the calculated standard error (2SE) or the external reproducibility, 0.030‰, whichever is larger.

*N*: analytical runs on different days; *n*: total sample-standard bracket measurements from *N* days. Chondrule classification adapted from (Lauretta et al, 2006), and is expressed as ‘Mineralogy\_Chondrule Type\_additional information’. For instance, PO\_1+altRim means a type 1 chondrule classified as porphyritic Olivine with altered rim. Other abbreviations include BO – barred Olivine; POP – porphyritic Olivine/Pyroxen.

**Table 2.**  
K isotope composition of ordinary chondrites.

Sample Name	Component	Classification	Weight (mg) <sup>†</sup>	K [ppm] <sup>‡</sup>	$\delta^{41}\text{K}$ (‰)	2SE <sup>§</sup>	N	n
<b><i>Elenovka (L5)</i></b>								
N1826–Mx1	Matrix	N/A	136.3	768	–0.433	0.038	3	12
N1826–Mx2	Matrix	N/A	60.3	765	–0.501	0.033	4	16
Ch#1	Chondrule	POP_2	46.3	80	–0.616	0.038	3	11
Ch#2	Chondrule	PO_2	31.2	693	–0.374	0.030	5	23
Ch#3 [f]	Chondrule	RP_1	35.9	810	–0.447	0.030	5	23
Ch#4	Chondrule	GO_1	30.5	705	–0.386	0.030	5	20
Ch#11	Chondrule	POP_2	17.9	536	–0.356	0.030	6	30
Ch#12 [f]	Chondrule	PO_2	19.5	757	–0.458	0.030	6	30
Ch#13 [f]	Chondrule	BO_2	11.5	712	–0.420	0.030	6	30
<b><i>Saratov (L4)</i></b>								
N311–Mx	Matrix	N/A	76.1	631	–0.835	0.033	4	16
Ch#5 [f]	Chondrule	RP_2	33.6	96	–0.573	0.030	5	23
Ch#6 [f]	Chondrule	POP_2	30.3	160	–0.702	0.030	4	18
<b><i>Ochansk (H4)</i></b>								
N75–Mx (dark)	Matrix	N/A	88.9	628	–0.960	0.033	4	16
N76–Mx (light)	Matrix	N/A	95.1	537	–0.881	0.033	4	16
Ch#7 (dark)	Chondrule	PO_2	6.3	932	–0.449	0.030	6	30
Ch#8 (light) [f]	Chondrule	POP_2	5.3	916	–0.722	0.030	6	30
Ch#9 (dark) [f]	Chondrule	RP_2	3.6	738	–0.441	0.030	7	35
Ch#10 (light)	Chondrule	RP_2	7.0	527	–0.649	0.030	6	30
Mean of the H chondrites <sup>¶</sup>	Whole rock	N/A	N/A	780	–0.672	0.037		
Mean of the L chondrites <sup>#</sup>	Whole rock	N/A	N/A	825	–0.675	0.028		

<sup>†</sup> Dissolved weights for Ordinary matrices components. Individual chondrule studied and dissolved.

<sup>¶</sup> The mean value is based on 6 different meteorites: Kernouve, Dresden, Forest City, Grady, Guareña, and Estacado. Details in Ku and Jacobsen, 2020.

<sup>#</sup> The mean value is based on 5 different meteorites: Marion Iowa, Homestead, Bruderheim, PeaceRiver (2 pieces), and Holbrook (3 pieces). Details in Ku and Jacobsen, 2020.

Classification abbreviations: RP – radial Pyroxene; GO – granular Olivine. Other footnotes are described in table 1.

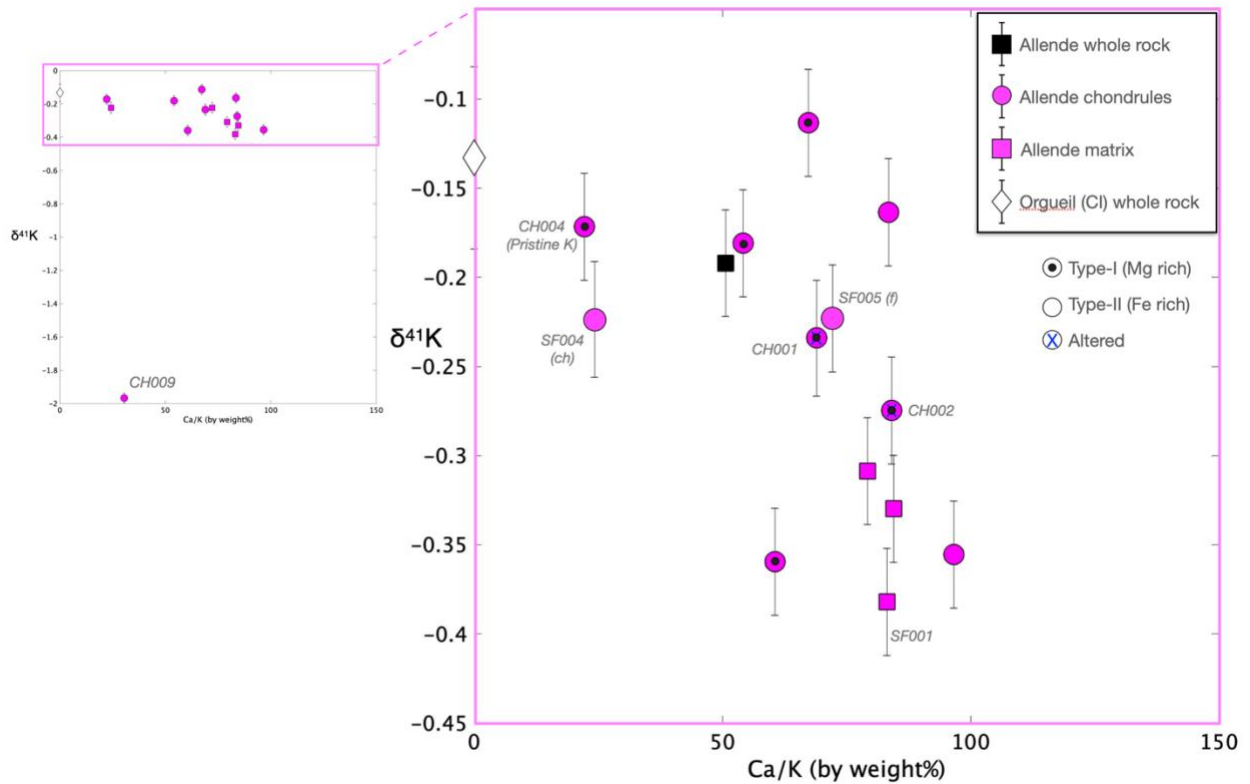


**Figure 5. K isotopic compositions ( $\delta^{41}\text{K}$ ) of Allende chondrites and matrices.** Nine chondrules and five matrices are plotted versus the K/Mg ratio. Two whole rock samples from Allende and Orgueil are also plotted for comparison (Ku and Jacobsen, 2020). The  $\delta^{41}\text{K}$  compositions for Allende chondrules do not correlate with either petrologic type or chondrule type. Additionally, chondrules with apparent alteration rims (CH001 and CH002) reveal similar  $\delta^{41}\text{K}$  values to chondrules with pristine K, indicating that aqueous alteration does not affect  $\delta^{41}\text{K}$  to any significant degree in Allende meteorites. The finest Allende matrix (SF001) has the lightest  $\delta^{41}\text{K}$  value, and the two coarse samples (SF004 and SF005), which potentially contain tiny chondrule fragments, are indistinguishable from one another and from other chondrules and the bulk Allende. Overall, Allende chondrules and matrices showed  $\delta^{41}\text{K}$  ranges that are similar to that of the bulk Allende, and the CI chondrite from Orgueil has a  $\delta^{41}\text{K}$  that is different from the Allende matrices, which should not be used to chemically or isotopically represent carbonaceous matrix.

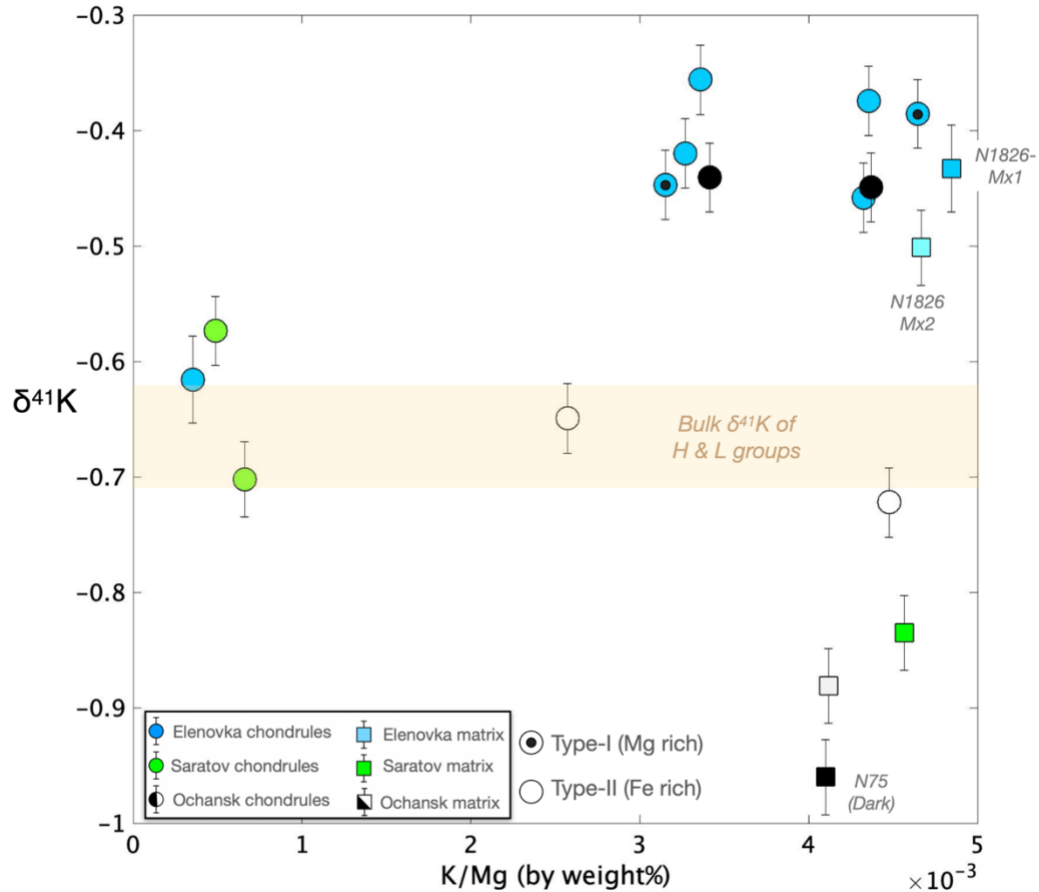


**Figure 6. K isotopic compositions ( $\delta^{41}\text{K}$ ) of chondrites and matrices from Elenovka (L5), Saratov (L4), and Ochansk (H4) meteorites.** For Elenovka, matrices without and with small chondrules (Mx1 v.s. Mx2) have similar  $\delta^{41}\text{K}$  compositions, and most chondrules have similar  $\delta^{41}\text{K}$ , except for Ch #1. For Saratov, the matrix has a lighter  $\delta^{41}\text{K}$  than 2 chondrules. For Ochansk, the dark matrix (N75) has a lighter  $\delta^{41}\text{K}$  than the light matrix (N76), and the  $\delta^{41}\text{K}$  range between the dark materials has a wider isotope variation than that between the light materials. Similar to Allende, there is no correlation with either petrologic type or chondrule type. Samples with higher metamorphic degrees (Elenovka L5) show a smaller K isotope difference between matrix and chondrules. Overall,  $\delta^{41}\text{K}$  values in matrices and in chondrules are very different within ordinary chondrites, so no single  $\delta^{41}\text{K}$  value can represent matrix and chondrule reservoirs.



## Discussion

Within few million years after their formation in the solar nebula, the chondritic components, once suspended in the H<sub>2</sub>-rich gas, have accreted into meteorite parent bodies where they have experienced interaction with each other in the presence of various fluids, often H<sub>2</sub>O-rich, at elevated temperatures and pressures, as well as brecciation and shock metamorphism during impacts caused by parent body collisions. All these processes could have changed primary K concentrations and isotopic compositions of individual chondritic components that needs to be taken into account before considering their nebular history.

The extent of fluid-assisted metasomatism and thermal metamorphism, collectively known as secondary parent body alteration, is reasonably assessed by a petrologic type of a particular meteorite (*e.g.*, Weisberg et al., 2006), with chondrites of types 3.0-3.1 being considered the least altered by the parent body processes. The higher or lower petrologic types indicate a larger extent of thermal or aqueous alteration, respectively. Because K can be mobilized by both aqueous fluids and high temperatures, such a secondary processing is expected to diminish primary chemical and isotopic differences among chondritic components.

The impact processing of a meteorite, besides brecciation, can subject it to high shock pressures typically indicated by a shock stage varying from S1 to S6 to describe progressive damage of mineral crystal structures, mineral transformations and eventually incipient melting. The shock processing is highly localized and dis-equilibrium process that is typically isochemical except for the highest shock stages when maskelynitization of plagioclase and incipient melting can result in evaporative loss of volatile elements, including K. Because of highly dis-equilibrium nature of this process, it may induce mass-dependent K isotope fractionation. Also, the brecciation can mix together clasts which experienced different shock and thermal histories.

### **Parent Body Processes**

Once the various chondrite components formed in the nebula, they accreted into meteorite parent bodies. There, thermal metamorphism, aqueous alteration, and shock modification, collectively known as parent body processes, began to modify the primary chondritic components, causing a redistribution of mobile elements such as K and potentially the fractionation of K isotopes. Both carbonaceous and ordinary chondrites experienced such processes to different degrees. Thermal metamorphism can be affected by the presence of water, so the line between aqueous alteration and thermal metamorphism is sometimes hard to draw. Few meteorites show evidence of both, implying that metasomatism likely represents aqueous alteration followed by thermal metamorphism.

### **Thermal Metamorphism**

Among the ordinary chondrites studied here, we focus our discussion on the difference between Saratov and Elenovka, because Ochansk is a heterogeneous breccia which has a potentially complex thermal history. Our K isotope data for matrix and chondrule components from Saratov and Elenovka revealed no apparent correlations between samples with high degrees of metamorphism. The  $\delta^{41}\text{K}$  values of bulk meteorites from each petrologic type also show no correlation (Ku and Jacobsen, 2020). One might argue that Elenovka (L5), when compared to both Saratov (L4) and Ochasnk (H4), reveals a smaller  $\delta^{41}\text{K}$  variation between the matrix component and the major cluster of chondrule samples, which implies that  $\delta^{41}\text{K}$  can be equilibrated through thermal metamorphism. Nevertheless, one Elenovka chondrule sample (#1) lies outside of the major chondrule cluster, making the overall  $\sim 0.2\%$  variation similar to that of Saratov. Indeed, our data did not reveal any systematic trend between  $\delta^{41}\text{K}$  value and petrologic type, which could potentially be due to limitations in the types of samples studied. So far, our data implies that the

observed variations in  $\delta^{41}\text{K}$  among and within Elenovka and Ochansk reflect the heterogeneity of the samples rather than effects of thermal metamorphism.

The overall  $\delta^{41}\text{K}$  variations among chondrule components in our type 4 and type 5 chondrite samples are larger than those among the bulk ordinary chondrites, suggesting the possibility that thermal metamorphism might fractionate K isotopes only locally. However, the identical  $\delta^{41}\text{K}$  values among the bulk type 3-6 ordinary chondrites (Ku and Jacobsen, 2020) suggest that thermal metamorphism led to re-equilibration and, consequently, elimination of the primary differences in  $\delta^{41}\text{K}$  for the bulk.

As for the two carbonaceous meteorites studied here, Allende and Murchison, thermal metamorphism events likely occurred with aqueous alteration, and the resulting effects on K isotopes are discussed in the following section.

### **Aqueous Alteration**

One Allende chondrule, CH004, shows an indistinguishable K concentration between the core and the rim (EDS data), and we are relatively certain that the  $\delta^{41}\text{K}$  of  $-0.172\text{‰}$  from this sample represents the primary composition of K isotopes in unaltered chondrules. On the other hand, Allende chondrules with clear alteration in the rim and an enrichment in K relative to the core – CH001 and CH002 (Fig. 7-8) – have slightly lighter  $\delta^{41}\text{K}$  values than the chondrule with no alterations – CH004 (Fig. 9). The  $\delta^{41}\text{K}$  values from the altered chondrules show that K is not a primary product which condensed from the nebula but is instead from a secondary source such as the parent body. However, the magnitude of K fractionation between the altered and unaltered chondrules is about  $0.1\text{‰}$ , which is smaller than the overall variations among all the Allende chondrules, and is also smaller than the differences between the matrix, bulk, and altered

chondrules. Thus, our data show no systematic trend of  $\delta^{41}\text{K}$  changes in chondrules caused by aqueous alteration.

A recent study (Jiang et al., 2021) concluded that the wide range of  $\delta^{41}\text{K}$  observed among Allende chondrules, especially those with high K/Al ratios, is the result of interactions with and addition of an *ad hoc* K-bearing fluid in the chondrule rims. This is based on data from what they believed were CAIs (something which is now questionable) and the analogue of terrestrial chemical weathering processes, which show an enrichment of heavy K isotopes in aqueous solutions relative to terrestrial igneous rocks. However, no direct K isotope data from meteoritic fluids has been measured so far, suggesting that the analogue between terrestrial weathering processes and Allende aqueous alteration is not supported. Moreover, even if the physicochemical processes were universal, the  $\delta^{41}\text{K}$  values of the unaltered chondrules and the interacting fluid likely differ drastically from those of terrestrial rocks and seawater, meaning that the resulting  $\delta^{41}\text{K}$  values of the altered chondrules may be very difficult to estimate. In fact, many studies have shown no systematic enrichment or shift in the K isotope composition between heavily altered and unaltered oceanic crust materials (Hu et al., 2020; Liu et al., 2021). Since no correlations between  $\delta^{41}\text{K}$  and elevated mobile elements (*i.e.*, K/Mg, Na/Mg) have been observed, and no further petrographic evidence was supported in Jiang et al. (2021), our data suggests that the  $\delta^{41}\text{K}$  variations found in Allende chondrules and among Allende components are not primarily due to aqueous alteration; instead, they are reflective of chondrule heterogeneity.

As for Murchison, because only one matrix sample was studied here, it is challenging to draw any concrete conclusion about whether the  $\delta^{41}\text{K}$  of matrix reflects such aqueous alteration, even though this matrix sample reveals a lighter  $\delta^{41}\text{K}$  value compared to the bulk sample (Ku and Jacobsen, 2020).

As for ordinary chondrites, especially those of types 3 and 4, the porosity is a relatively well-preserved texture which enables estimation of the degree of secondary aqueous alteration (Grossman et al., 2000; Dobrică and Brearley, 2014). In particular, it was found that type-4 chondrites have the highest average density in bulk porosity and that two Saratov chondrules show a porosity of ~2 volume% (Macke, 2010). This implies that the transport of mobile elements out of the chondrules largely arises from the dissolution of chondrule mesostasis (Lewis et al., 2018). It is, however, difficult to conclude if our Saratov chondrules have also experienced the same processes due to a lack of porosity data for these chondrules. For chondrites of higher petrologic degree (5-6), any prior phases related to aqueous alteration are likely to have disappeared or re-equilibrated after metamorphism (Grossman and Brearley, 2005). Hence, our current data cannot distinguish whether the variations in  $\delta^{41}\text{K}$  values observed in ordinary chondrules are the result of aqueous alteration or sample heterogeneity.

### **Impact, Shock and Brecciation**

Ochansk, a breccia complex with pristine Fe-Ni grains and cloudy taenite (Scott et al., 2014), contains dark and light materials of potentially different thermal history, where the heating has likely never exceeded the temperature experienced in the lowest-metamorphized-grade materials for both dark and light components. This complex also shows a larger range of  $\delta^{41}\text{K}$  values compared to both Elenovka (L5) and Saratov (L4). Specifically, the dark components of Ochansk have a wider  $\delta^{41}\text{K}$  variation (~0.5‰) between matrix and chondrules relative to the light components (~0.2‰), despite the identical chemical compositions of the dark and light samples (Appendix C, Fig. 4). The matrices of the dark and light materials have similar  $\delta^{41}\text{K}$  values, whereas the  $\delta^{41}\text{K}$  of light chondrules is identical to that of the bulk H chondrites, and the dark chondrules have a significantly heavier  $\delta^{41}\text{K}$  compared to the other Ochansk components.

However, the mean  $\delta^{41}\text{K}$  value of  $-0.783\%$  for the light components is similar to that of the dark components,  $-0.703\%$ . Such observations indicate that shock effects may significantly redistribute opaque minerals, resulting in a larger magnitude of K isotope fractionation in the dark components. Despite this, the net loss of K could remain minimal, leading to the observed similarity of the bulk chemical compositions.

In fact, a previous study revealed a wide overall  $\delta^{41}\text{K}$  variation, up to  $\sim 1\%$ , within chondrules from Hamlet (LL4) meteorites with a shock stage of S3 (Koefoed et al., 2020). The similarity of the large K isotope fractionations observed in Hamlet and Ochansk relative to the other ordinary chondrites studied further supports the notion that impacts from shock or brecciation are likely the main cause of the wide variations in  $\delta^{41}\text{K}$ . However, the evolution histories of light and dark lithologies remain unknown, and the timing of impact events which fractionated the dark materials is still hard to resolve based solely on K isotope data.

In short, because no direct evidence is found in our data which supports a systematic K fractionation caused by aqueous alteration or thermal metamorphism, the most likely explanation for the variations in  $\delta^{41}\text{K}$  values observed between chondrules and matrix is sample heterogeneity. In addition, the wider range of  $\delta^{41}\text{K}$  values observed in Ochansk breccia appears to be related to secondary parent body shock and impact events. Despite the variations between different components, the lack of correlation between  $\delta^{41}\text{K}$  and K loss or gain, as well as the lack of open-system K isotope fractionation, suggest that there were no large, mass-dependent fractionation processes occurring in the nebula during the last stage of chondrule formation.

#### **Separate Matrix Reservoirs for Carbonaceous Chondrites**

Across three matrix samples from Allende, samples, SF003(Mx) and SF002(Mx), show identical, albeit slightly negative,  $\delta^{41}\text{K}$  values compared to the bulk Allende. The finest matrix

sample, SF001(Mx) has the most negative  $\delta^{41}\text{K}$  among all. Meanwhile, matrix from Murchison has a  $\delta^{41}\text{K}$  of  $-0.197\%$ , which is slightly more negative than the bulk Murchison (Table 1), consistent with the matrix-chondrule-bulk relations observed in other meteorites. However, none of the analyzed matrix components from the carbonaceous chondrites have  $\delta^{41}\text{K}$  values which are identical to that of the CI chondrites ( $-0.133\%$ ).

Previously, it was suggested that a carbonaceous chondrite matrix is elementally and isotopically similar to an anhydrous and reduced CI-like composition (Alexander, 2019a). A recent study also suggested that the linear correlation observed between  $\delta^{41}\text{K}$  and  $\delta^{87}\text{Rb}$  is due to a binary mixing between a CI-like matrix and a universal chondrule component (Nie et al., 2021). Nevertheless, the isotopic and elemental compositions of both the matrix and the chondrule components used in their mixing model are pure calculated values, and no real measurements on the end members were conducted or used in their study. Here, our data of the matrix components for CV, CM, and ordinary chondrites show that the  $\delta^{41}\text{K}$  values for each group are actually distinguishable from one another, and neither of the matrix samples has a CI-like isotopic composition. Specifically, both matrix of Allende and Murchison, the two carbonaceous chondrites analyzed here, have lighter  $\delta^{41}\text{K}$  values than the bulk compositions which are of opposite trend of what Nie et al. (2021) predicted. Therefore, our data argue that the binary mixing between CI-like matrix and chondrules are not the explanation to explain the K isotopic composition in the bulk carbonaceous meteorites.

One might argue that the differences in  $\delta^{41}\text{K}$  between CI and other carbonaceous matrices are very small, and that such discrepancies might result from secondary alteration. Indeed, matrices from Allende and Murchison both have  $\delta^{41}\text{K}$  values which are more negative overall than the CI chondrites. Considering the bulk components, however, especially that of Allende, which also has

a slightly negative  $\delta^{41}\text{K}$  value, it is quite challenging to quantitatively justify the notion that all carbonaceous chondrite matrices started with a CI-like composition. Instead, a comparison of the elemental depletion patterns supports the idea that the CI chondrites do not chemically or isotopically represent matrices of either carbonaceous or ordinary chondrites. Additionally, the matrix of carbonaceous chondrites should have condensed or accreted from reservoirs in the protoplanetary disk that are isotopically distinct with respect to K.



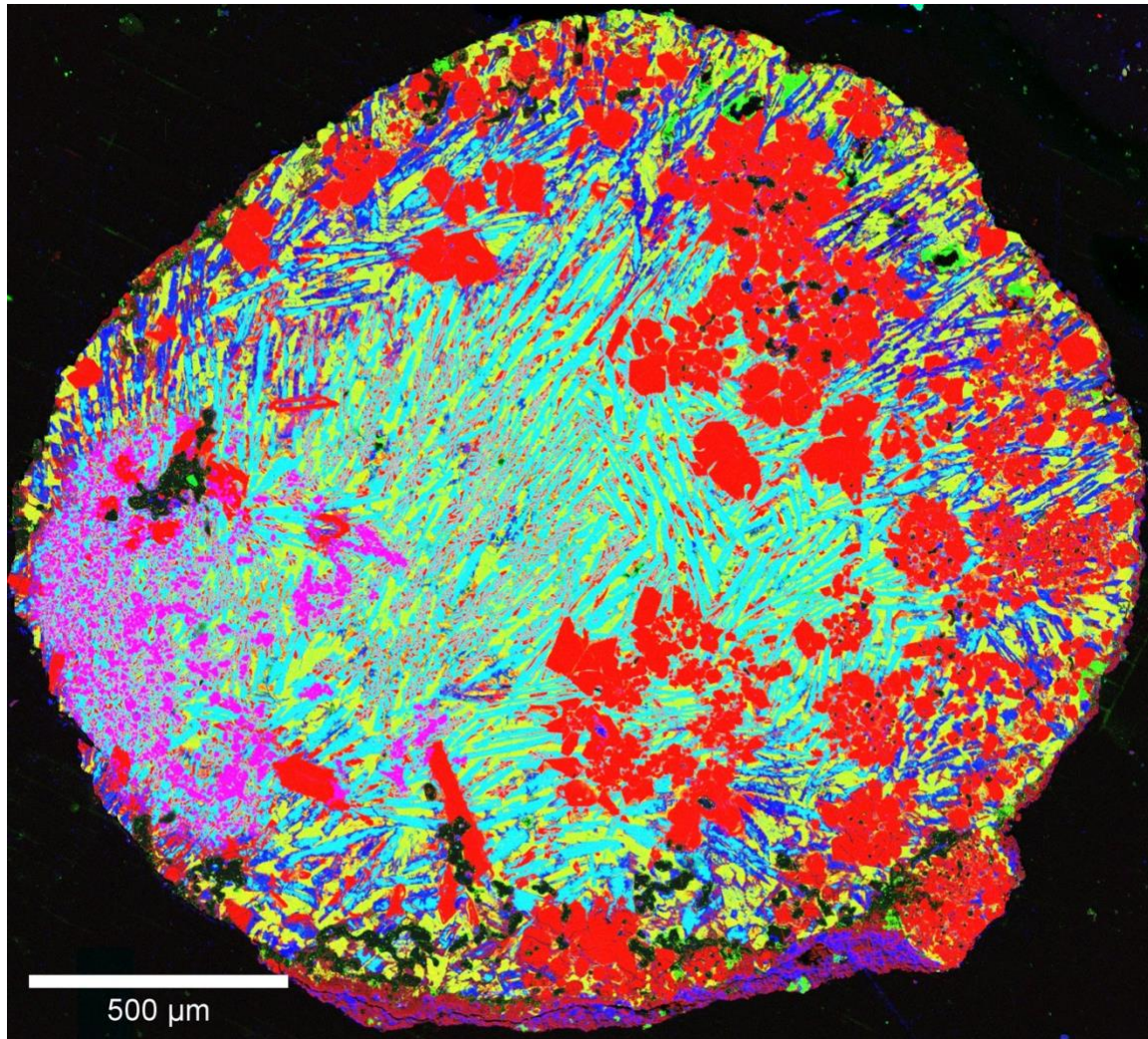


**Figure 7. Combined elemental map of the CH001 thin section in Mg (red), Ca (green), and Al (blue)  $K\alpha$  X-rays.** Mineral colors: red – forsterite, pink – spinel, yellow – Al-diopside, cyan – anorthite, blue – secondary sodalite and/or nepheline partially or completely replacing primary anorthite, light green – secondary salitic clinopyroxene, black – Ni-rich pyrrhotite.

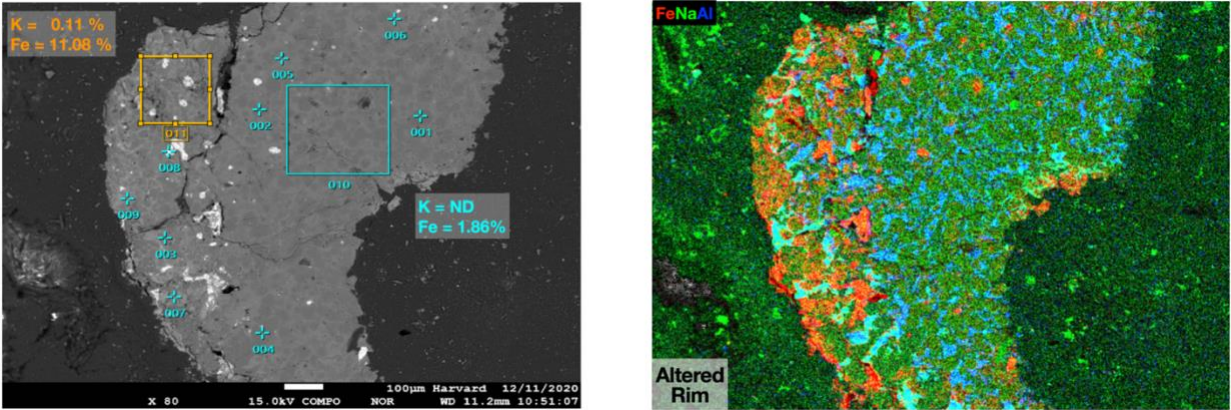


**Figure 8.** Allende - CH002: type-I chondrule, porphyritic Olivine with an altered rim. The surface EDS analysis show that K is concentrated in the rim (orange box) and is not detected in the core (blue box). Furthermore, Fe and Na are highly mobile during low temperature aqueous alteration, and both elements are highly concentrated in the rim area. Therefore, the K isotope data ( $\delta^{41}\text{K} = -0.275 \text{ ‰}$ ) from this sample represents aqueous alteration activities.



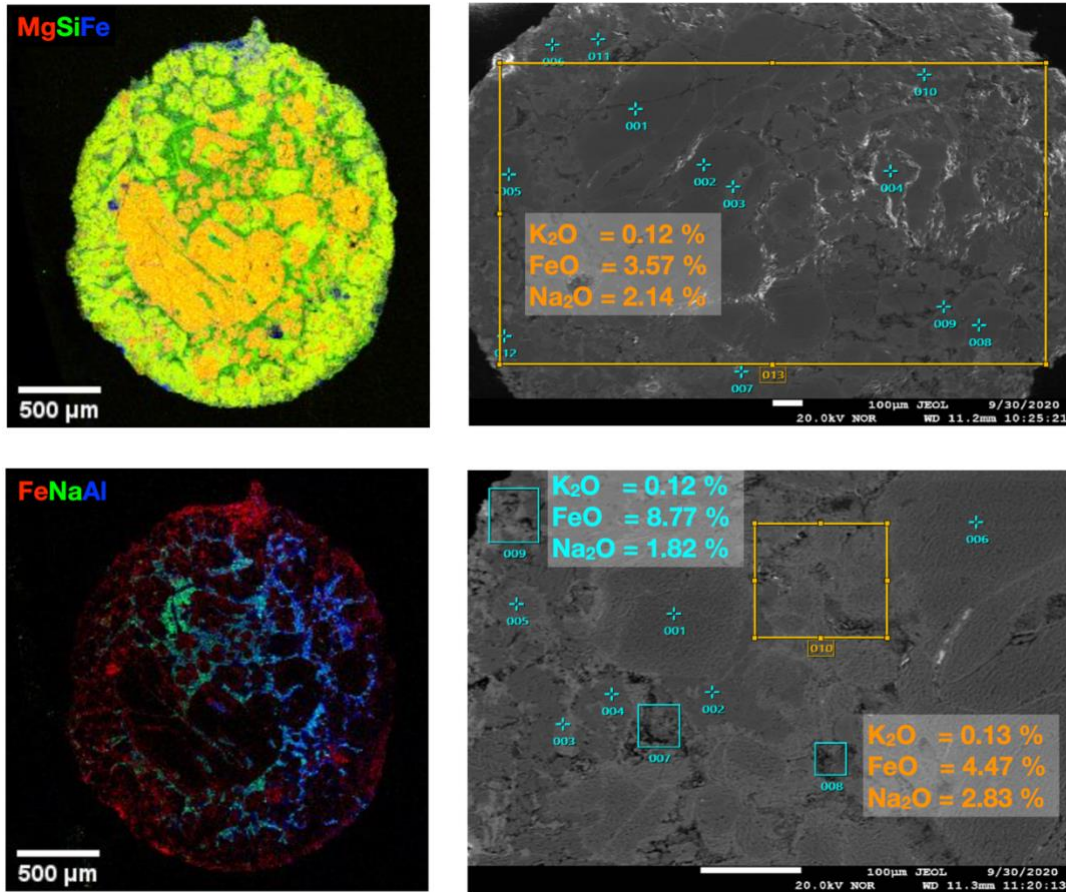


**Figure 9.** Allende - CH004: type-I chondrule, porphyritic Olivine with unaltered rim. The surface EDS analysis shows a homogeneous K distribution across the entire chondrule, and K concentrations in the rim and core are identical: K<sub>2</sub>O of the bulk (top right) is 0.12 %; K<sub>2</sub>O of the rim (bottom right – blue box) is 0.12 %; K<sub>2</sub>O of the core (bottom right – orange box) is 0.13 %. In comparison, the elemental concentration obtained from bulk solution using Q-ICP-MS is 243 ppm. Our data suggests that this chondrule did not experience extensive aqueous alteration, and that the rim of CH004 is a primary igneous rim. Therefore, the K isotope data ( $\delta^{41}\text{K} = -0.172 \text{ ‰}$ ) from this sample represents the primitive K isotope composition of this chondrule. Considering the analytical uncertainties and the overall range in  $\delta^{41}\text{K}$  among all Allende chondrules, our data suggests that aqueous alteration does not affect  $\delta^{41}\text{K}$  to any significant degree in Allende meteorites.

## Conclusions

Prior to this study, small fractionations between chondritic components were suspected to be caused by either the nebular chondrule formation conditions while cooling or by secondary parent body alteration. Our data, in contrast, suggest that while the latter process might have moved mobile elements such as Fe, Na, and K around, it did not fractionate K isotopes to any significant extent. Rather, the wider variation of  $\delta^{41}\text{K}$  in chondrules and matrix, compared to the bulk, likely reflects the sample heterogeneity from the nebular environment instead of secondary processes. In addition, the lack of open-system behavior for the K isotopes suggests that a closed-system or near-equilibrium environment, which is associated with a high ambient gas pressure, existed during the last chondrule formation event. Overall, the observed variations in  $\delta^{41}\text{K}$  in various chondritic components are limited, which may be the result of closed-system formation of chondrules from heterogeneous precursor materials.

In summary, our study finds that:

(1) The  $\delta^{41}\text{K}$  compositions for chondrules do not correlate with their petrologic type (*e.g.*, L4, H4) or the chondrule type (*e.g.*, Type-I, Type-II), nor do they correlate with the elemental depletion. There also appears to be no correlation between the  $\delta^{41}\text{K}$  composition and the chondrule mineralogy classification (*e.g.*, porphyritic Olivine).

(2) Allende chondrules with secondary K (CH001 and CH002 – secondary K in the rim) have  $\delta^{41}\text{K}$  values similar to the chondrule with pristine K, which implies that aqueous alteration does not affect  $\delta^{41}\text{K}$  to any significant degree.

(3) Our measurements reveal that no single  $\delta^{41}\text{K}$  value can accurately represent matrix or chondrule reservoirs. Both chondrules and matrix of ordinary and carbonaceous chondrites have

different K isotopic compositions, which implies that neither can be approximated by a common nebular component.

(4) Based on the observed wide  $\delta^{41}\text{K}$  variations from Ochansk (H4), especially in the dark components, K isotopes might be fractionated during local impact and brecciation events.

(5) The lack of Rayleigh-type fractionation between all chondritic phases, including chondrules, matrices, and the bulk, suggests that the nebula-wide thermal processing which may have depleted other volatile elements in the solar system bodies did not significantly fractionate K isotopes.

### **Acknowledgement**

This work is collaborated with Dr. Skripnik and Dr. Ivanova from Vernadsky Institute of Russian Academy of Sciences. We acknowledge Dr. Philipp R. Heck from the Field Museum for generously providing the Murchison sample (catalog number: ME2640.32) used in this work. We are also thankful to Dr. Natasha V. Krestina for preparing Allende chondrules and matrices for this study. Y. K. thanks the Harvard Origins of Life Initiative, NASA (grant number 80NSSC20K0346 to SBJ), and the DOE-NNSA (grant number DE-NA0003904 to SBJ) for supporting her graduate research.

## Chapter 5

### Conclusion

Potassium is an useful proxy in geological systems due to its volatility in high temperature nebula processes and its mobility during low temperature geological processes. Such characteristics make it a good candidate for tracing mass-dependent isotopic fractionation. Moreover, radiogenic  $^{41}\text{K}$ , arising from short-lived  $^{41}\text{Ca}$  decay, also provides valuable constraints on the precise chronology of solar system formation. This thesis includes studies of both behaviors of K, and the common theme among these studies is chondritic meteorites which bear information on early solar system formation and evolution of planetary objects.

Beyond the major scope of this thesis, K isotopes have also been studied for various differentiated planetary bodies. For example, it has been argued that the volatile depletion of eucrites, and the variations of K isotopes in Martian samples result from degassing of crystallizing magmas; on the other hand, the isotopic fractionation of K between the bulk silicate Earth (BSE) and Moon (BSM) is explained by Moon's formation impact mechanism (Wang and Jacobsen, 2016b).

One significant aspect of studying the moderate volatile elements, such as K, and their isotopes is that their elemental and the isotopic composition could help us to evaluate the high-energy impacting processes that result in volatile depletion as well as isotopic fractionations. One potential work is to test models of Moon formation.

The classic giant impact models (Canup and Asphaug, 2001) are unable to satisfactorily explain isotopic similarity between the Moon and Earth. Most dynamic simulations have shown that the Moon should be largely derived from the impactor and, therefore, the isotopic composition of the Moon is expected to be different from that of the Earth. However, the Moon and Earth are

strikingly similar in many isotopic compositions. For instance, the Moon deviates by less than 0.02‰ from the  $^{17}\text{O}/^{16}\text{O}$  terrestrial fractionation line (Wiechert et al., 2001; Spicuzza et al., 2007), and Ca and Ti isotopes, which vary among different types of chondrites and planetary bodies, have nearly identical compositions in the Moon and Earth (Simon and DePaolo, 2010; Millet et al., 2016). This needs to be explained by any Moon formation model, as it contrasts strongly with large oxygen isotope variations among other solar system bodies, such as Mars, Vesta, and chondritic meteorites. High precision measurements of isotopic compositions of moderately volatile elements will help to resolve the isotopic differences between the Moon and Earth and test the Moon forming models.

In order to better estimate the K isotopic composition in the BSM, measurements of more lunar samples, including different types from different regions and especially low-K mare basalts, are needed. My preliminary results on terrestrial crustal samples reveal variations in K isotopic compositions among terrestrial rocks (Appendix C), but it is not clear whether such variations are caused by igneous processes. Moreover, it has been shown that feldspar and plagioclase groups have heavier values of  $\delta^{41}\text{K}$  (Kuhnel et al., 2021). Therefore, the same inter-mineral isotopic fractionation during plagioclase-melt segregation should have happened in lunar rocks and such an effect must be taken into consideration.

A future work proposed is to study K isotopic compositions of more terrestrial and lunar rocks derived from various sources to obtain more representative BSE and BSM compositions. Samples, such as different mid-ocean ridge basalts from various Earth reservoirs, as well as lunar basalts of various kinds (high-Ti, low-Ti and KREEP) would be the priority work in order to (i) better constrain the K isotope fractionation magnitude between BSE and BSM, (ii) to understand whether K depletion and isotopic fractionation can be affected by large-scale magmatic activities

during planetary differentiation, and (iii) to test models of Moon formation using these new chemical and isotopic data.



# Appendix

## Appendix A

### Supporting Information for Chapter 2

#### Samples and standards

Samples studied here were dissolved completely, except for the ordinary chondrite Estacado and a separate piece of the enstatite chondrite Abee (Abee-1b). These two solutions were centrifuged and separated from the undissolved material (*e.g.*, graphite). The K isotopic composition of Estacado is similar to other ordinary chondrites; Abee-1b yielded value indistinguishable from Abee-1a (Table 1 in chapter 2).

Samples containing water soluble phases (*e.g.*, enstatite chondrites) are typically cut using ethanol or oils as a coolant. A piece of Abee (EH4) studied here was cut using oil; the surface was cleaned with ethanol in our lab. The sample Indarch-1 (EH4) is a cut-off piece with unknown handling history. The sample Indarch-2 (EH4), an internal fragment with no cut surfaces, was not treated with water during our fragmentation and crushing procedure. As our high precision K isotopic analyses detect very small variations that are not detectable before, extra caution and care are needed in interpretation of data for samples that were not directly handled in our lab. While a previous study (Zhao et al., 2019) also reported a wide range of  $\delta^{41}\text{K}$  in 8 Antarctic enstatite chondrites, we suspect that such a large variation might be, at least partially, due to improper handling of the samples prior to laboratory work. Therefore, we consider the  $\delta^{41}\text{K}$  values of  $-0.293\text{‰}$  and  $-0.333\text{‰}$  for Abee-1 and Indarch-2 to be more representative for EH chondrites as they were handled properly. MacAlpine Hills 88184 (EL3), a find from an Antarctic ice sheet, might have lost some K-bearing phases during interaction with ice and/or water; its  $\delta^{41}\text{K}$  value is  $-0.556\text{‰}$ . The sample of the EL6 chondrite Eagle, which is a cut-off piece with unknown handling

history, has a very different  $\delta^{41}\text{K}$  value of +0.082‰. Therefore, we did not discuss the group mean of EL chondrites in this paper.

The K isotopic compositions are reported relative to the Merck Suprapur (lot no. B0982265). It is a single dissolution of the 50-g sample of  $\text{KNO}_3$  dissolved in MilliQ produced water under clean lab conditions into a Teflon bottle to make sure it is homogeneous. There is no guarantee that the batches of the NIST clinical concentration standard SRM-3141a sold to different investigators are uniform in isotopic composition. Therefore, we prefer to use only our reference standard, and report values for SRM-3141a, seawater potassium, and potassium separated from the USGS BHVO-2 standard relative to our standard (Appendix A, Fig. 5 and table 1). This laboratory has determined the SRM-3141a  $\delta^{41}\text{K}$  value of  $+0.047 \pm 0.003$ ‰ relative to Merck Suprapur. Reference (Chen et al., 2019) claims that the Suprapur and SRM 3141-a have indistinguishable  $\delta^{41}\text{K}$  values, and they used them interchangeably (Zhao et al., 2019; Chen et al., 2019; Tian et al., 2019; Bloom et al., 2020) without correction.

Also, most available K isotope data for chondrites were reported relative to Suprapur [*e.g.*, (Humayun and Clayton, 1995; Wang and Jacobsen, 2016b)]. In particular, many samples measured in the current study are the same as those measured by (Wang and Jacobsen, 2016b). Although the most recent paper by Bloom et al. (2020) reports K isotope data relative to SRM-3141a and uses some of the data from (Wang and Jacobsen, 2016b), they did not take into account the discrepancy between these two standards. An additional column with  $\delta^{41}\text{K}_{\text{NIST}}$  converted values based on our measurements can be found in table 1.

The K isotopic compositions, denoted in  $\delta^{41}\text{K}$ , is defined here as recommended in (Teng et al., 2017),  $\delta^{41}\text{K}$  (‰) =  $[(^{41}\text{K}/^{39}\text{K})_{\text{sample}}/(^{41}\text{K}/^{39}\text{K})_{\text{standard}} - 1] \times 10^3$ . An alternative  $\delta$  notation without the factor of  $10^3$  has been suggested by the IUPAC for expression of stable isotope ratios

(Coplen, 2011) to avoid any confusion of ‰ added to the value, which is indeed equivalent to the one in (Teng et al., 2017). However, this work compares the  $\delta^{41}\text{K}$  data with other literature isotope data [*e.g.*, (Wang and Jacobsen, 2016b; Bloom et al., 2020)] that often have notations in  $\delta$ ,  $\epsilon$ , and  $\mu$  (Appendix A, Fig. 9). Therefore, we currently decide to use the above expression but to add additional notes of (‰) for  $\delta$ , (ppt) for  $\epsilon$ , and (ppm) for  $\mu$  to clear up any potential confusion for the readers.

### **Contamination test and the true $\delta^{41}\text{K}$ value for Orgueil**

Concentrations of both major and trace elements in each sample were measured with a quadrupole ICP-MS to check for potential terrestrial contamination. We included the elements, which are particularly enriched and common in the terrestrial crustal materials (*e.g.*, K, Rb, Nb, Cs, Ba, Th, U and the REEs) and are good indicators of contamination. No obvious contamination has been found in desert and Antarctic meteorites studied by us.

It is important to know the right  $\delta^{41}\text{K}$  value of the carbonaceous chondrite Orgueil, as it chemically represents the solar system composition. We have re-analyzed a piece of the same Orgueil fragment (labeled as Orgueil-1 here) that was analyzed before by (Wang and Jacobsen, 2016b). In the two separately dissolved aliquots of Orgueil-1, we found very high concentration of mobile and moderately volatile elements such as K, Rb, Nb, Cs, Ba, Th and U, which are often found in terrestrial upper continental crust samples. In addition, the Rare Earth Elements (REEs) are strongly fractionated and enriched in the light REEs which is also typical for terrestrial upper continental crust materials (Appendix A, Fig. 3). This shows that the Orgueil-1 sample is contaminated by terrestrial upper crustal materials (approximately 8 weight % inferred from the mass balance calculation). The K isotopic compositions of these samples also yielded terrestrial values of  $-0.512\text{‰}$  and  $-0.447\text{‰}$  (Appendix A, Fig. 4). The Orgueil-2 and Orgueil-3 samples

prepared from separate chips obtained from different sources show no signs of contamination. The REEs show no fractionation and are in chondritic abundance like other trace elements. Thus, our CI chondrite group mean  $\delta^{41}\text{K}$  of  $-0.133\text{‰}$  is based on these two clean samples.

### **Comparison of our $\delta^{41}\text{K}$ data with literature values**

We compare our K isotope data mainly with those from three studies, which analyzed CI and O-chondrites (Wang and Jacobsen, 2016b), enstatite chondrites (Zhao et al., 2019), and C- and O-chondrite (Bloom et al., 2020). We reproduced  $\delta^{41}\text{K}$  values for three ordinary chondrites that were measured in (Wang and Jacobsen, 2016b), and identified a contaminated sample of the CI chondrite Orgueil. Literature  $\delta^{41}\text{K}$  values for enstatite chondrites show a very large variability among 8 Antarctica finds with  $\delta^{41}\text{K}_{\text{suprapur}} = -0.423 \pm 0.057\text{‰}$ . On the other hand, the EH chondrites studied by us are all meteorite falls that have well-documented elemental and isotopic data.

### **Evaluating thermal processing under equilibrium and non-equilibrium conditions**

We evaluate whether K isotopic fractionation among meteorite groups can be explained by evaporation/condensation processes under either equilibrium or kinetic (non-equilibrium) conditions. In the case of equilibrium ( $P_i/P_{i,\text{sat}} = 1$ ), the isotopic composition of the condensed phase is expected to be heavier than the bulk system for both evaporation residues and condensates. The magnitude of fractionation depends on the temperature and K-bearing phases (*i.e.*, plagioclase, feldspar) (Li et al., 2019), but the K isotopic fractionation is expected to be smaller than the analytical uncertainty.

Non-equilibrium (or kinetic, usually under very low gas pressure) processes are considered as uni-directional fluxes, with fractionation factor  $\alpha = \sqrt{m_1/m_2}$  if evaporation occurs into vacuum ( $P_i/P_{i,\text{sat}} = 0$ ). Ambient gas pressure ( $P_i/P_{i,\text{sat}} \sim 1$ ) can suppress the magnitude of fractionation. The

evaporation residue would be enriched in heavier isotopes up to 22‰ (Richter et al., 2011), with the magnitude of fractionation decreasing as  $P_i/P_{i,sat}$  increases:

$$\Delta \delta^{41}\text{K}_{\text{CI-Sample}} = \Delta_{\text{kinetic}} \times (1 - P_i/P_{i,sat}) \times \ln(f) + \Delta_{\text{eq}},$$

where the kinetic fractionation  $\Delta_{\text{kinetic}}$  is -22‰, and  $f$  is the K depletion relative to the CI chondrites. When  $P_i/P_{i,sat} \sim 1$ ,  $\Delta \delta^{41}\text{K}_{\text{CI-Sample}}$  approaches an equilibrium fractionation value,  $\Delta_{\text{eq}}$  (the horizontal dotted line in Fig. 1).

During non-equilibrium condensation, the condensed phase is expected to be enriched in lighter isotopes. If in a closed system, the isotopic composition of the condensed phase will be getting progressively heavier and become equal to the starting composition when an element of interest is completely condensed. The net magnitude of fractionation, similarly to evaporation, can be suppressed by surrounding pressure. Non-equilibrium condensation can potentially explain the correlation among carbonaceous chondrites except for CI chondrites (Fig. 1), but requires the starting composition to be chemically and isotopically close to the most  $\delta^{41}\text{K}$ -rich end member (*i.e.*, CM chondrites). Thus, neither equilibrium nor non-equilibrium condensation/evaporation apparently can explain the overall nebula-wide  $\delta^{41}\text{K}$  variations.

### **Discussion of parent body processes (thermal metamorphism and aqueous alteration)**

No systematic correlations between  $\delta^{41}\text{K}$  and petrologic types (1-6) was observed. Each group of meteorites has nearly identical K isotopic composition within uncertainty (*e.g.*, H3, H5 and H6). The variability among three LL3 chondrites likely results from non-representative small sample sizes of 1 to 1.5 g (Table 1).

Aqueous alteration in the parent body could potentially alter the K isotope signature if transport of K in fluids occurred at a larger scale than the meteorite samples. This process could potentially result in a large mass-dependent fractionation of K at relative low temperature (*i.e.*,

350K). Multiple studies show that the mobility of K and some other elements follows the sequence (high to low), Cs > Rb > K > Ba > Sr during low temperature aqueous alteration (Verma, 1981). To investigate if element mobility in aqueous fluids has affected the K in the meteorites studied, we compare K and Rb concentrations in the samples (Appendix A, Fig. 7A).

CI and CM meteorites are the only classes containing substantial amounts of water, so they are expected to differ from the other C-chondrites if their bulk chemical compositions are severely affected by aqueous alteration. However, both of them as well as Earth have an essentially constant K/Rb ratio, indicating that the differences in K and Rb concentrations in carbonaceous chondrites and Earth are unlikely due to aqueous alteration, because Rb is more mobile than K. The enstatite chondrites have definitely escaped aqueous alteration as suggested by the presence of water-soluble sulfides. The highly unequilibrated ordinary (H, L, LL) chondrites of petrologic type 3 show mineralogical evidence of minor aqueous alteration on a highly localized scale that disappears as petrologic type increases. Since most of the ordinary chondrites studied in this work are equilibrated ones of petrologic types 5 and 6, the observed K isotope variations must be due to some process(es) other than aqueous alteration.

Aluminum is highly immobile during aqueous alteration and metamorphism of terrestrial igneous and sedimentary rocks, and is used as a reference immobile element for evaluating chemical data of rocks that have suffered various degree of aqueous metasomatism (Kuwatani et al., 2020). We plot  $\delta^{41}\text{K}$  with four elements, which Al and Cr are likely immobile, while Fe and Ni are mobile during aqueous alteration (Appendix A, Fig. 7B). All the plots in the Appendix A-Fig. 7B show the same pattern regardless of whether the element K is compared to is mobile or immobile.

**Calculation of variations in  $^{41}\text{K}/^{39}\text{K}$  resulting from the  $^{41}\text{Ca}$  decay in the early solar system**

Variations of  $^{41}\text{K}/^{39}\text{K}$  in meteorites could be traced back to a possible heterogeneous distribution of  $^{41}\text{Ca}$  as  $^{41}\text{K}$  is the decay product of this radionuclide. Short-lived isotope  $^{41}\text{Ca}$  can be made through secondary thermal neutron capture, *in situ* irradiation in the early solar system, or the *s*-process (Ramaty et al., 1996). *In situ* irradiation could produce  $^{41}\text{Ca}$  in the solar nebula by non-thermal nuclear reactions between energetic charged particles and gas or/and solid targets (Lee et al., 1998; Gounelle et al., 2001). The thermal neutron capture processes ( $^{40}\text{Ca} + n \rightarrow ^{41}\text{Ca}$ ) are unlikely to explain a nearly 0.5‰ fractionation since the reactions are limited to the surfaces of meteorites and require an environment with very high density of neutrons. Also,  $^{41}\text{Ca}$  can be synthesized via the *s*-process in stars. Such scenarios imply that the live  $^{41}\text{Ca}$  found in CAIs (Goswami, 1998) could have formed in the solar system, or been injected by stellar winds (*e.g.*, originating from a Wolf-Rayet star). We evaluate how much  $^{41}\text{K}$  excesses in CAIs due to  $^{41}\text{Ca}$  decay can contribute to observed  $^{41}\text{K}/^{39}\text{K}$  variations among different meteorites, especially chondrites, by a simplified two-component (CAIs and matrix) mixing model. Due to the very low abundance (Liu et al., 2012) and short half-life of  $^{41}\text{Ca}$ , there is barely any live  $^{41}\text{Ca}$  left in them by the time of chondrule formation (Bollard et al., 2017).

To determine the  $^{41}\text{K}/^{39}\text{K}$  ratio in CAIs, we first calculated the contribution of each K isotope to the total K amount in CAIs ( $K_{\text{tot}}$ ) as follows:

$$K_{\text{tot}} = ^{39}\text{K} + ^{40}\text{K} + ^{41}\text{K} + ^{41}\text{K}^* \quad (1),$$

where  $^{41}\text{K}^*$  is radiogenic  $^{41}\text{K}$ , the decay product of  $^{41}\text{Ca}$ .

Here we neglect  $^{40}\text{K}$  because of its extremely low abundance (0.012%) and replace stable  $^{41}\text{K}$  with  $0.072 \times ^{39}\text{K}$ :

$$K_{\text{tot}} = ^{39}\text{K} + 0.072 \times ^{39}\text{K} + ^{41}\text{K}^* \quad (2).$$



The  $^{41}\text{K}^*$  can be estimated from the  $^{41}\text{Ca}$  concentration in CAIs using the total Ca concentration ( $\text{Ca}_{\text{tot}}$ ) and the initial  $^{41}\text{Ca}/^{40}\text{Ca}$  ratio,  $[\text{}^{41}\text{Ca}/^{40}\text{Ca}]_i$ :

$$^{41}\text{K}^* = ^{41}\text{Ca} = \text{Ca}_{\text{tot}} \times 0.97 \left( ^{40}\text{Ca} / \text{Ca}_{\text{tot}} \right) \times [\text{}^{41}\text{Ca}/^{40}\text{Ca}]_i \quad (3),$$

where the atomic ratio  $[\text{}^{41}\text{Ca}/^{40}\text{Ca}]_i = 4.2 \times 10^{-9}$ , data from (Liu et al., 2012); and  $\text{Ca}_{\text{tot}} = 222455$  ppm (mean of 10 CAIs) (Sylvester et al., 1993), corresponding to a  $^{41}\text{Ca}$  atomic abundance of  $1.36 \times 10^{13} \text{ g}^{-1}$ .

The total K ( $\text{K}_{\text{tot}}$ ) concentration of 34.5 ppm in CAIs (mean of 9 CAIs)(Sylvester et al., 1993), corresponding to a  $^{41}\text{K}$  atomic abundance of  $5.31 \times 10^{17} \text{ g}^{-1}$ , translates to the  $^{41}\text{K}$  ( $0.72 \times ^{39}\text{K} + ^{41}\text{K}^*$ )/ $^{39}\text{K}$  ratio =  $7.203 \times 10^{-2}$  (eq. 2) in CAIs, which results in  $\delta^{41}\text{K}^*_{\text{CAI}} = 0.382\%$  where we define  $\delta^{41}\text{K}^*$  as radiogenic  $^{41}\text{K}^*$  excess compared to matrix ( $\delta^{41}\text{K}^*_{\text{matrix}} = 0$ ).

The highest estimates of CAI abundances in carbonaceous (CV) and ordinary chondrites are 10 vol% and 0.1 vol% (Scott and Krot, 2003), with K concentration in bulk meteorites of 310 ppm and 798 ppm (Alexander, 2019a, b), respectively. Factors ( $F_K$ ) of K distribution in the CAIs compared to the bulk K are 1.113% and 0.004%, so  $\delta^{41}\text{K}^*_{\text{chondrite}}$  in each sample can be calculated as follows:

$$\delta^{41}\text{K}^*_{\text{chondrite}} = \delta^{41}\text{K}^*_{\text{CAI}} \times F_K + \delta^{41}\text{K}^*_{\text{matrix}} \times (1 - F_K) \quad (4).$$

where  $\delta^{41}\text{K}^*_{\text{matrix}} = 0$  because of assuming no  $^{41}\text{K}^*$  excess.

The resulting  $\delta^{41}\text{K}^*_{\text{CV}} = 0.0042\%$  and  $\delta^{41}\text{K}^*_{\text{ordinary chondrites}} = 0.000016\%$  are too small to explain the observed differences in  $\delta^{41}\text{K}$  ( $\sim 0.5\%$ ). In fact, due to the very different bulk K concentrations in CAIs and matrix, a chondrite fragment containing 99% CAIs can only yield a  $\sim 0.065\%$  difference in  $\delta^{41}\text{K}$  compared to matrix.

Thus, we concluded that the  $^{41}\text{K}^*$  from the decay of live  $^{41}\text{Ca}$  in CAI cannot account for the observed K isotopic variations in meteorites, which points to an explanation of a heterogeneous distribution of  $^{41}\text{K}$  before the solar nebula formation.

Based on the calculation in the Appendix, we converted the  $\delta^{41}\text{K}^*$  (excess from  $^{41}\text{K}^*$ ) to  $\delta^{41}\text{K}$  assuming CI chondrites represents the  $\delta^{41}\text{K}$  value of the matrix component. Thus,  $\delta^{41}\text{K}^*_{\text{matrix}} = 0$  becomes  $\delta^{41}\text{K}_{\text{matrix}} = -0.133\text{‰}$  (CI chondrites), and  $\delta^{41}\text{K}^*_{\text{CAI}} = 0.382\text{‰}$  becomes  $\delta^{41}\text{K}_{\text{CAI}} = 0.249\text{‰}$ . This value was used in the modified three-component mixing regions shown in Fig. 2 and the Appendix A Fig. 8.

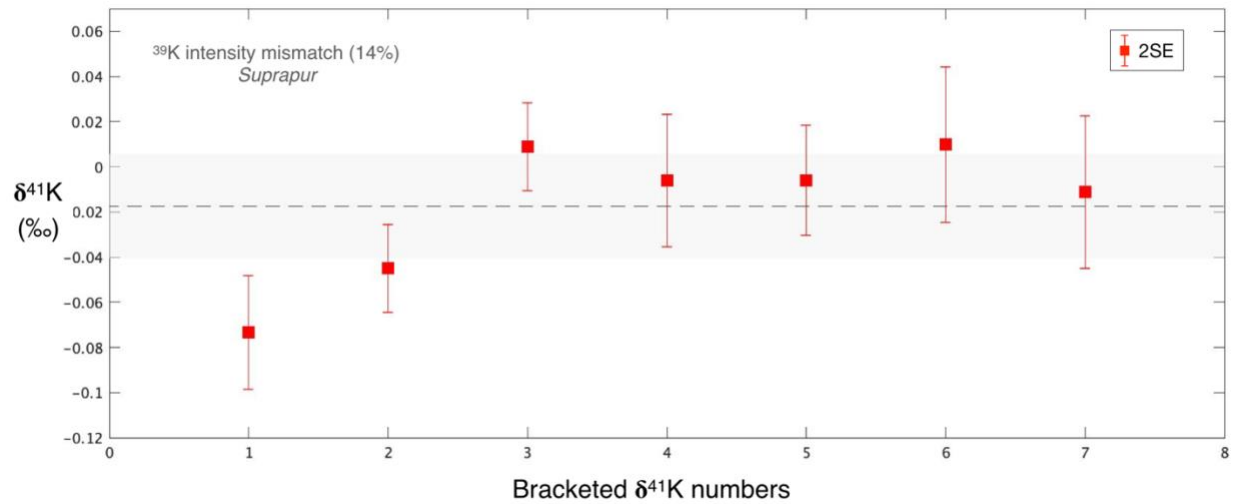


**Figure 1. Standard mismatching with one analytical run.** We made one  $^{39}\text{K}$  intensity-mismatch solution in each run along with other samples to monitor the quality of data (reported in Table 1). One example of a standard solution with 14%  $^{39}\text{K}$  intensity-mismatch has the mean  $\delta^{41}\text{K}$  value of  $-0.017 \pm 0.023\%$  (2SE) from one analytical run.

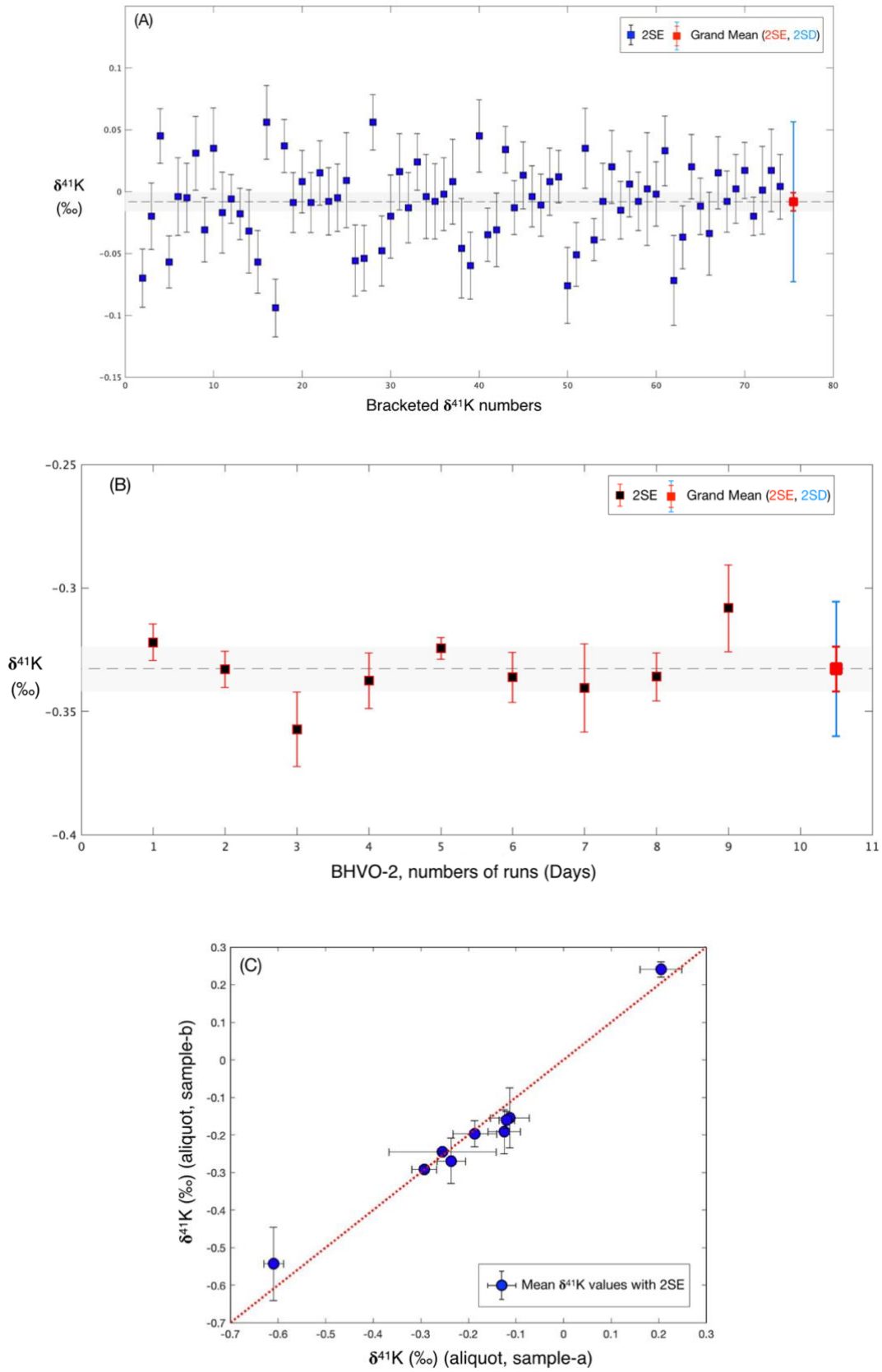


**Figure 2. Analytical internal uncertainties and external reproducibility.** (A) Within-run uncertainty (internal). We estimate a within-run uncertainty by calculating the standard deviation (SD) and standard error (SE) of standard self-bracketing within an analytical run. Data from each bracketed number are shown as blue squares with uncertainties (2SE) in black. The variation (2SD) is 65 ppm, and the corresponding uncertainty for a sample is 30 ppm (5 repeats). Note that the uncertainty shown here (in red) are the calculated 2SE based on the 73 self-bracketing numbers. (B) Day-to-day instrument variability (external). We estimate the instrument day-to-day variability by calculating the SD and the corresponding SE from multiple days' measurements of a single analytical aliquot. Data from each day are shown as black squares with uncertainties (2SE) in red. This reflects only instrument variability, as each data point represents a  $\delta^{41}\text{K}$  value measured from a single aliquot. The calculated variation (2SD) is 27 ppm and the uncertainty (2SE) is 9 ppm. The first eight  $\delta^{41}\text{K}$  values plotted from BHVO-2 were measured from October-December 2018, and the last  $\delta^{41}\text{K}$  value was analyzed in October 2019. (C) Comparison of sample powder aliquots, a and b, of nine meteorites. Aliquots a and b were dissolved and separated through column chemistry independently. Each aliquot was analyzed on different days on the ICP-MS. The data points are the mean  $\delta^{41}\text{K}$  from multiple days ( $N$ ) for each aliquot, shown as blue circles with two-sigma uncertainties (2SE); all are within error with the 1:1 line, showing that the uncertainties due to column chemistry and dissolution processes are negligible, and the instrument performance is sufficient for reproducibility. Samples plotted here include: Orgueil-2, Murray, Mighei, Murchison, Allende-1, Vigarano, Abee, Indarch-1, and Tuxuac (Table 1).

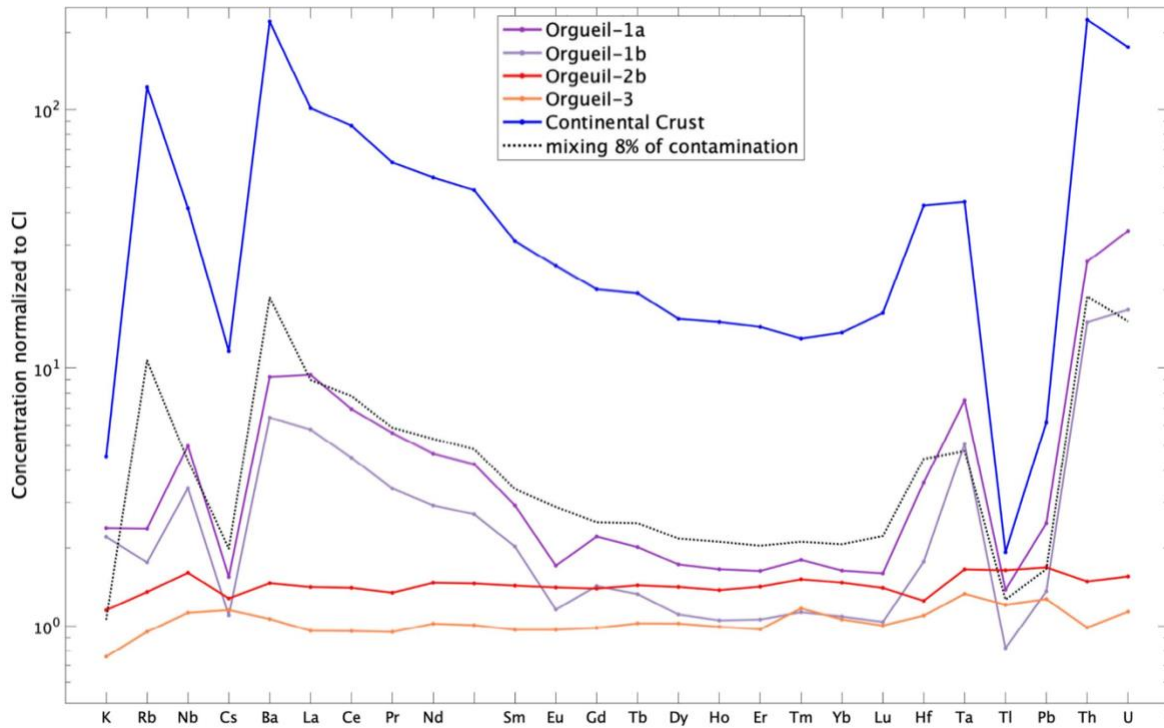


**Figure 3. Elemental composition of the studied samples of the CI chondrite Orgueil.** Two aliquots of a coarsely crushed Orgueil-1 sample shown in purple lines, which are the same materials as in (Wang and Jacobsen, 2016b), have fractionated elemental patterns similar to that of the continental crust (Rudnick and Gao, 2003), shown in heavy blue line. The mass balance calculation suggests that the sample is contaminated by ~8 wt % terrestrial crustal materials (dotted black line). Flat elemental patterns of the Orgueil-2 and Orgueil-3 samples (red and orange lines, respectively), made from separate chips, show no signs of contamination.

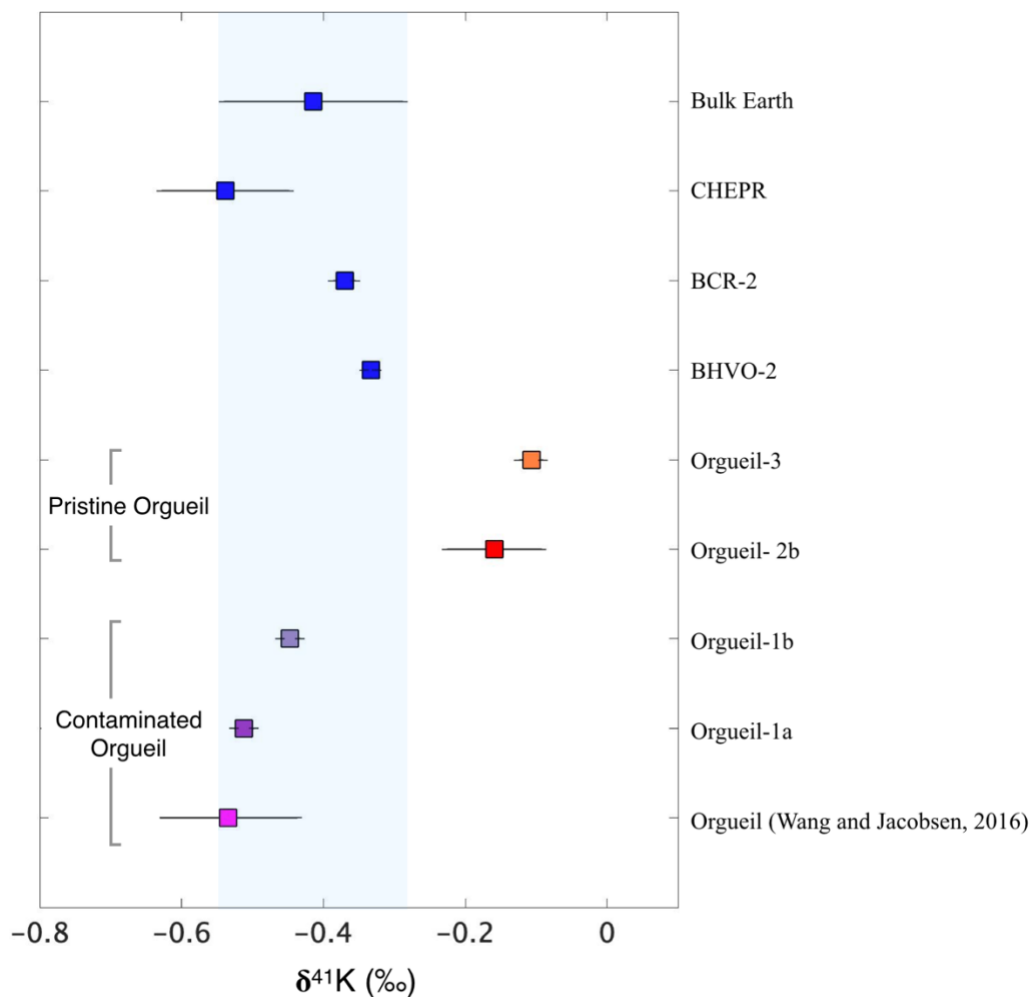


**Figure 4. The K isotopic compositions of the contaminated Orgueil samples and other reference samples.** Orgueil-2 and Orgueil-3 have similar  $\delta^{41}\text{K}$  values, both of which notably differ from Orgueil-1. The latter plots within the terrestrial range (in shaded blue), consistent with the terrestrial contamination inferred from the elemental pattern (Appendix A, Fig. 3).

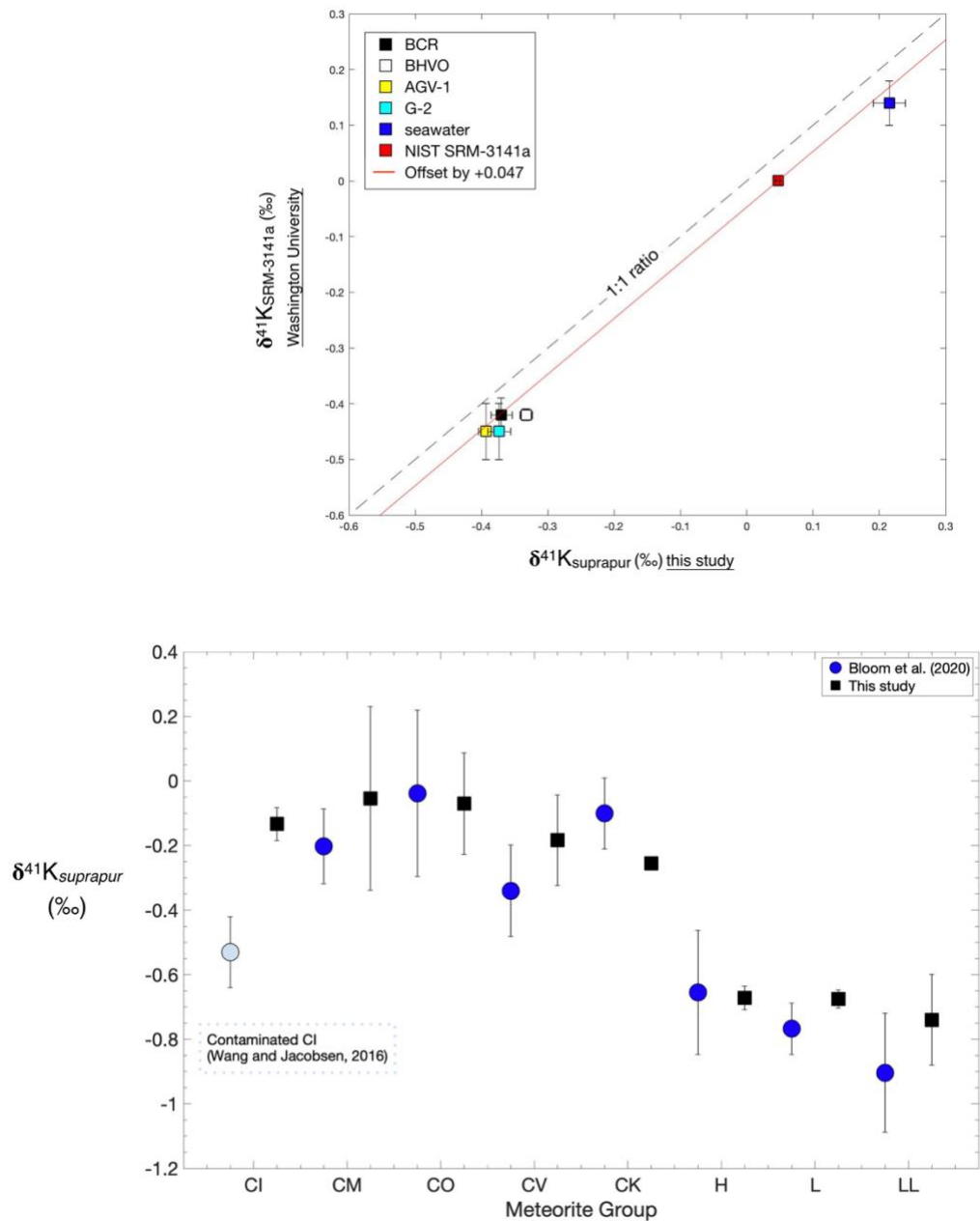


**Figure 5.  $\delta^{41}\text{K}$  comparison with the literature.** (Top) Comparison of common rock and seawater samples between (Hu et al., 2018) and this study. It shows a  $\sim 0.047\text{‰}$  shift between Suprapur and NIST SRM-3141a standards. The additional USGS measurements can be found in table S1. (Bottom) The K isotopic compositions of each meteorite group in this study compared to Bloom et al. (2020).



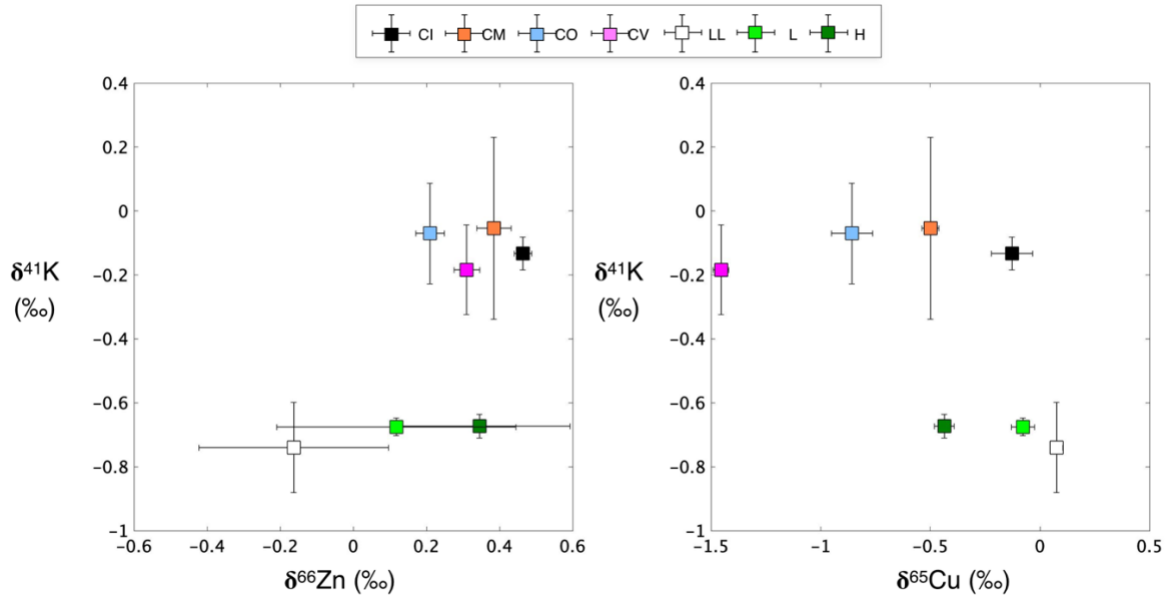


**Figure 6. Comparison of  $\delta^{41}\text{K}$  with other MVEs:  $\delta^{41}\text{K}-\delta^{66}\text{Zn}$  and  $\delta^{41}\text{K}-\delta^{66}\text{Cu}$ .** K, Zn and Cu are all moderately volatile elements, with  $T_c$  (50% condensation temperature) of 1006K, 726 K, and 1037 K, respectively. However, there are no correlations indicating similar behaviors among them. This suggests the main mechanisms to explain the isotope variation among the three elements are different. A similar conclusion and plots can be found in Bloom et al. (2020) and  $\delta^{66}\text{Zn}$   $\delta^{66}\text{Cu}$  are from previous work (Luck et al., 2003, 2005).

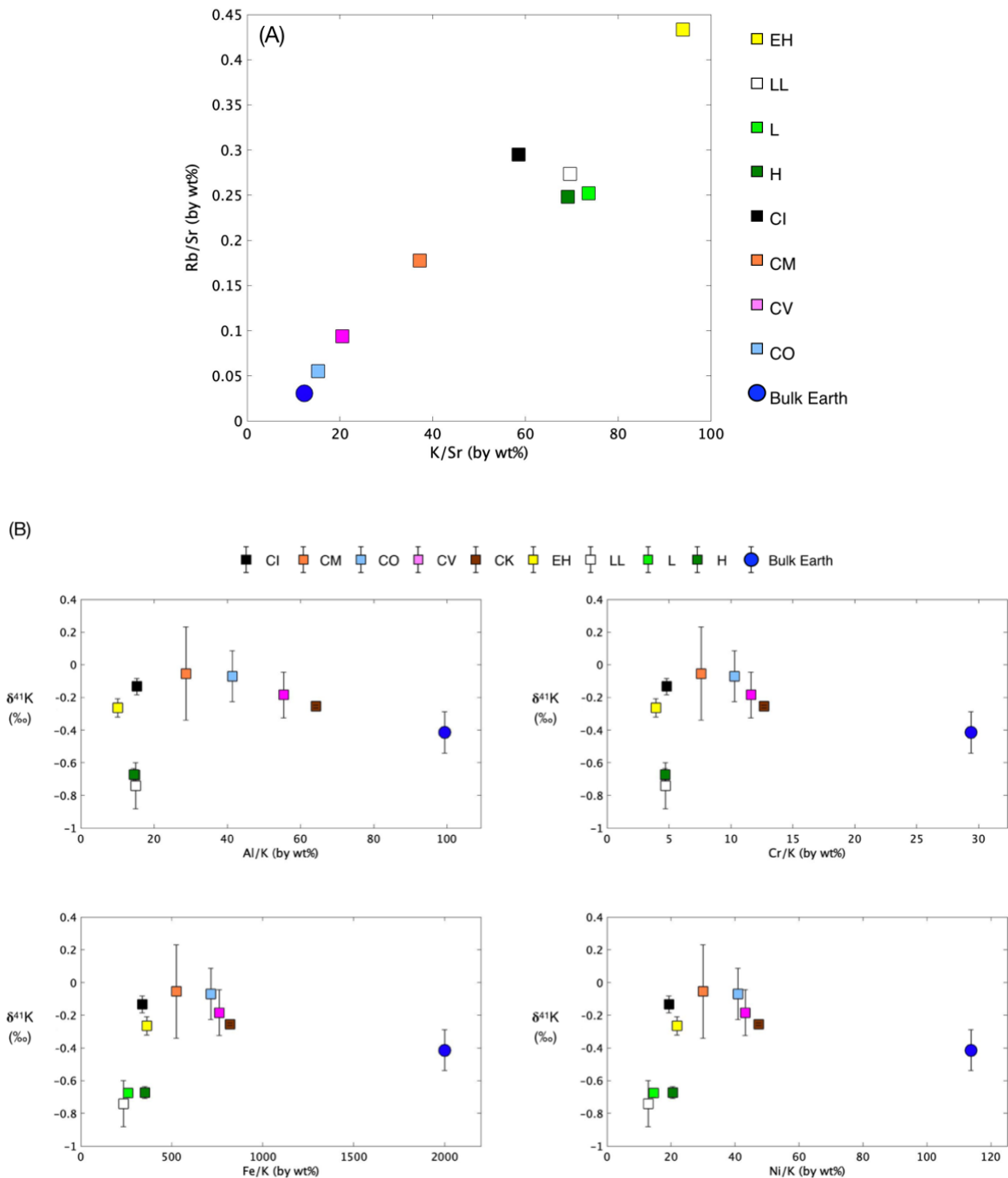


**Figure 7. Evaluation of parent body processes.** (A) The comparison of K-Rb concentrations normalized to Sr in different chondrite groups studied in this work and for the Earth (McDonough, 2003). This shows that the Earth and carbonaceous chondrites lie on a line with essentially constant K/Rb ratio, and thus, it's unlikely that the differences in K and Rb concentrations in carbonaceous

chondrites and Earth are due to aqueous alteration. (B) Plots of  $\delta^{41}\text{K}$  vs Al/K, Cr/K, Fe/K and Ni/K in different chondrite groups and Earth. Figure 1 of our manuscript shows a similar plot of  $\delta^{41}\text{K}$  vs Ca/K. Calcium is mobile during aqueous alteration (Ca, Fe-rich rims are abundant in carbonaceous chondrites). The coherent patterns among all plots regardless the mobility of elements, suggests that  $\delta^{41}\text{K}$  is not affected by any observable aqueous alteration. The elemental concentrations in each group are taken from literature (McDonough, 2003; Taylor, 2013; Alexander, 2019a, b).

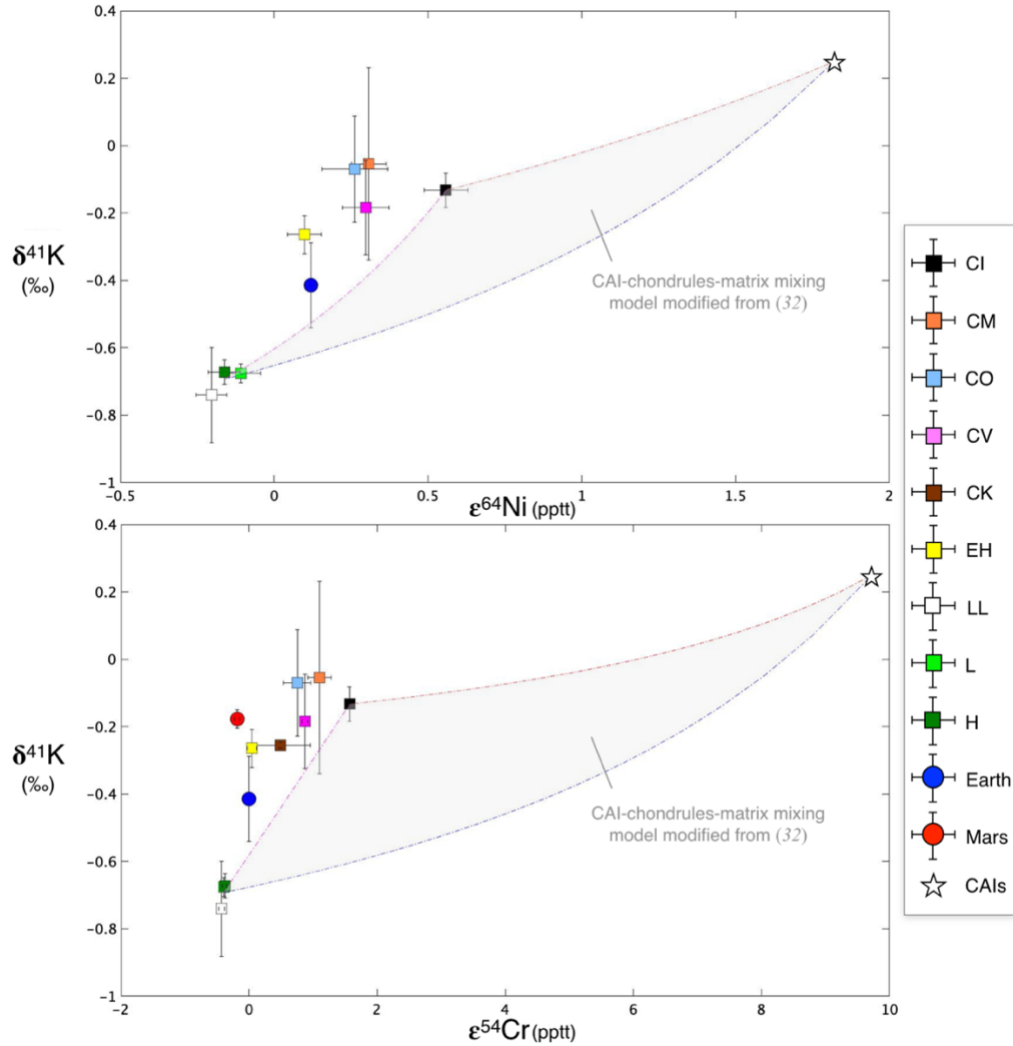


**Figure 8. Three-component mixing fields of CAIs, chondrules, and matrix of  $\delta^{41}\text{K}$ ,  $\epsilon^{64}\text{Ni}$  and  $\epsilon^{54}\text{Cr}$  modified from a previous work (Alexander, 2019a).** The mixing regions shows that none of the samples are the mixture of these three components, implying that mixing between multi-major chondrite components cannot explain the K isotope variations. The individual  $\epsilon^{64}\text{Ni}$  and  $\epsilon^{54}\text{Cr}$  values used for calculating group means are from the literature (Shukolyukov and Lugmair, 2006; Regelous et al., 2008; Dauphas et al., 2008; Trinquier et al., 2009; Qin et al., 2010; Larsen et al., 2011; Steele et al., 2012; Tang and Dauphas, 2012, 2014; Schiller et al., 2014; Göpel et al., 2015). Details of the estimation of  $\delta^{41}\text{K}$  for CAIs are discussed in the Appendix.

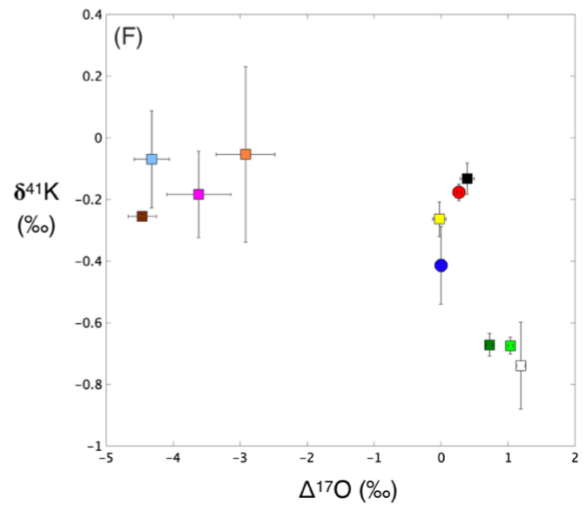
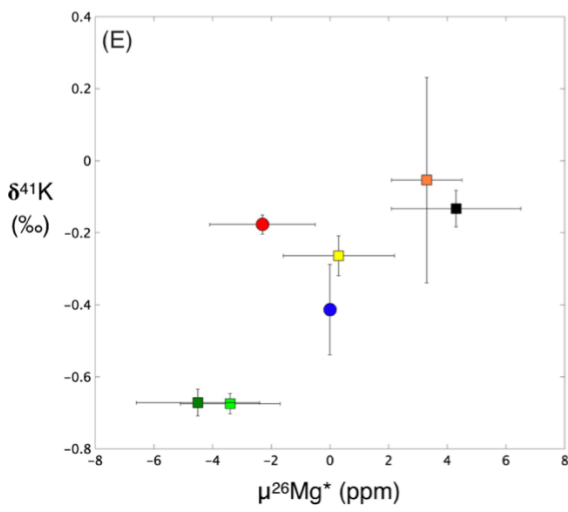
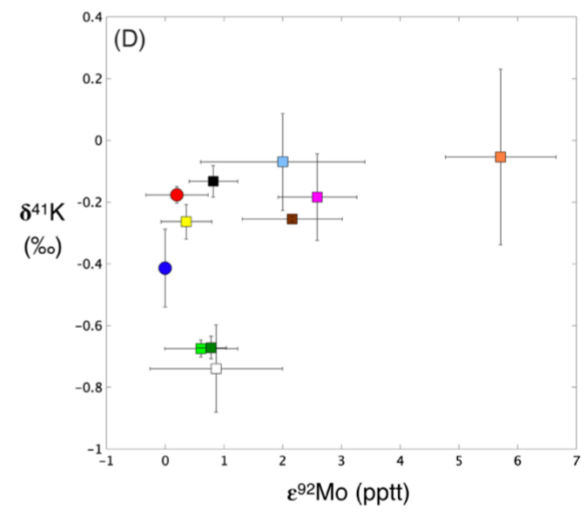
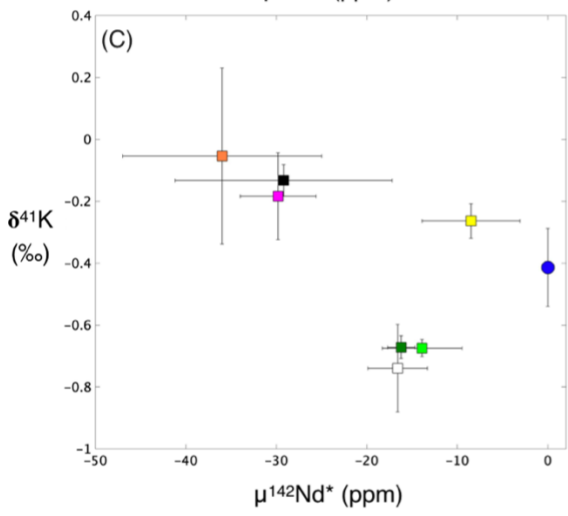
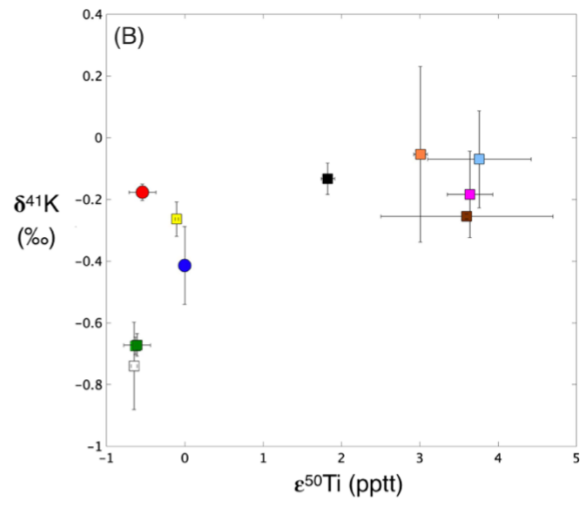
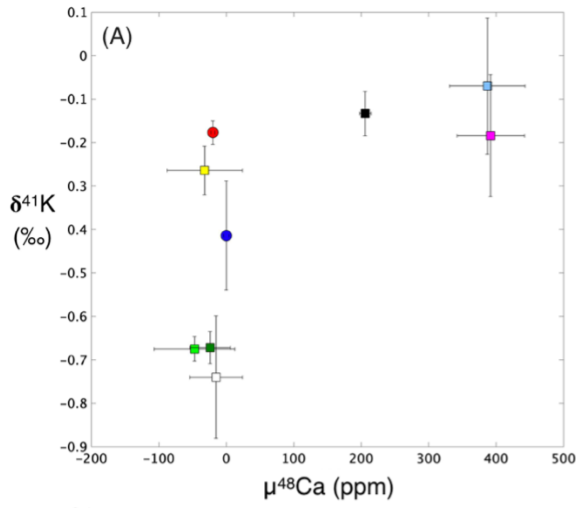


**Figure 9. Mean values for  $\delta^{41}\text{K}$  plotted with various nuclides for each meteorite group (Dauphas, 2017).** (A) (B) The correlation of  $\mu^{48}\text{Ca}$  and  $\varepsilon^{50}\text{Ti}$  with  $\delta^{41}\text{K}$  might be affected by the different concentration in CAIs. Ti and Ca are enriched in CAIs compared to K. The individual  $\mu^{48}\text{Ca}$  and  $\varepsilon^{50}\text{Ti}$  values used for calculating group means are from the literature (Trinquier et al., 2009; Zhang et al., 2011, 2012; Chen et al., 2011; Dauphas et al., 2014; Schiller et al., 2015, 2018). (C) A correlation among carbonaceous, enstatite chondrites, and Earth is shown between  $\delta^{41}\text{K}$  and  $\mu^{142}\text{Nd}^*$ , the product of  $^{146}\text{Sm}$  decay. Ordinary chondrites have intermediate  $\mu^{142}\text{Nd}^*$  values between carbonaceous chondrites and Earth. Note that, Earth, in this case, is an end member which has the most positive  $\mu^{142}\text{Nd}^*$  values. (D) Similar to  $\mu^{142}\text{Nd}^*$ , Earth is an end member in this  $\delta^{41}\text{K}$ – $\varepsilon^{92}\text{Mo}$  plot: it has the most negative  $\varepsilon^{92}\text{Mo}$  value. Both (C) and (D) might imply that the stellar sources of  $\mu^{142}\text{Nd}^*$  and  $\varepsilon^{92}\text{Mo}$  are distinct from  $\delta^{41}\text{K}$ ,  $\varepsilon^{64}\text{Ni}$  and  $\varepsilon^{54}\text{Cr}$ , since Earth has an intermediate isotopic composition in  $\delta^{41}\text{K}$ ,  $\varepsilon^{64}\text{Ni}$  and  $\varepsilon^{54}\text{Cr}$ . There must be more than two nucleosynthetic components in the solar system to explain the different end members between the  $\delta^{41}\text{K}$ – $\varepsilon^{64}\text{Ni}$  ( $\delta^{41}\text{K}$ – $\varepsilon^{54}\text{Cr}$ ) and  $\delta^{41}\text{K}$ – $\mu^{142}\text{Nd}^*$  ( $\delta^{41}\text{K}$ – $\varepsilon^{92}\text{Mo}$ ) plots. The individual  $^{142}\text{Nd}^*$  and  $\varepsilon^{92}\text{Mo}$  values used for calculating groups means are from the literature (Dauphas et al., 2002a, b; Boyet and Carlson, 2005; Rankenburg et al., 2006; Andreasen and Sharma, 2006; Carlson et al., 2007; Bouvier et al., 2008; Boyet et al., 2010; Gannoun et al., 2011; Burkhardt et al., 2011, 2014, 2016; Sprung et al., 2013; Bouvier and Boyet, 2016). (E) A broad correlation between  $\delta^{41}\text{K}$  and  $\mu^{26}\text{Mg}^*$  (decay product of extinct  $^{26}\text{Al}$ ) hints at a common source of  $^{41}\text{K}$  and  $^{26}\text{Mg}$ . The individual  $\mu^{26}\text{Mg}^*$  values are from the literature (Larsen et al., 2011; Van Kooten et al., 2016). (F) There are three main clusters: lower  $\Delta^{17}\text{O}$  and higher  $\delta^{41}\text{K}$  in carbonaceous chondrite (except CI chondrites), intermediate values in planetary bodies, enstatite chondrites, and CI chondrites, and higher  $\Delta^{17}\text{O}$  and lower  $\delta^{41}\text{K}$  value. The origins of  $\Delta^{17}\text{O}$  anomalies might involve more than two nucleosynthetic

components. The individual  $\Delta^{17}\text{O}$  values for each group are from the literature (Clayton et al., 1976, 1981, 1984a, b, 1991, 1997; Clayton and Mayeda, 1977, 1984, 1985, 1996, 1999; Mayeda et al., 1983, 1987, 1989, 1995; Onuma et al., 1983; Halbout et al., 1984, 1986; Recca et al., 1986; Grady et al., 1987; Grossman et al., 1987; Brearley et al., 1989; Zolensky et al., 1989, 1997; Sears et al., 1990; Bischoff et al., 1991; Franchi et al., 1992, 1999; Keller et al., 1994; Rowe et al., 1994; Ruzicka et al., 1995; Simon et al., 1995; Weber et al., 1996; Bridges et al., 1997, 1999; Weisberg et al., 1997; Romanek et al., 1998; Jabeen et al., 1998; Young and Russell, 1998; Young et al., 2016).

**Table 1.**  
Additional  $\delta^{41}\text{K}$  measurements for USGS standards.

Group	Sample	Type	$\delta^{41}\text{K}_{\text{Suprapur}}$ (‰)	$\pm 2\text{SE}$	$N$	$n$	Sources	$\delta^{41}\text{K}_{\text{SRM-3141a}}$ (‰)
Earth	AGV-1	Basalt	-0.393	0.012	1	6	USGS	-0.440
	G-2	Granite	-0.373	0.017	5	23	USGS	-0.420
	seawater		0.215	0.014	15	64		0.168

*NIST* SRM-3141-a was measured with respect to *Suprapur* =  $+0.047 \pm 0.003\text{‰}$

The uncertainty (2SE) is calculated based on  $N$  days of analyses; the internal analytical uncertainty is 30 ppm.

$N$ : numbers of independent analytical runs.

$n$ : total number of the bracketed  $\delta^{41}\text{K}$  values from  $N$  days.



## Appendix B

### Supporting Information for Chapter 3

#### Samples

We analyzed 6 samples – one matrix (Mx), one chondrule (CH001), and four CAIs (3 chips of SJ101 and whole CH007). Mineralogy and mineral chemistry of CH001 and CH007 were studied by EPMA/SEM techniques using the JXA-8230 electron microprobe at Harvard University. Detailed petrologic and chemical studies of the SJ101 CAI have also been done earlier by Petaev and Jacobsen (2009). The SJ101 CAI is a very large ( $\sim 2.5 \times 1.5$  cm in size, 6.34 g) forsterite-bearing Type B (FoB) CAI that consists of several igneous lithologies representing multiple spinel-melilite-anorthite-clinopyroxene-bearing CAIs of previous generations ‘glued’ together by forsterite-clinopyroxene bands of variable thicknesses. The latter were formed by the melting of forsterite-rich rims and adjacent portions of primary CAIs while the CAIs’ cores have remained solid. The type II REE pattern of SJ101 (Fig. 4) points to a condensation origin of its precursors while the lack of Si and Mg isotope fractionations rules out an evaporative loss of these elements during the last melting episode. Secondary alteration involving exchange of Ca, Si, Fe, Na and Cl between the matrix, chondrules and CAIs, typical for many Allende samples, is very minor and affects only limited areas in the melilite. The three dissolved samples (A, B and C) are fresh chips from the interior of the inclusion.

The CH001 chondrule, a nearly ideal spherule of  $\sim 3$  mm across weighing  $\sim 15$  mg, was mounted in epoxy and sliced off-center; the smaller chip was used for preparation of a polished thin section. The larger chip (8.8 mg) after extraction from epoxy and thorough cleaning was powdered and used for K isotope analysis. The epoxy was analyzed and found to contain

insignificant K. The chondrule consists mainly of groundmass of intergrown anorthite (< 1 wt% Na<sub>2</sub>O, no detectable K<sub>2</sub>O) and Al-diopside laths and minor forsterite that encloses clusters of large forsterite (<1 wt% FeO) or spinel (<1 wt% FeO and Cr<sub>2</sub>O<sub>3</sub>) or Fe,Ni sulfide grains (Fig. 5). The chondrule exhibits an alteration rind of variable thickness where the anorthite is nearly completely replaced by sodalite or nepheline, or both, and olivine and spinel grains show significant outward increase in FeO contents. The alteration rind is enriched in Na and K by ~2× compared to the central unaltered part of the chondrule.

The rounded polyhedral sample CH007 (19.1 mg) was imaged intact (Fig. 6) in order to save material and classified as a fragment of a Type B1 CAI with a pronounced melilite mantle and clear Wark-Lovering rim. The CAI is partially covered by adhered fine-grained Mg-rich material mainly filling the depressions on the sample surface (Fig. 6a). The core consists of gehlenitic melilite and Al, Ti-rich clinopyroxene both enclosing euhedral spinel grains (Fig. 6b,d). The melilite of the rim is enriched in Al and depleted in Mg and Si compared to the core melilite. The Wark-Lovering rim is partially replaced by secondary sodalite and nepheline as suggested by the presence of Na and Cl. An area at the CAI edge not covered by matrix (Fig. 6c,d) shows only minor secondary alteration of melilite along grain boundaries and/or cleavage cracks (Fig. 6d). This clean area (Fig. 6d) has much lower Na and K concentrations compared to the bulk. This could suggest that the higher Na and K concentrations in the bulk CAI are due to addition of the matrix to the CAI material, however the plots in figure 2 suggests that such an effect must be rather minimal.

The Allende whole rock sample was prepared by powdering a 34 g chunk of the meteorite. The Allende sample matrix was separated by sequential sieving of a crushed 43 g sample fragmented by the SELFRAG company. All samples were carefully handpicked under a binocular

microscope and sonicated in ethanol to further ensure their purity. The finest fraction (<23  $\mu\text{m}$ ) weighing 107 mg contains no visible chondrule fragments.

### **K Isotope Analytical Methods and Data**

Aliquots (10-40 mg) of the matrix as well as chondrule and CAI powders were dissolved in multiple steps using mixtures of concentrated HF, HCl and HNO<sub>3</sub>. The first step requires adding a mixture of 0.5 mL HF, 2 mL HNO<sub>3</sub>, and 1 mL HCl acids, which was then heated to 160°C on a hotplate for a day. For the second dissolution step, the resulting solutions were dried down, and a mixture of 2 mL HNO<sub>3</sub>, 6 mL HCl, and 1 mL purified MQ H<sub>2</sub>O was added to Teflon coated EasyPrep vessels for high-temperature and high-pressure dissolution applications. The samples were then repeatedly heated to 210°C in a CEM MARS 6 microwave digestion system. After complete digestion, the aliquots were re-dissolved in a dilute 0.5N HNO<sub>3</sub> solution for K ion-exchange column chemistry.

To separate K, the bulk solutions were loaded into 13 mL fused silica chromatography columns filled with Bio-Rad AG50W-X8 cation-exchange resin (100-200 mesh) using our established procedure (Ku and Jacobsen, 2020). Here, all samples were passed through the columns 3 times in order to purify the K-cuts (> 99% yield). The K solutions were then dried down and re-dissolved in dilute HNO<sub>3</sub> (~2%) for MC-ICP-MS analysis.

Potassium (K) isotopes were measured at Harvard University using a multi-collector ICP-MS Nu Sapphire (serial #SP001) that is equipped with a hexapole collision cell to eliminate mass interference from Ar-bearing ions such as ArH<sup>+</sup>, Ar<sup>+</sup>, and ArO<sup>+</sup>. The samples and standard were matched for <sup>39</sup>K intensity to within 1%. The measured K isotope values are expressed relative to our lab standard, a batch of Merck KgaA high-purity KNO<sub>3</sub> Merk Suprapur:

$$\delta^{41}\text{K} (\text{‰}) = [(\delta^{41/39}\text{K}_{\text{sample}}) / \delta^{41/39}\text{K}_{\text{Suprapur}} - 1] \times 10^3.$$

As K solutions could be contaminated with very small amounts of Ca, we corrected for any possible Ca-related interference on mass 41 ( $^{41}\text{K}$ ), such as Ca-hydride  $^{41}({}^{40}\text{CaH}^+)$ , of both sample and standard solutions. The amount of correction is inferred from monitoring mass 40 intensity, and is calculated based on the difference in 41/39 ratios between a Ca-spiked and unspiked standard solutions:

$${}^{41}\text{CaH}/{}^{40}\text{Ca} = ({}^{41/39}\text{R}_{\text{Ca-spiked}} - {}^{41/39}\text{R}_{\text{standard}}) / ({}^{40/39}\text{R}_{\text{Ca-spiked}} - {}^{40/39}\text{R}_{\text{standard}}),$$

where  ${}^{41/39}\text{R}_{\text{spiked-solution}}$  is the ratio of intensity in mass 41 to mass 39 after subtracting the blank. Thus, the excess in  ${}^{41/39}\text{K}$  caused by Ca-related species can be expressed as

$$\delta^{41}\text{K}_{\text{error}} = \{ [({}^{41}\text{K} + {}^{41}\text{CaH}) / {}^{39}\text{K}]_{\text{measured}} - ({}^{41}\text{K} / {}^{39}\text{K})_{\text{real}} \} / ({}^{41}\text{K} / {}^{39}\text{K})_{\text{standard}} \times 10^3,$$

so the real  $\delta^{41}\text{K}_{\text{real}} = \delta^{41}\text{K}_{\text{measured}} - ({}^{40/41}\text{R}_{\text{sample}} \times {}^{41}\text{CaH}/{}^{40}\text{Ca} \times 10^3)$ . The formation of  $^{41}({}^{40}\text{CaH}^+)$  is also described in the literature (Moynier et al., 2021). Additionally, for each analytical run we monitored the matrix effect arising from concentration mismatch among solutions by analyzing an extra standard solution with up to 15% concentration mismatch. The data reported here are obtained from analytical runs where the  $\delta^{41}\text{K}$  values from the ‘mismatched’ standard are less than 0.05 (Ku and Jacobsen, 2020).

We used an uncertainty of 0.03‰ in the K isotope data of each sample, that was established following the experimental, chemical, and instrumental procedures used in Ku and Jacobsen, 2020 (Ku and Jacobsen, 2020). The within-run uncertainty of 0.03‰ is the calculated standard error ( $2\sigma_m$ ) of a K standard solution that was repeatedly measured within an analytical run, and the

external reproducibility of 0.027‰ is the calculated variation obtained by measuring a rock sample, BHVO-2, repeatedly on different days. The consistency between the two values implies that no additional variability of dissolution or column chemistry was present in the data, so we used the former value as the best estimate of the analytical uncertainty for each sample.

### Calculation of initial $^{41}\text{Ca}/^{40}\text{Ca}$ from $^{41}\text{Ca} - ^{41}\text{K}$ isochrons in figure 1

The equation for a  $^{41}\text{Ca}-^{41}\text{K}$  fossil isochron is:

$$\left(\frac{^{41}\text{K}}{^{39}\text{K}}\right)_{meas} = \left(\frac{^{41}\text{K}}{^{39}\text{K}}\right)_{initial} + \left(\frac{^{41}\text{Ca}}{^{40}\text{Ca}}\right)_{initial} \left(\frac{^{40}\text{Ca}}{^{39}\text{K}}\right)_{meas}$$

This equation can be converted to use  $\delta^{41}\text{K}$ -values by using:

$$\delta^{41}\text{K}_{meas} = \left[ \frac{\left(\frac{^{41}\text{K}}{^{39}\text{K}}\right)_{meas}}{\left(\frac{^{41}\text{K}}{^{39}\text{K}}\right)_{std}} - 1 \right] \times 10^3$$

Thus, in this notation the fossil isochron is:

$$\delta^{41}\text{K}_{meas} = \delta^{41}\text{K}_{initial} + \left[ \frac{10^3}{\left(\frac{^{41}\text{K}}{^{39}\text{K}}\right)_{std}} \right] \left(\frac{^{41}\text{Ca}}{^{40}\text{Ca}}\right)_{initial} \left(\frac{^{40}\text{Ca}}{^{39}\text{K}}\right)_{meas}$$

The value of  $^{41}\text{K}/^{39}\text{K} = 0.0721677$  for the standard (Naumenko et al., 2013). Thus, the slope of the isochron determined in the  $\delta^{41}\text{K}$  vs.  $^{40}\text{Ca}/^{39}\text{K}$  diagram (slope) can be converted to give initial  $(^{41}\text{Ca}/^{40}\text{Ca})_I$  ratio:

$$\left(\frac{^{41}\text{Ca}}{^{40}\text{Ca}}\right)_{initial} = slope \times \left[ 10^{-3} \left(\frac{^{41}\text{K}}{^{39}\text{K}}\right)_{std} \right]$$

### Isochron fitting and the mean squared weighted deviation

We compare weighted least squares fits of our data with the NWA3118 #1Nb (Liu, 2017) using the method of Williamson 1968. The goodness of fit of the isochron (straight line) can be

tested by calculating the mean squared weighted deviation (MSWD) or a mean value for chi [ $\chi = (\text{MSWD})^{1/2}$ ] (Wendt and Carl, 1991). This parameter should be about 1 when the deviations of the measurements for the isochron are within analytical error of the best-fit line. It can be used to expand the errors on the slope and intercept of the isochron. As we do not think we have underestimated our analytical errors, these expanded error estimates for the isochron are not used in the discussion and comparison to previous studies. The excess scatter of the data around our CAI best fit isochrons is most likely due to the complex histories of these CAIs and the expanded error would in such a case give uncertainties for the mean values of the isochron parameters that are too large. The multipliers for Liu (2017) NWA3118 and our isochron are about 4. By using such a multiplier,  $(^{41}\text{Ca}/^{40}\text{Ca})_{\text{I}}$  from Liu (2017) is no longer resolved from zero, while our results are still well-resolved. As can be seen in figure 2 of Liu (2017), the slope of their isochron appears visually resolved from zero; thus, we prefer to compare our data with the figure 3 of Liu (2017) without showing the expanded error bars. The isochron based on the four CAI data points in figure 1 gives  $(^{41}\text{Ca}/^{40}\text{Ca})_{\text{I}} = (2.20 \pm 0.18) \times 10^{-8}$  and an intercept  $\delta^{41}\text{K} = -0.55 \pm 0.05$  ( $2\sigma_{\text{m}}$ ). If the matrix is added to the isochron, we obtain  $(^{41}\text{Ca}/^{40}\text{Ca})_{\text{I}} = (1.87 \pm 0.11) \times 10^{-8}$  and an intercept  $\delta^{41}\text{K} = -0.45 \pm 0.03$  ( $2\sigma_{\text{m}}$ ), only marginally different from the isochron without the matrix.

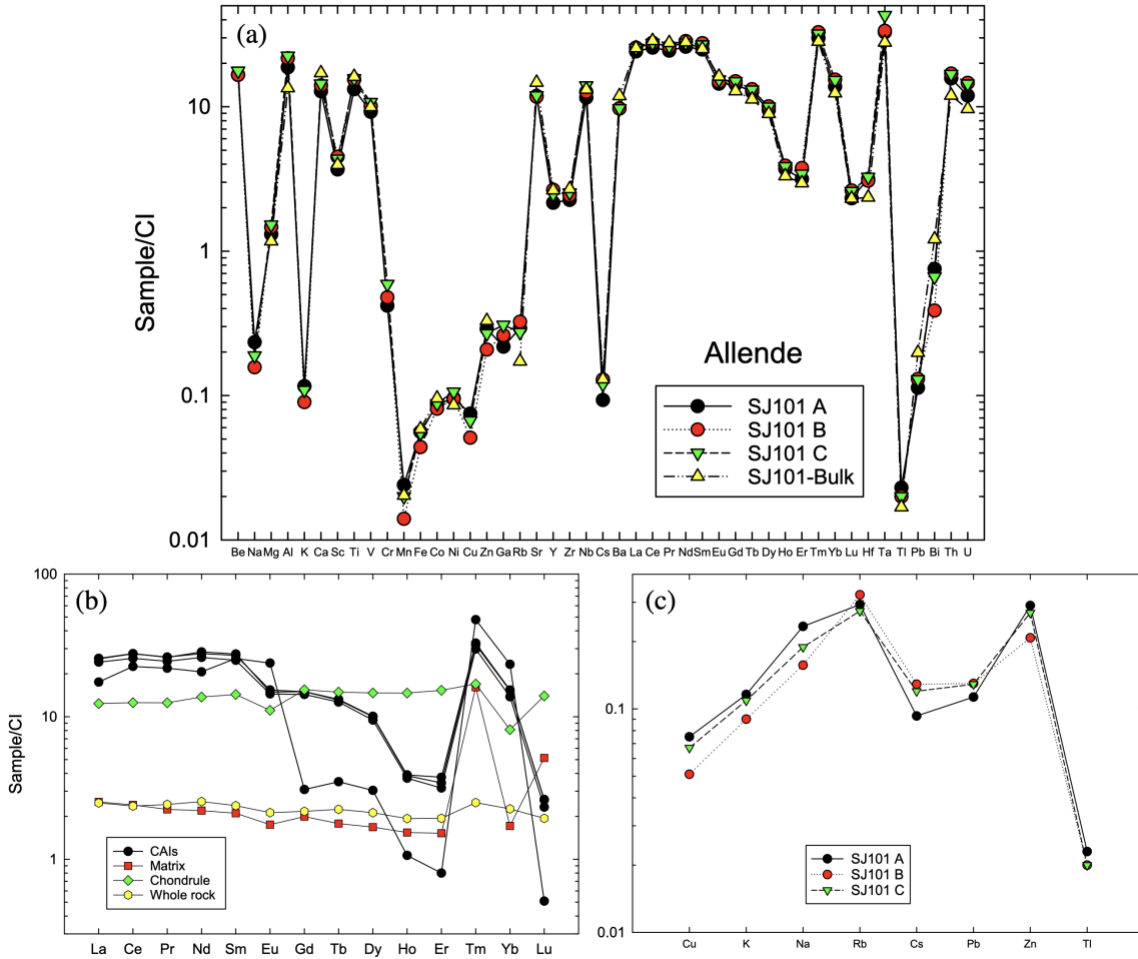


**Figure 1.** Major and trace elements concentration for all samples studied. (a) The extremely coherent elemental patterns of the three SJ101 chips are essentially identical to that of a bulk SJ101 sample analyzed by Petaev & Jacobsen (2009). Especially, Sr as a refractory but mobile element, shows consistent concentrations, eliminating significant effect from aqueous alteration in these samples. (b): All CAIs have a Group II Rare Earth element (REE) pattern – depleted in the most refractory REEs (heavy REEs except for Tm and Yb). The Allende bulk, matrix and the chondrule samples show relatively flat REE patterns. The CI meteorite data from (McDonough and Sun, 1995). Concentrations of the REEs are listed in Table 3. (c) The coherent behavior of selected volatile elements in three SJ101 chips suggests that there is no major effect of fractionation from evaporation related to K loss.

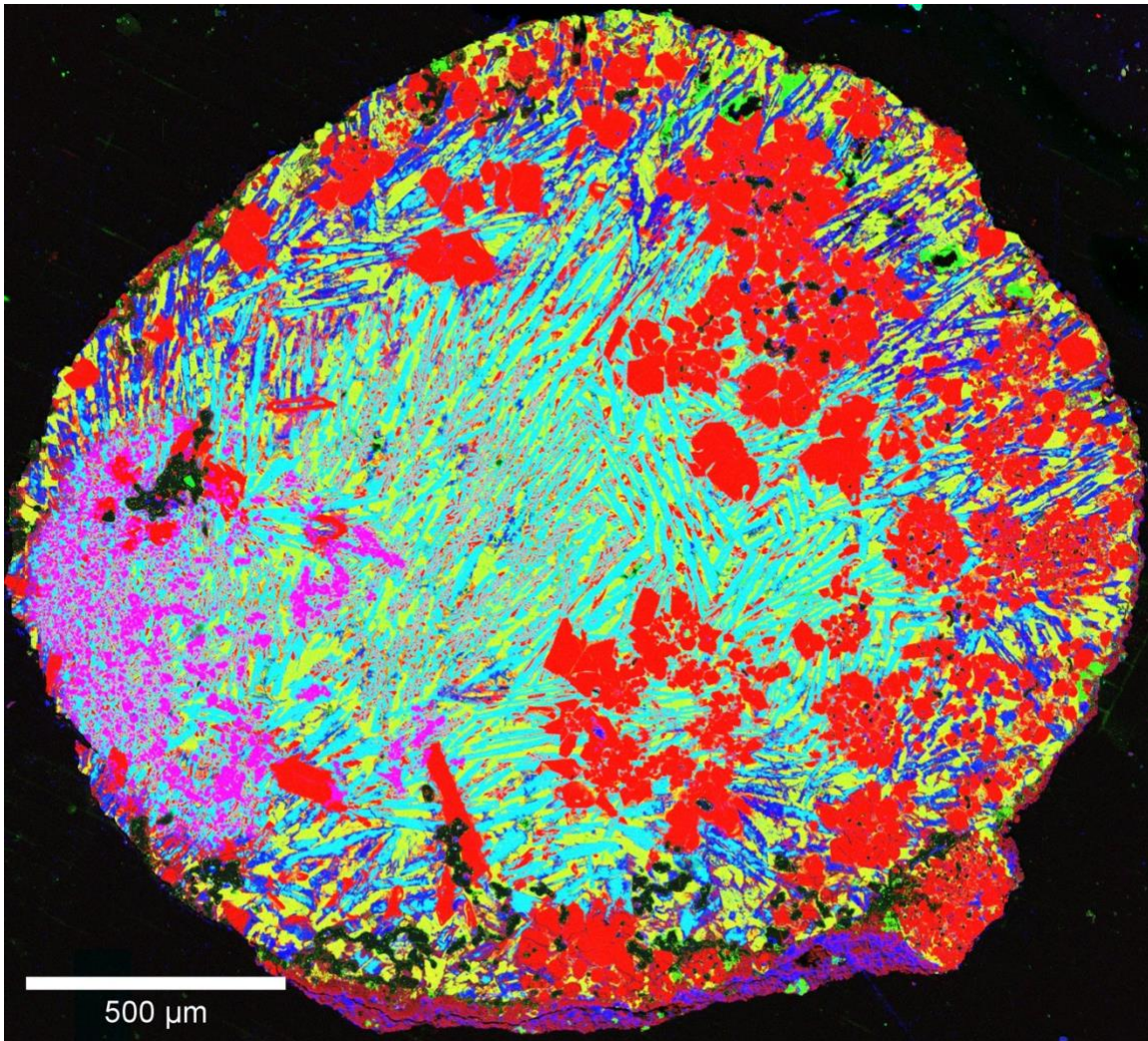


**Figure 2.** Combined elemental map of the CH001 thin section in Mg (red), Ca (green), and Al (blue)  $K\alpha$  X-rays. Mineral colors: red – forsterite, pink – spinel, yellow – Al-diopside, cyan – anorthite, blue – secondary sodalite and/or nepheline partially or completely replacing primary anorthite, light green – secondary salitic clinopyroxene, black – Ni-rich pyrrhotite.



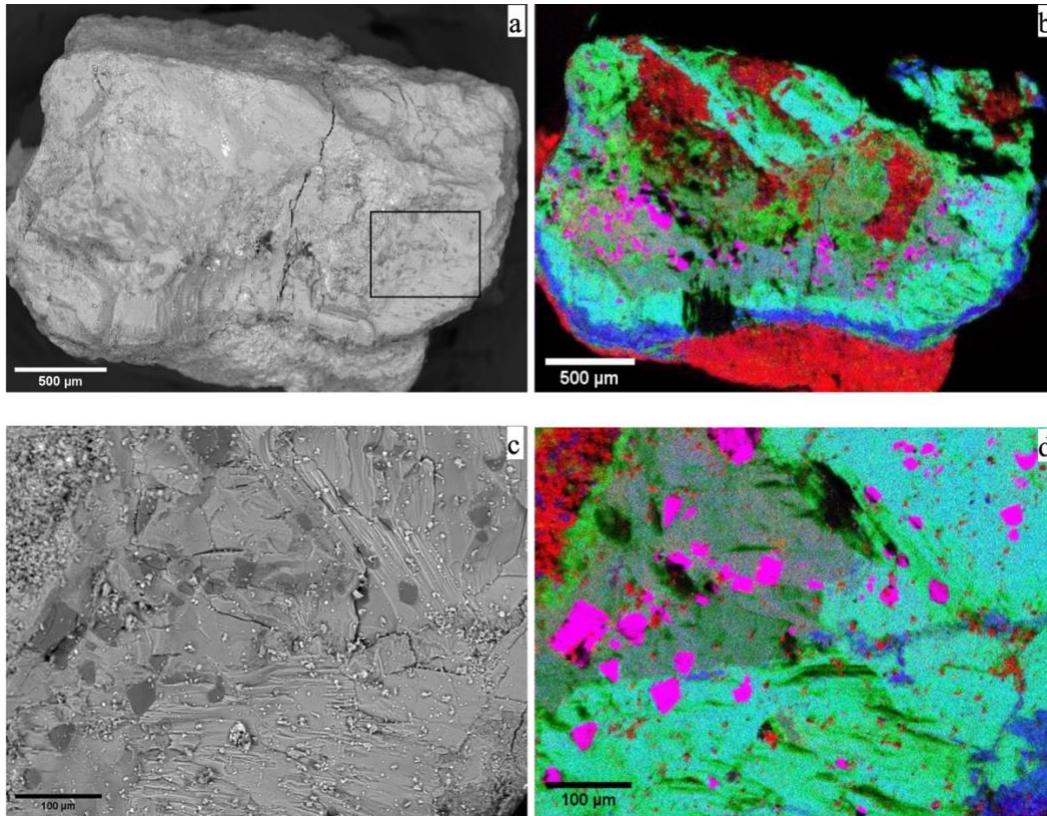


**Figure 3.** The BSE images (a,c) and combined elemental maps (b,d) of CH007 in Mg (red), Ca (green), and Al (blue)  $K\alpha$  X-rays. The whole CAI fragment (a) has irregular fracture surface with the depressions being completely or partially filled with fine-grained matrix. The black box outlines the area shown in panels c and d. Mineral colors (b,d): red – matrix olivine, pink – spinel, cyan/light green – melilite, ‘dirty’ green – Al, Ti-rich clinopyroxene, blue – secondary sodalite and nepheline replacing melilite adjacent to the Wark-Lovering rim, black – deep depressions or very steep slopes. The dotted appearance and blurry grain outlines in panel (b) are due to the roughness of the CH007 surface; these effects are much less pronounced on a more even surface at the CAI edge (c,d). The green to cyan transition in melilite color is caused largely by the increase of Al contents outward due to evaporative loss of Si and Mg during CAI crystallization. Thin blue bands along grain boundaries or cleavage planes of melilite in panel (d) show secondary alteration by Al-rich minerals depleted in Ca and Mg such as nepheline and sodalite.

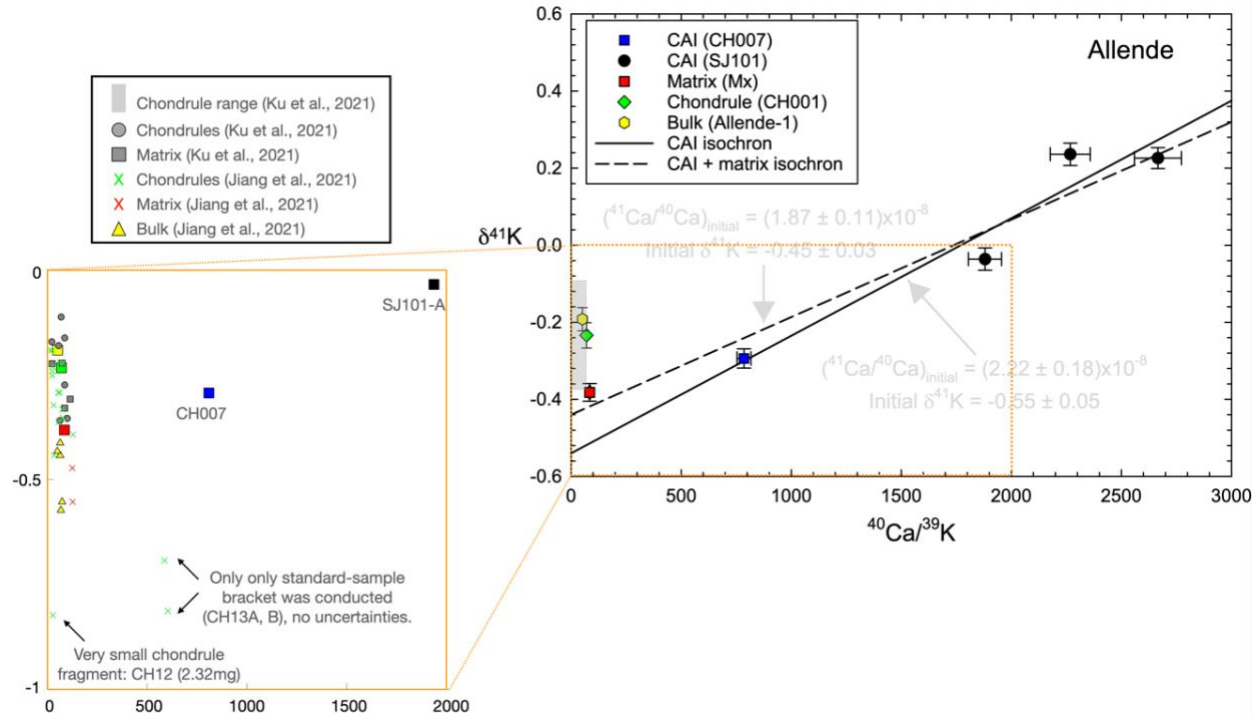


**Figure 4. Comparison of our  $\delta^{41}\text{K}$  data with the literature.** The  $\delta^{41}\text{K}$  values of 26 chondrules [18 from Jiang et al. 2021 and 8 from Ku et al. 2021] range from  $-0.4\%$  to  $-0.1\%$ . Three outliers (Jiang et al., 2021) are most likely due to small sample sizes ( $\sim 2$  mg) which lack reproducibility ( $n=1$ ). None of the chondrules lie on the  $^{41}\text{Ca}$ - $^{41}\text{K}$  bulk isochron. The difference in the bulk Allende values between Jiang et al. and Ku and Jacobsen are likely due to the large difference in sample size. Ku and Jacobsen used an aliquot of a large (34 grams) powdered representative sample of the bulk Allende, while the five bulk Allende samples analyzed by Jiang et al. are separate chips weighing  $\leq 0.090$  g each.

**Table 1.**

Weighted least squares fits for figures 1 and 3 in the main text.

Isochron	Error multi-plier ( $\chi$ )	Initial $^{41}\text{Ca}/^{40}\text{Ca}$	Initial $^{41}\text{Ca}/^{40}\text{Ca}$ error ( $2\sigma$ )	Expanded $^{41}\text{Ca}/^{40}\text{Ca}$ error ( $2\sigma$ )	Initial $\delta^{41}\text{K}$	Initial $\delta^{41}\text{K}$ error ( $2\sigma$ )	Expanded $\delta^{41}\text{K}$ error ( $2\sigma$ )
NWA3118	3.8	$4.70 \times 10^{-9}$	$1.90 \times 10^{-9}$	$7.16 \times 10^{-9}$	-5.7	1.5	5.65
4 CAIs	4.2	$2.22 \times 10^{-8}$	$1.84 \times 10^{-9}$	$7.68 \times 10^{-9}$	-0.549	0.048	0.20
4 CAIs + matrix	4.6	$1.87 \times 10^{-8}$	$1.13 \times 10^{-9}$	$5.18 \times 10^{-9}$	-0.449	0.026	0.12

**Table 2 (source data for Fig. 2).**

Concentrations (ppm) of selected major and traced elements.

Sample Name	Na	Mg	Al	Ti	Cr	Mn	Fe	Cs	Tl	Pb
Allende-1 (bulk)	3705	146014	17511	827	3243	1406	224066	0.101	0.068	1.24
Mx	2498	119531	14421	532	2781	1320	248573	0.083	0.165	18.1
CH001	17083	153167	88853	3659	4020	755	141363	0.066	0.0597	1.52
CH007	6568	40631	194124	7028	410	195	23891	0.027	0.0062	0.64
SJ101-A	1191	126016	161300	5820	691	46	10209	0.018	0.0032	0.28
SJ101-B	800	141642	186227	6780	788	27	7933	0.024	0.0028	0.32
SJ101-C	962	147030	193195	6898	973	38	10009	0.023	0.0027	0.32

**Table 3 (source data for REEs in Fig. 2).**

Concentrations (ppm) of rare Earth elements (REEs).

Sample Name	La	Ce	Pr	Nd	Sm	Eu	Gd	Tb	Dy	Ho	Er	Tm	Yb	Lu
Allende-1 (bulk)	0.588	1.447	0.225	1.160	0.352	0.119	0.431	0.081	0.521	0.105	0.310	0.062	0.363	0.048
Mx	0.598	1.473	0.208	1.002	0.311	0.098	0.396	0.064	0.413	0.084	0.244	0.397	0.276	0.126
CH001	2.929	7.690	1.161	6.279	2.118	0.624	3.072	0.537	3.611	0.800	2.451	0.418	1.306	0.344
CH007	4.145	13.795	2.031	9.435	3.788	1.337	0.614	0.126	0.748	0.058	0.128	1.182	3.749	0.013
SJ101-A	5.721	15.717	2.270	11.898	3.680	0.813	2.851	0.457	2.329	0.202	0.505	0.738	2.222	0.057
SJ101-B	6.082	16.985	2.421	13.009	4.072	0.838	2.986	0.477	2.474	0.213	0.602	0.810	2.476	0.065
SJ101-C	6.036	16.919	2.430	12.657	3.985	0.866	2.979	0.472	2.458	0.211	0.548	0.790	2.456	0.064

**Table 4 (source data for Fig. 3a).**Summary of initial ( $^{41}\text{Ca}/^{40}\text{Ca}$ )<sub>I</sub> and ( $^{26}\text{Al}/^{27}\text{Al}$ )<sub>I</sub> ratios from various CAIs.

Meteorite	Sample Name	Isochron Type	( $^{41}\text{Ca}/^{40}\text{Ca}$ ) <sub>I</sub>	( $^{26}\text{Al}/^{27}\text{Al}$ ) <sub>I</sub>	Data Source $^{41}\text{Ca}/^{40}\text{Ca}$	Data Source $^{26}\text{Al}/^{27}\text{Al}$
Allende	Allende	Bulk CAI	$(2.22\pm 0.18)\times 10^{-8}$	$(5.23\pm 0.13)\times 10^{-5}$	This study	1
Allende	SJ101	Bulk/ mineral	$(2.22\pm 0.18)\times 10^{-8}$	$(5.20\pm 0.53)\times 10^{-5}$	This study	2
Allende	Alvin	Mineral	N/A	$(4.17\pm 0.43)\times 10^{-5}$	N/A	2
Efremovka	E65	Mineral	$(1.4\pm 0.6)\times 10^{-9}$	$(4.42\pm 0.38)\times 10^{-5}$	3	4
NWA 3188	#1Nb (NWA)	Mineral	$(4.6\pm 1.9)\times 10^{-9}$	$(4.64\pm 0.09)\times 10^{-5}$	5	6

**Reference.** 1. (Jacobsen et al., 2008) 2. (MacPherson et al., 2017) 3. (Liu et al., 2012) 4. (Srinivasan and Chaussidon, 2013) 5. (Liu, 2017) 6. (MacPherson et al., 2013)

**Table 5 (source Data for Fig. 3b).**

Nucleosynthetic production ratios of  $^{26}\text{Al}/^{27}\text{Al}$  and  $^{41}\text{Ca}/^{40}\text{Ca}$  for Type II supernova, AGB stars, Wolf-Rayet winds, and the solar initial (defined by the bulk CAI isochrons).

Nucleosynthetic Source	Data Source	$M_{\odot}$	$^{26}\text{Al}/^{27}\text{Al}$	$^{41}\text{Ca}/^{40}\text{Ca}$	$(^{41}\text{Ca}/^{40}\text{Ca})/(^{26}\text{Al}/^{27}\text{Al})$	t (Myr) before CAI Formation
SN-II	1	15	$5.7 \times 10^{-3}$	$1.5 \times 10^{-2}$	2.63	1.45
TP-AGB	1	1.5	$5.8 \times 10^{-3}$	$4.2 \times 10^{-4}$	0.0724	0.852
TP-AGB	1	2	$3.6 \times 10^{-3}$	$2.6 \times 10^{-4}$	0.0722	0.852
TP-AGB	1	3	$2.9 \times 10^{-3}$	$3.0 \times 10^{-4}$	0.103	0.911
TP-AGB	1	5	$5.3 \times 10^{-4}$	$1.2 \times 10^{-4}$	0.226	1.04
WR-wind*	2-4	60	$4.3 \times 10^{-2}$	$6.9 \times 10^{-4}$	0.016	0.60
CAI-Bulk	this study and 5		$5.23 \times 10^{-5}$	$2.22 \times 10^{-8}$	$4.24 \times 10^{-4}$	0.00
CAI processing	6		$4.31 \times 10^{-5}$	$5.50 \times 10^{-9}$	$1.28 \times 10^{-4}$	-0.204

\* WR-wind mass production  $^{26}\text{Al}$  and  $^{41}\text{Ca}$  is from Table 2 of Young (2014) for a 60 solar mass ( $M_{\odot}$ ) rotating Wolf Rayet star. It lists  $^{26}\text{Al} = 7 \times 10^{-5} M_{\odot}$  from Gounelle and Meynet (2012) and  $^{41}\text{Ca} = 8 \times 10^{-7} M_{\odot}$  from Arnould et al. (2006). When combined with the  $^{27}\text{Al}/^{40}\text{Ca} = 1.43$  for the Solar System from Anders and Grevesse (1989), this gives  $(^{41}\text{Ca}/^{40}\text{Ca})/(^{26}\text{Al}/^{27}\text{Al}) = 0.016$  for the protosolar molecular cloud right after the last WR-wind injection. The  $(^{41}\text{Ca}/^{40}\text{Ca}) = 6.9 \times 10^{-4}$  is from figure 6 of Arnould et al. (2006) by using their dilution factor of 2160 and correcting to their  $\Delta^*$  (free decay) = 0. This gives  $(^{26}\text{Al}/^{27}\text{Al}) = 4.3 \times 10^{-2}$  to be consistent with the values listed in Table 2 of Young (2014). Reference. 1. (Wasserburg et al., 2006) 2. (Arnould et al. 2006) 3. (Gounelle & Meynet, 2012) 4. (Young 2014) 5. (Jacobsen et al., 2008) 6. (MacPherson et al., 2017)

**Table 6.**

Calculated abundances of  $^{41}\text{Ca}/^{40}\text{Ca}$  and  $^{26}\text{Al}/^{27}\text{Al}$  in the protosolar molecular cloud; details can be found in (Jacobsen, 2005).

	$^{41}\text{Ca}/^{40}\text{Ca}$	$^{26}\text{Al}/^{27}\text{Al}$
$(N_{\text{R}}/N_{\text{S}})/(P_{\text{R}}/P_{\text{S}})$ for Interstellar Medium (ISM)	$4 \times 10^{-5}$	$2 \times 10^{-4}$
$(N_{\text{R}}/N_{\text{S}})/(P_{\text{R}}/P_{\text{S}})$ for Molecular Cloud (MC)	$4 \times 10^{-8}$	$2 \times 10^{-6}$
$P_{\text{R}}/P_{\text{S}}$	$1 \times 10^{-3}$	$5.4 \times 10^{-3}$
$(N_{\text{R}}/N_{\text{S}})$ for ISM	$4 \times 10^{-8}$	$1.1 \times 10^{-6}$
$(N_{\text{R}}/N_{\text{S}})$ for MC	$4 \times 10^{-11}$	$1.1 \times 10^{-8}$

**Note.**

R: radioactive isotope; S: stable isotope;  $N_{\text{R}}/N_{\text{S}}$ : initial solar ratios of radioactive to stable isotopes;  $P_{\text{R}}/P_{\text{S}}$ : nucleosynthetic production ratios.



## Appendix C

### Supporting Information for Chapter 4

**Table 1.**

Concentrations of Tl and Pb for 5 separated fractions of Allende fine materials.

	<b>[Tl] in ppm</b>	<b>[Pb] in ppm</b>
SF001(Mx)	0.16526	18.14581
SF002(Mx)	0.27132	34.99256
SF003(Mx)	0.09957	3.73609
SF004(Ch)	0.00476	0.25472
SF005(f)	0.08163	1.41099

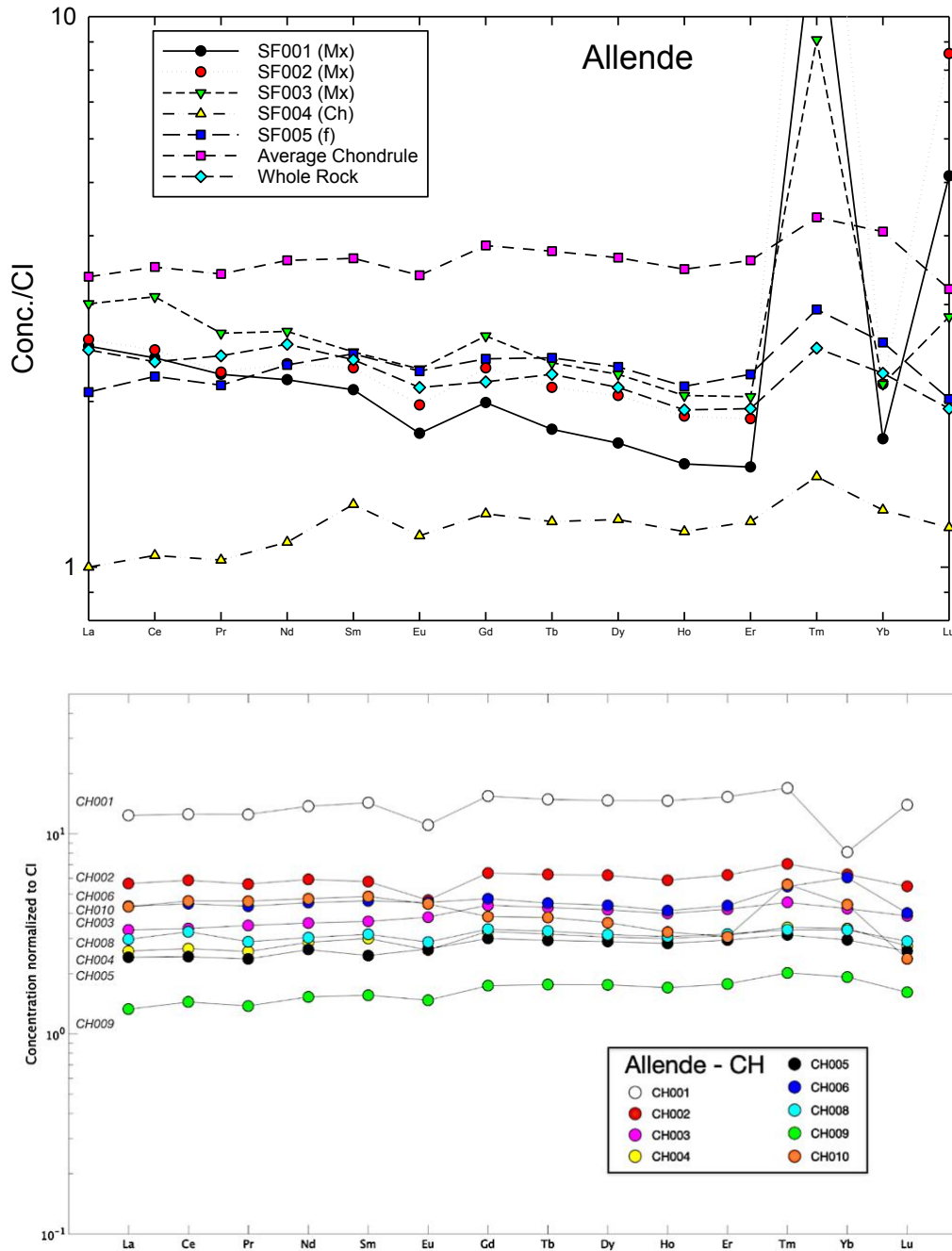


**Figure 1. (Top) Rare Earth element (REE) for the five separated fractions of Allende fine samples (SF) studied; (Bottom) Rare Earth element (REE) for the Allende chondrules studied.** Each elemental concentration is normalized to CI meteorites (McDonough and Sun, 1995). They all show relatively flat and unfractionated REE patterns, except the Tm anomalies for the Allende matrix samples (SF001-003).

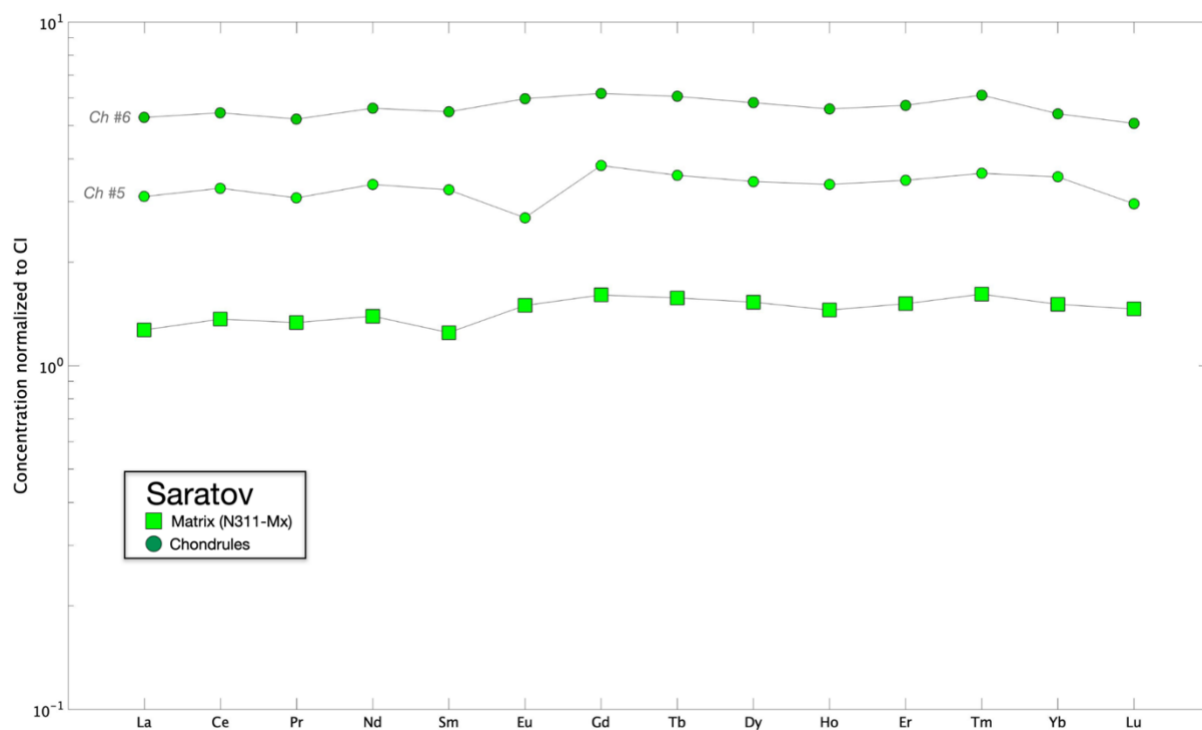


**Figure 2. Rare Earth element (REE) for the Saratov matrix and chondrules studied.** Each elemental concentration is normalized to CI meteorites (McDonough and Sun, 1995). Both matrix and chondrules samples have relatively flat and unfractionated REE patterns.

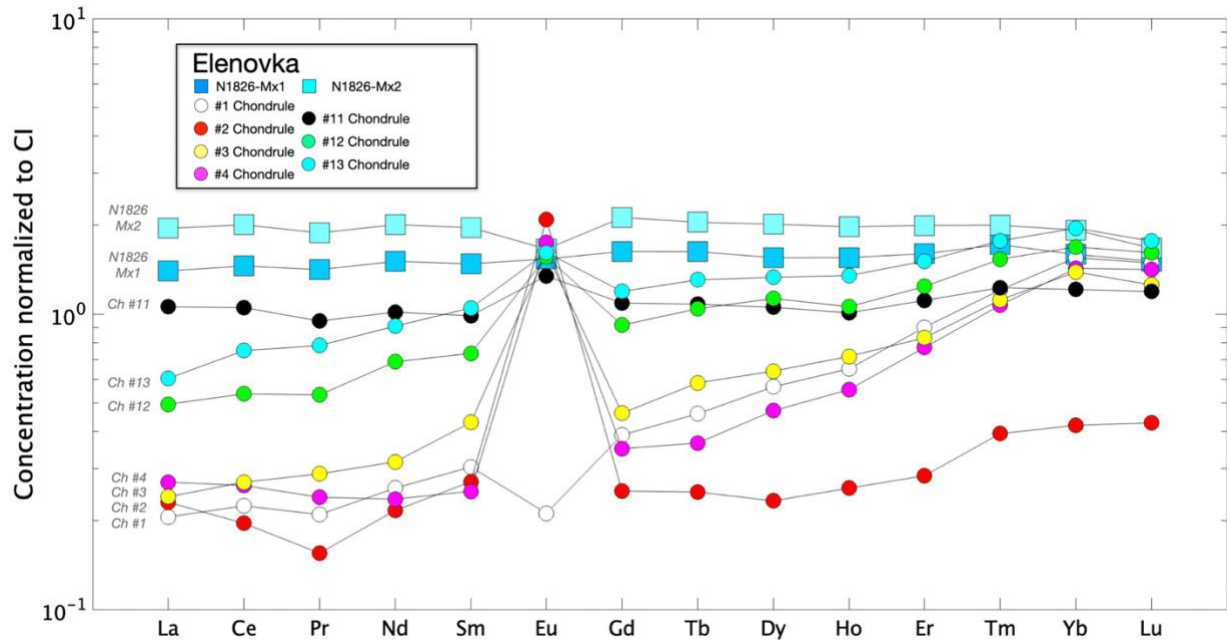


**Figure 3. Rare Earth element (REE) for the Elenovka matrix and chondrules studied. Each elemental concentration is normalized to CI meteorites (McDonough and Sun, 1995). All Elenovka' chondrules are slightly enriched in heavy REE elements, especially for chondrules #1, #3, and #4. The slightly fractionated patterns within these chondrules might reflect the presence of clinopyroxene. All chondrules also have positive anomaly in Eu (which usually substitutes Ca in some mineral phases under reduced environment), except for chondrule #1, which shows a negative Eu anomaly. Such Eu anomaly is likely related to the mineral phases present, such as plagioclase, within each chondrule samples.**

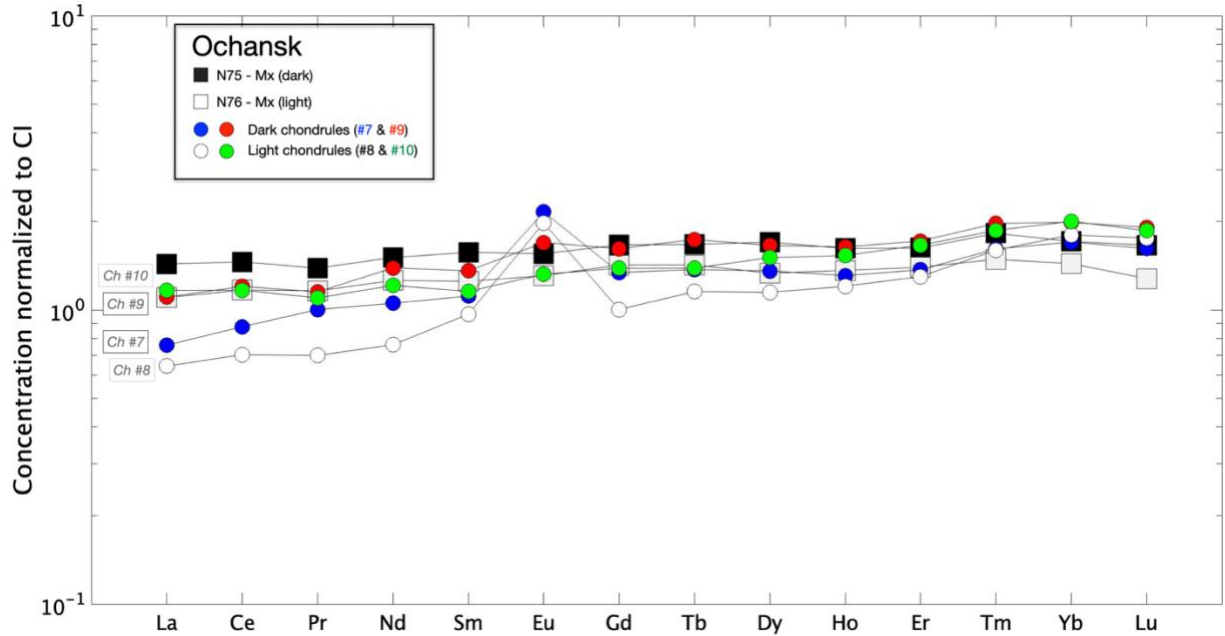


**Figure 4. Rare Earth element (REE) for the Ochansk matrix and chondrules studied. Each elemental concentration is normalized to CI meteorites (McDonough and Sun, 1995).** There are no systematic differences between the dark and the light materials, and one dark (#7) and one light chondrules (#8) show the positive Eu anomalies, which likely relate to the present minerals. Both matrix from the dark and light materials do show similar REE patterns.

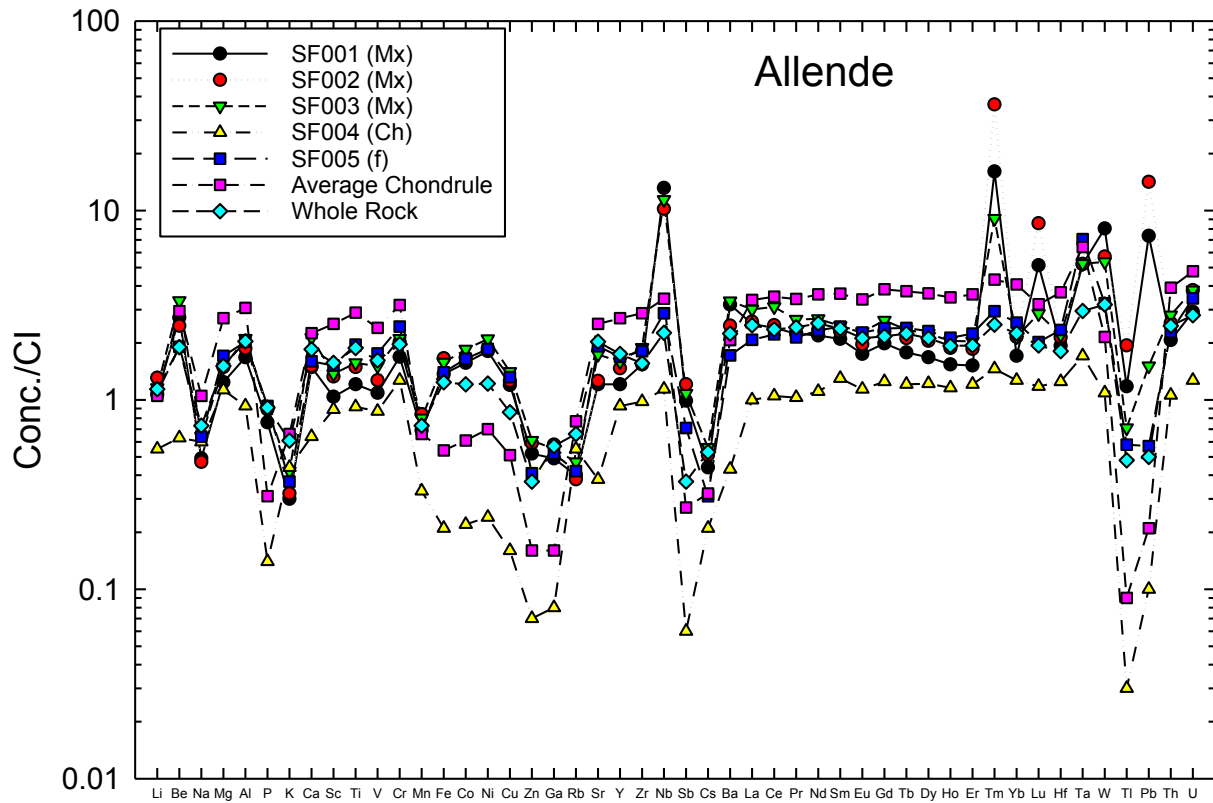


**Figure 5. Elemental concentrations of Allende whole rock, average Allende chondrules, and Allende separated fraction samples (SF001 to SF005).** Each elemental concentration is normalized to CI meteorites (McDonough and Sun, 1995). The break-down figures of each Allende separation could be found in Appendix C Fig. 6-8.

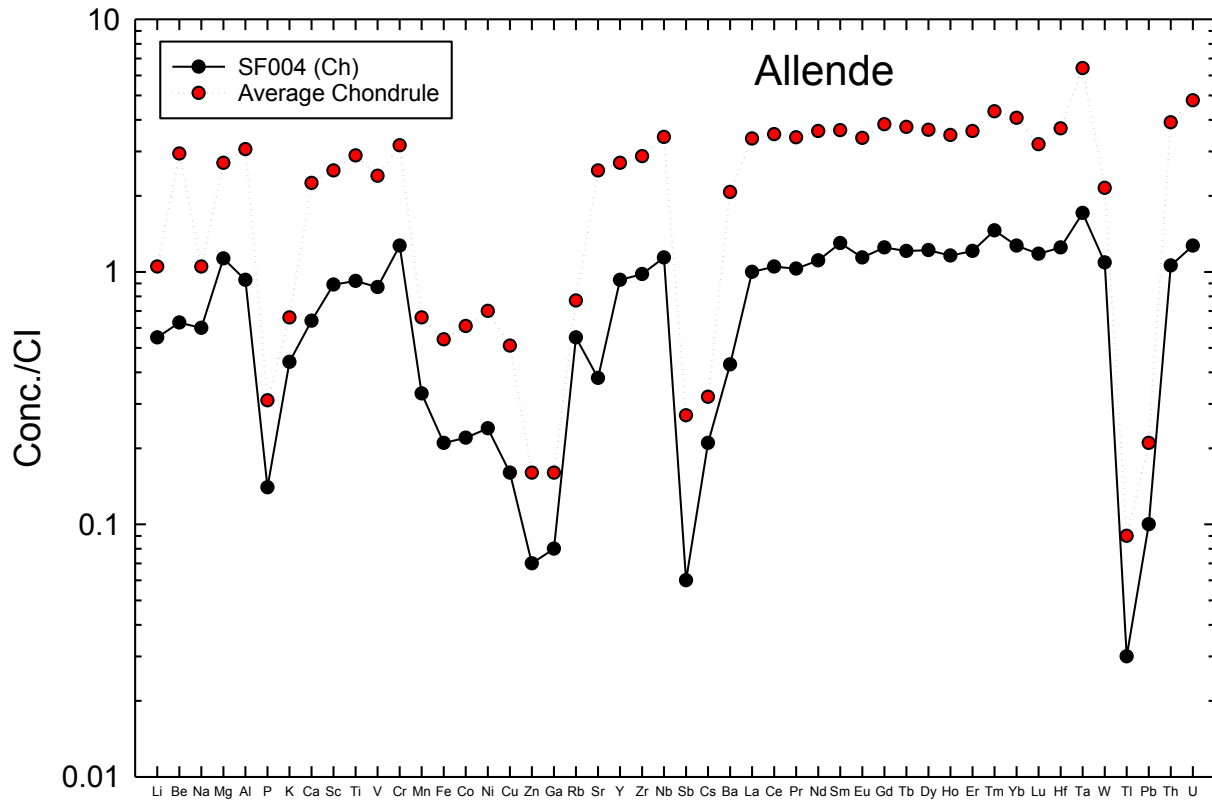


**Figure 6. Elemental concentrations of SF004(Ch) and the average Allende chondrules studied.** The coherent and similar patterns between this Allende fraction, SF004(Ch), and the average chondrules implies that this sample likely is the chondrule assemblages instead of Allende matrix materials. The absolute concentration of chondrules vary individually, therefore, a perfect overlap of all elemental concentrations is not expected. Each elemental concentration is normalized to CI meteorites (McDonough and Sun, 1995).

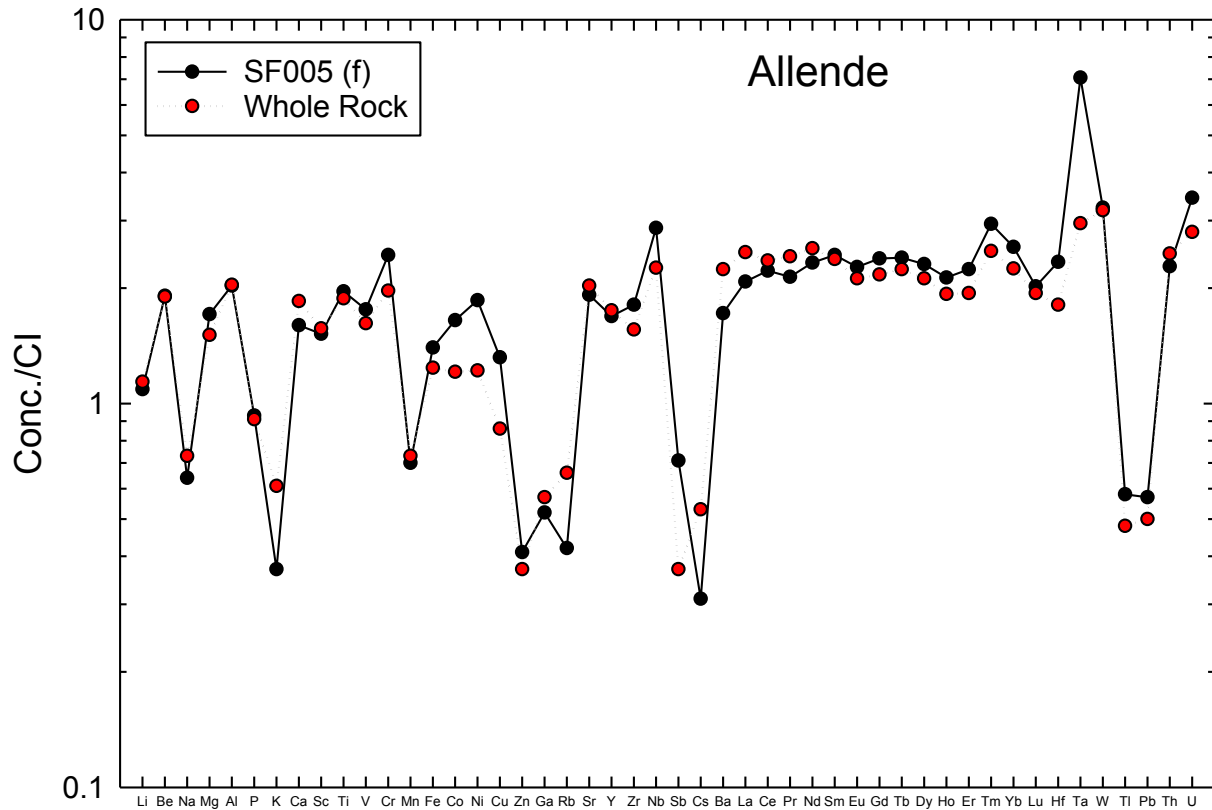


**Figure 7. Elemental concentrations of SF005(f) and Allende whole rock (Ku and Jacobsen, 2020).** The identical patterns between this Allende fraction, SF005(f), and the Allende whole rock (~34 g) implies that this sample likely is the assemblages of broken tiny Allende rock fragment instead of Allende matrix materials. Each elemental concentration is normalized to CI meteorites (McDonough and Sun, 1995).



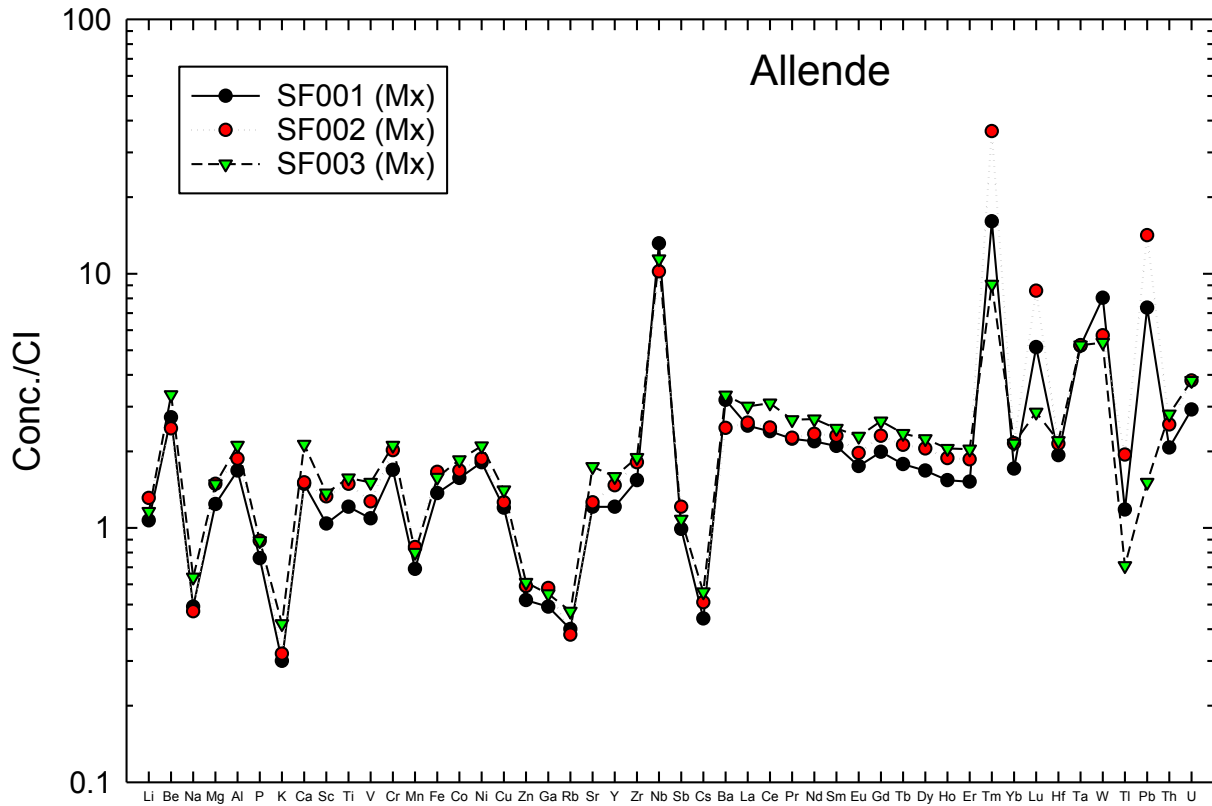


**Figure 8. Elemental concentrations of Allende matrix samples.** SF001(Mx) and SF002(Mx) are the two finest separated fractions, and the high concentrations of Pb and Tl in them supports that such fractions are the Allende matrix materials. SF003(Mx) contains courser materials compared to SF001(Mx) and SF002(Mx), and the relatively low Pb and Tl implies that very tiny chondrules were present in this Allende fraction. However, due to the consistent and coherent patterns of their elemental concentrations among SF001(Mx), SF002(Mx) and SF003(Mx), we still considered SF003(Mx) as one of the Allende matrix materials as well. Each elemental concentration is normalized to CI meteorites (McDonough and Sun, 1995).

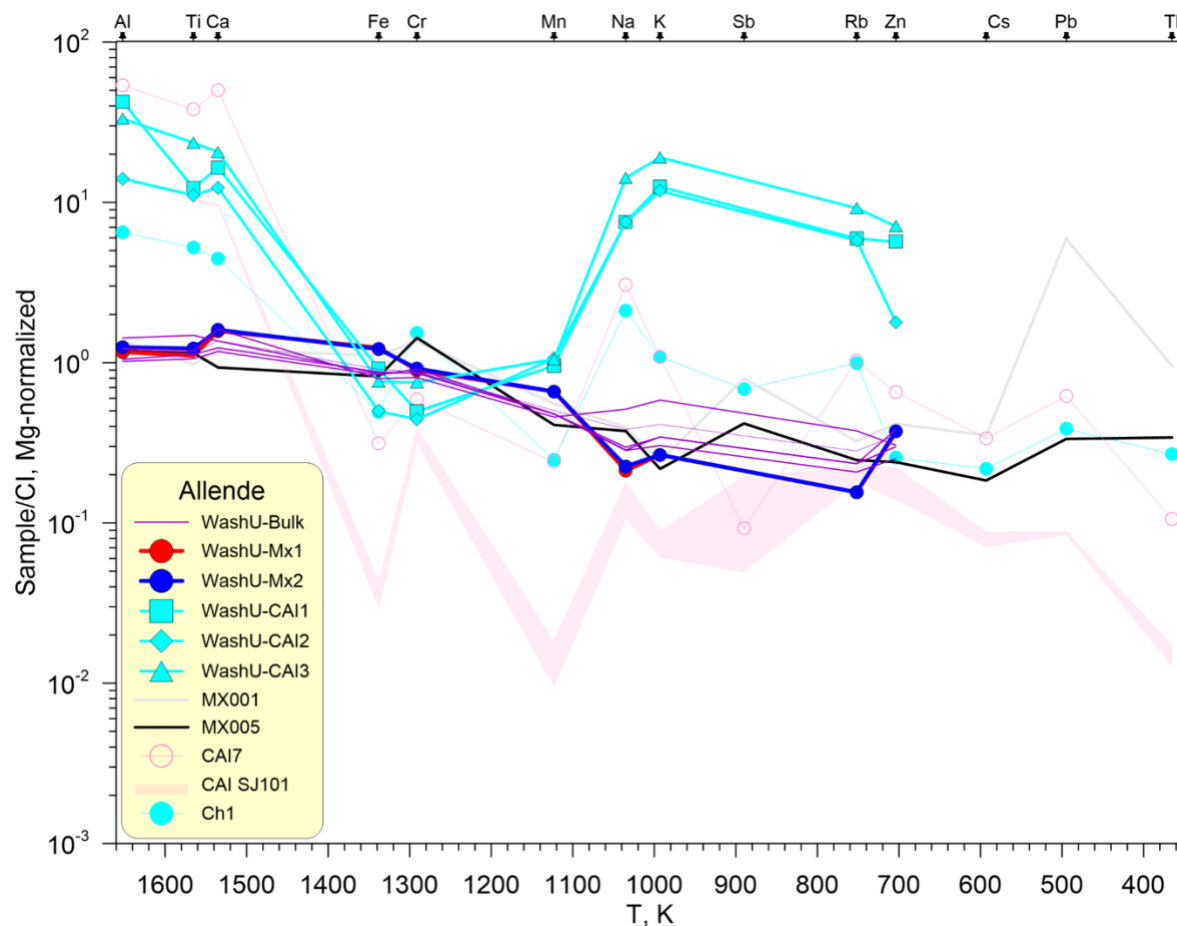


**Figure 9. Depletion patterns of the CAIs and Allende bulk from Jiang et al. (2021) (labeled as WashU), CAIs studied here (CAI7, and CAI SJ101), matrix (SF001) studied here, and Allende fragment (SF005) studied here.** The enrichment of moderately volatile elements, such as Na, K, Rb and Zn, suggests that the CAIs analyzed by Jiang et al. (2021) have been contaminated. The nearly identical patterns between Jiang et al.’s matrix samples and their bulk to our SF005(f), suggests that their Allende matrix (WashU-Mx1 and Mx2) are just like our SF005(f), which are the fine martials of Allende rock fragments. Also, the similar patterns between their bulk (WashU-Bulk) and our SF005(f) also suggests that their bulk materials are not representative, and are, again, just Allende rock fragments.

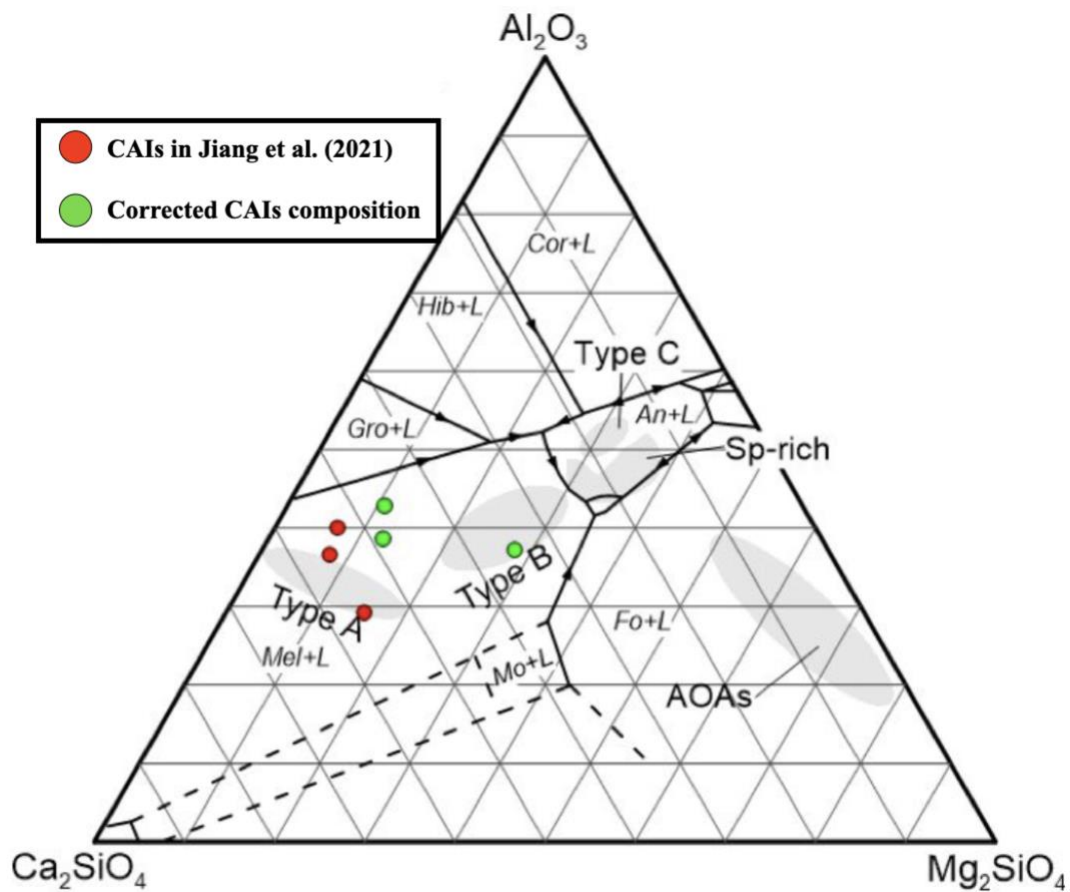


**Figure 10. Comparison of CAIs in Jiang et al. (2021) study in the Glen's diagram.** The previously reported  $\delta^{41}K$  values of 3 CAIs (Jiang et al., 2021) are indistinguishable from the bulk Allende. Additionally, given the lack of petrographic description of these CAIs and unreasonably high concentrations of FeO, Na<sub>2</sub>O, and K<sub>2</sub>O in them, suggestive of contamination, we prefer not to compare their CAIs data to this study.

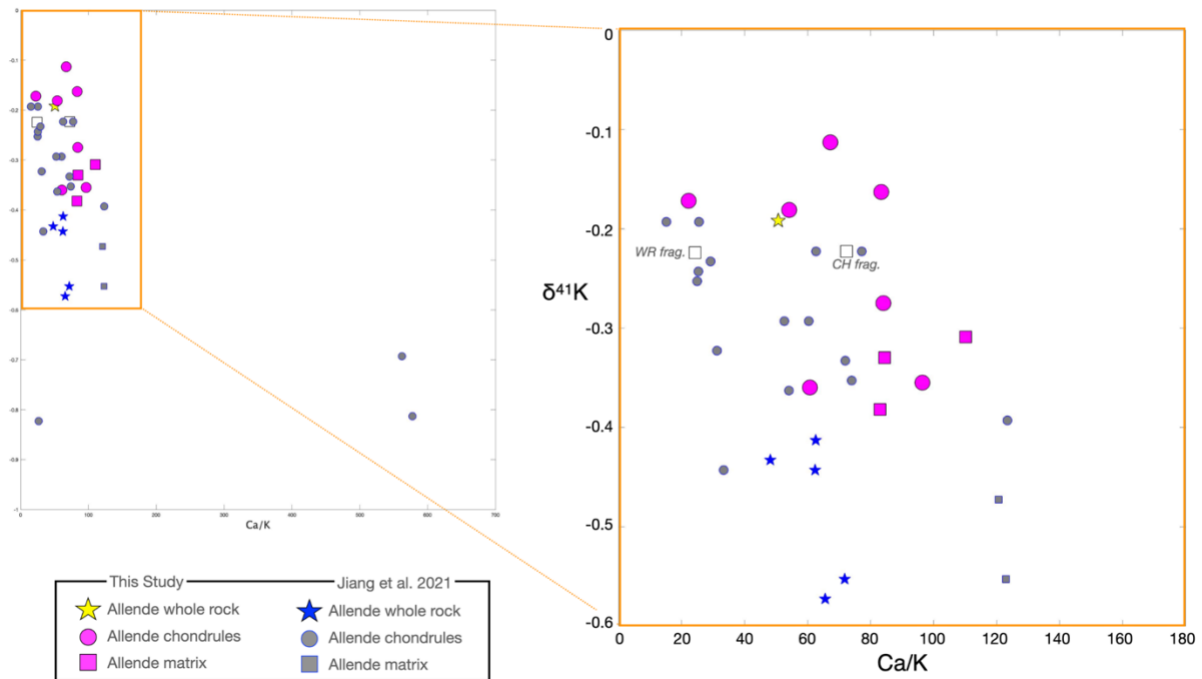


**Figure 11. Comparison of our  $\delta^{41}\text{K}$  data with the literature (Jiang et al., 2021).** The  $\delta^{41}\text{K}$  values of 26 chondrules [18 from Jiang et al. 2021 and 8 from this study] range from  $-0.4\text{‰}$  to  $-0.1\text{‰}$ . Three outliers (Jiang et al., 2021) are most likely due to small sample sizes ( $\sim 2$  mg) which lack reproducibility ( $n=1$ ). The difference in the bulk Allende values between Jiang et al. (2021) and Ku and Jacobsen (2020) are likely due to the large difference in sample size; Ku and Jacobsen (2020) used an aliquot of a large (34 grams) powdered representative sample of the bulk Allende, while the five bulk Allende samples analyzed by Jiang et al. (2020) are small Allende chips weighing  $\leq 0.090$  g each.

## Appendix D

### Supporting Information for Chapter 5

**Table 1.**  
 $\delta^{41}\text{K}$  measurements for USGS terrestrial standards.

Group	Sample	Type	$\delta^{41}\text{K}_{\text{Suprapur}}$ (‰)	$\pm 2\text{SE}$	$N$	$n$
Earth	BCR-2	Basalt	-0.370	0.022	9	46
	BHVO-2	Basalt	-0.333	0.022	9	46
	AGV-1	Basalt	-0.393	0.065	1	6
	G-2	Granitoid	-0.373	0.029	5	23
	RGM-1	Rhyolite	-0.308	0.029	5	26
	W-2	Diabase	-0.428	0.046	2	9
	GSP-2	Granitoid	-0.382	0.029	5	23
	BIR	Basalt	-0.283	0.065	1	5

**Table 2.**  
 $\delta^{41}\text{K}$  measurements for selected Earth samples.

Group	Sample	Type	$\delta^{41}\text{K}$ (‰)	$\pm 2\text{SE}$	$N$	$n$	Publication
Earth	HE-5	Granite	-0.412	0.033	4	20	
	GN-12-03	Granite	-0.496	0.033	4	20	
	Ram-3	Granite	-0.313	0.025	7	35	
	K410	Gabbro	-0.371	0.029	5	25	
	E-58	Diorite	-0.165	0.029	5	25	
	CP5.5	Gabbro	-0.350	0.033	4	20	Kuhnel et al., 2021
	CP5.5 – Plag.	Plagioclase	-0.019	0.033	4	17	Kuhnel et al., 2021
	BR-02	Basalt	-0.446	0.029	5	25	
	K1714	Andesite	-0.446	0.033	4	20	
	CGJ-02	Camptonite	-0.309	0.023	8	40	
	R-B-1	Basalt	-0.388	0.065	1	5	
	RC2D-1	Basalt	-0.212	0.065	1	5	
	W-B-1	Basalt	-0.357	0.065	1	5	

*NIST* SRM-3141-a was measured with respect to *Suprapur* =  $+0.047 \pm 0.003\text{‰}$   
The uncertainty (2SE) is calculated based on  $N$  days of analyses; the internal analytical uncertainty is 30 ppm.

$N$ : numbers of independent analytical runs.

$n$ : total number of the bracketed  $\delta^{41}\text{K}$  values from  $N$  days.

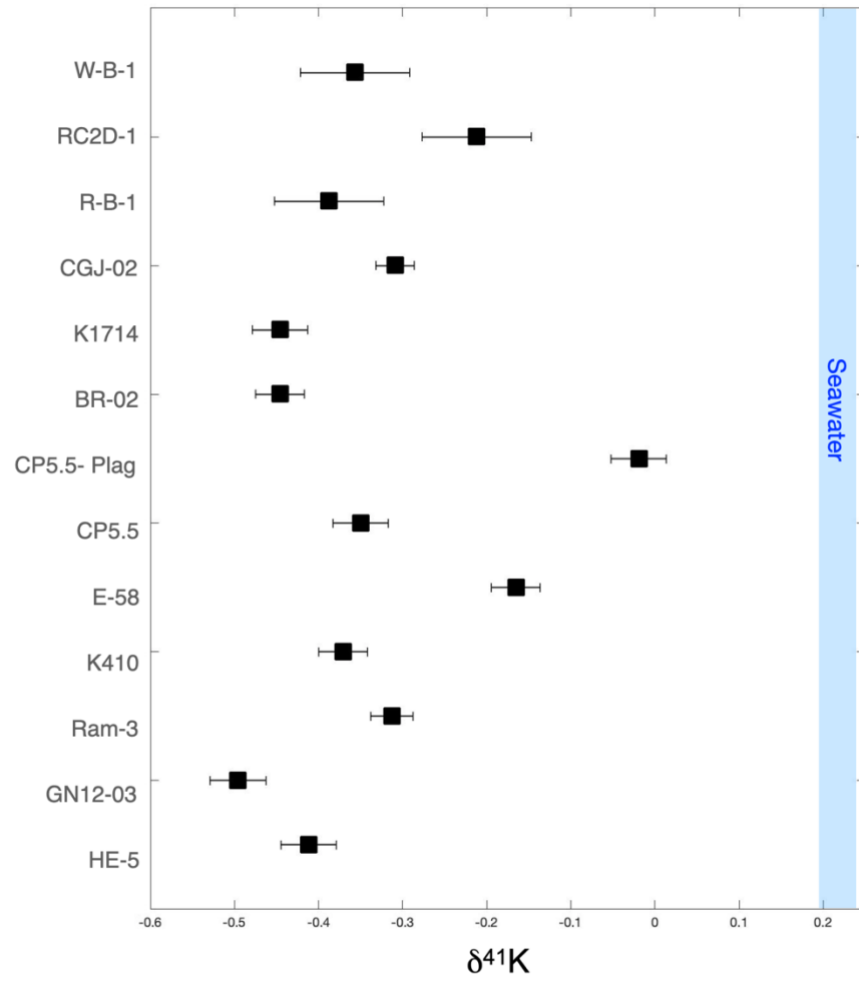


**Figure 1.**  $\delta^{41}\text{K}$  measurements for selected Earth samples. The sample origins and data can be found in Appendix D - table 2.

## References

- Adams F. C. (2010) The Birth Environment of the Solar System. *Annual Review of Astronomy and Astrophysics* **48**, 47–85.
- Alexander C. M. O. (2019a) Quantitative models for the elemental and isotopic fractionations in chondrites: The carbonaceous chondrites. *Geochimica et Cosmochimica Acta* **254**, 277–309.
- Alexander C. M. O. (2019b) Quantitative models for the elemental and isotopic fractionations in the chondrites: The non-carbonaceous chondrites. *Geochimica et Cosmochimica Acta* **254**, 246–276.
- Alexander C. M. O. and Grossman J. N. (2005) Alkali Elemental and Potassium Isotopic Compositions of Semarkona Chondrules. *Meteoritics & Planetary Science* **40**, 541–556.
- Amelin Y., Kaltenbach A., Iizuka T., Stirling C. H., Ireland T. R., Petaev M. and Jacobsen S. B. (2010) U–Pb chronology of the Solar System’s oldest solids with variable  $^{238}\text{U}/^{235}\text{U}$ . *Earth and Planetary Science Letters* **300**, 343–350.
- Anders E. and Grevesse N. (1989) Abundances of the elements - Meteoritic and solar. *Geochimica et Cosmochimica Acta* **53**, 197–214.
- Andreasen R. and Sharma M. (2006) Solar Nebula Heterogeneity in p-Process Samarium and Neodymium Isotopes. *Science* **314**, 806–809.
- Bakhtin A. I., Sonin G. V., Sungatullin R. Kh., Petrova R. D., Gusev A. V. and Kuzina D. M. (2017) Meteorite Ochansk: Genesis and Composition Peculiarities. **80**, 6114.
- Birck J. L. and Lugmair G. W. (1988) Nickel and chromium isotopes in Allende inclusions. *Earth and Planetary Science Letters* **90**, 131–143.
- Bischoff A., Palme H., Clayton R. N., Mayeda T. K., Grund T., Spettel B., Geiger T., Endreß M., Beckerling W. and Metzler K. (1991) New carbonaceous and type 3 ordinary chondrites from the Sahara Desert. *Meteoritics* **26**, 318.
- Bloom H., Lodders K., Chen H., Zhao C., Tian Z., Koefoed P., Petó M. K., Jiang Y. and Wang (王昆) K. (2020) Potassium isotope compositions of carbonaceous and ordinary chondrites: Implications on the origin of volatile depletion in the early Solar System. *Geochimica et Cosmochimica Acta*.
- Bollard J., Connelly J. N., Whitehouse M. J., Pringle E. A., Bonal L., Jørgensen J. K., Nordlund Å., Moynier F. and Bizzarro M. (2017) Early formation of planetary building blocks inferred from Pb isotopic ages of chondrules. *Science Advances* **3**.
- Bouvier A. and Boyet M. (2016) Primitive Solar System materials and Earth share a common initial  $^{142}\text{Nd}$  abundance. *Nature* **537**, 399–402.

- Bouvier A., Vervoort J. D. and Patchett P. J. (2008) The Lu-Hf and Sm-Nd isotopic composition of CHUR: Constraints from unequilibrated chondrites and implications for the bulk composition of terrestrial planets. *Earth and Planetary Science Letters* **273**, 48–57.
- Boyet M. and Carlson R. W. (2005)  $^{142}\text{Nd}$  Evidence for Early (>4.53 Ga) Global Differentiation of the Silicate Earth. *Science* **309**, 576–581.
- Boyet M., Carlson R. W. and Horan M. (2010) Old Sm–Nd ages for cumulate eucrites and redetermination of the solar system initial  $^{146}\text{Sm}/^{144}\text{Sm}$  ratio. *Earth and Planetary Science Letters* **1–4**, 172–181.
- Brearley A. J., Scott E. R. D., Keil K., Clayton R. N., Mayeda T. K., Boynton W. V. and Hill D. H. (1989) Chemical, isotopic and mineralogical evidence for the origin of matrix in ordinary chondrites. *Geochimica et Cosmochimica Acta* **53**, 2081–2093.
- Bridges J. C., Franchi I. A., Grady M. M., Sexton A. S. and Pillinger C. T. (1997) The  $\text{d}^{18}\text{O}$  composition of feldspar and other minerals in Lafayette. *Meteoritics and Planetary Science Supplement* **32**.
- Bridges J. C., Franchi I. A., Sexton A. S. and Pillinger C. T. (1999) Mineralogical controls on the oxygen isotopic compositions of UOCs. *Geochimica et Cosmochimica Acta* **63**, 945–951.
- Bullock E. S., Knight K. B., Richter F. M., Kita N. T., Ushikubo T., MacPherson G. J., Davis A. M. and Mendybaev R. A. (2013) Mg and Si isotopic fractionation patterns in types B1 and B2 CAIs: Implications for formation under different nebular conditions. *Meteoritics & Planetary Science* **48**, 1440–1458.
- Burkhardt C., Borg L. E., Brennecka G. A., Shollenberger Q. R., Dauphas N. and Kleine T. (2016) A nucleosynthetic origin for the Earth's anomalous  $^{142}\text{Nd}$  composition. *Nature* **537**, 394–398.
- Burkhardt C., Hin R. C., Kleine T. and Bourdon B. (2014) Evidence for Mo isotope fractionation in the solar nebula and during planetary differentiation. *Earth and Planetary Science Letters* **391**, 201–211.
- Burkhardt C., Kleine T., Oberli F., Pack A., Bourdon B. and Wieler R. (2011) Molybdenum isotope anomalies in meteorites: Constraints on solar nebula evolution and origin of the Earth. *Earth and Planetary Science Letters* **312**, 390–400.
- Canup R. M. and Asphaug E. (2001) Origin of the Moon in a giant impact near the end of the Earth's formation. *Nature* **412**, 708–712.
- Carlson R. W., Boyet M. and Horan M. (2007) Chondrite Barium, Neodymium, and Samarium isotopic heterogeneity and early Earth differentiation. *Science* **316**, 1175–1178.
- Cassen P. (1996) Models for the fractionation of moderately volatile elements in the solar nebula. *Meteoritics & Planetary Science* **31**, 793–806.



- Chaussidon M., Libourel G. and Krot A. N. (2008) Oxygen isotopic constraints on the origin of magnesian chondrules and on the gaseous reservoirs in the early Solar System. *Geochimica et Cosmochimica Acta* **72**, 1924–1938.
- Chen H., Tian Z., Tuller-Ross B., Korotev R. L. and Wang K. (2019) High-precision potassium isotopic analysis by MC-ICP-MS: an inter-laboratory comparison and refined K atomic weight. *J. Anal. At. Spectrom.* **34**, 160–171.
- Chen H.-W., Lee T., Lee D.-C., Jiun-San Shen J. and Chen J.-C. (2011)  $^{48}\text{Ca}$  Heterogeneity in Differentiated Meteorites. *The Astrophysical Journal Letters* **743**, L23.
- Clayton D. (2003) *Handbook of Isotopes in the Cosmos: Hydrogen to Gallium.*, Cambridge University Press.
- Clayton R. N. and Mayeda T. K. (1977) Correlated oxygen and magnesium isotope anomalies in Allende Inclusions, I: Oxygen. *Geophysical Research Letters* **4**, 295–298.
- Clayton R. N. and Mayeda T. K. (1996) Oxygen isotope studies of achondrites. *Geochimica et Cosmochimica Acta* **60**, 1999–2017.
- Clayton R. N. and Mayeda T. K. (1999) Oxygen isotope studies of carbonaceous chondrites. *Geochimica et Cosmochimica Acta* **63**, 2089–2104.
- Clayton R. N. and Mayeda T. K. (1985) Oxygen isotopes in chondrules from Enstatite chondrites: Possible Identification of a Major Nebular Reservoir. **16**, 142–143.
- Clayton R. N. and Mayeda T. K. (1984) The oxygen isotope record in Murchison and other carbonaceous chondrites. *Earth and Planetary Science Letters* **67**, 151–161.
- Clayton R. N., Mayeda T. K., Goswami J. N. and Olsen E. J. (1991) Oxygen isotope studies of ordinary chondrites. *Geochimica et Cosmochimica Acta* **55**, 2317–2337.
- Clayton R. N., Mayeda T. K., Hiroi T., Zolensky M. and Lipschutz M. E. (1997) Oxygen Isotopes in Laboratory-heated CI and CM Chondrites. *Meteoritics and Planetary Science Supplement* **32**.
- Clayton R. N., Mayeda T. K. and Rubin A. E. (1984a) Oxygen isotopic compositions of enstatite chondrites and aubrites. *Journal of Geophysical Research: Solid Earth* **89**, C245–C249.
- Clayton R. N., Mayeda T. K. and Yanai K. (1984b) Oxygen isotopic compositions of some Yamato meteorites. *National Institute Polar Research Memoirs* **35**, 267.
- Clayton R. N., McCrea W. H., Massey H. S. W., Runcorn S. K., Guest J. E., Hunt G. E. and Woolfson M. M. (1981) Isotopic variations in primitive meteorites. *Philosophical Transactions of the Royal Society of London. Series A, Mathematical and Physical Sciences* **303**, 339–349.

- Clayton R. N., Onuma N. and Mayeda T. K. (1976) A classification of meteorites based on oxygen isotopes. *Earth and Planetary Science Letters* **30**, 10–18.
- Coplen T. B. (2011) Guidelines and recommended terms for expression of stable-isotope-ratio and gas-ratio measurement results. *Rapid Communications in Mass Spectrometry* **25**, 2538–2560.
- Dale J. E. (2015) The modelling of feedback in star formation simulations. *New Astronomy Reviews* **68**, 1–33.
- Dauphas N. (2017) The isotopic nature of the Earth's accreting material through time. *Nature* **541**, 521–524.
- Dauphas N. and Chaussidon M. (2011) A Perspective from Extinct Radionuclides on a Young Stellar Object: The Sun and Its Accretion Disk. *Annual Review of Earth and Planetary Sciences* **39**, 351–386.
- Dauphas N., Chen J. H., Zhang J., Papanastassiou D. A., Davis A. M. and Travaglio C. (2014) Calcium-48 isotopic anomalies in bulk chondrites and achondrites: Evidence for a uniform isotopic reservoir in the inner protoplanetary disk. *Earth and Planetary Science Letters* **407**, 96–108.
- Dauphas N., Cook D. L., Sacarabany A., Fröhlich C., Davis A. M., Wadhwa M., Pourmand A., Rauscher T. and Gallino R. (2008) Iron 60 evidence for early injection and efficient mixing of stellar debris in the protosolar nebula. *Nippon rinsho. Japanese journal of clinical medicine* **686**, 560–569.
- Dauphas N., Marty B. and Reisberg L. (2002a) Molybdenum Evidence for Inherited Planetary Scale Isotope Heterogeneity of the Protosolar Nebula. *ApJ* **565**, 640–644.
- Dauphas N., Marty B. and Reisberg L. (2002b) Molybdenum Nucleosynthetic Dichotomy Revealed in Primitive Meteorites. *The Astrophysical Journal Letters* **569**, L139–L142.
- DeMeo F. E. and Carry B. (2014) Solar System evolution from compositional mapping of the asteroid belt. *Nature* **505**, 629–634.
- Dobrică E. and Brearley A. J. (2014) Widespread hydrothermal alteration minerals in the fine-grained matrices of the Tieschitz unequilibrated ordinary chondrite. *Meteoritics & Planetary Science* **49**, 1323–1349.
- Dwarkadas V. V., Dauphas N., Meyer B., Boyajian P. and Bojazi M. (2017) Triggered Star Formation inside the Shell of a Wolf–Rayet Bubble as the Origin of the Solar System. *ApJ* **851**, 147.
- Franchi I. A., Akagi T. and Pillinger C. T. (1992) Laser Fluorination of Meteorites--Small Sample Analysis of delta<sup>17</sup>O and delta<sup>18</sup>O. *Meteoritics* **27**.

- Franchi I. A., Wright I. P., Sexton A. S. and Pillinger C. T. (1999) The oxygen-isotopic composition of Earth and Mars. *Meteoritics & Planetary Science* **34**, 657–661.
- Gannoun A., Boyet M., Rizo H. and Goresy A. E. (2011)  $^{146}\text{Sm}$ – $^{142}\text{Nd}$  systematics measured in enstatite chondrites reveals a heterogeneous distribution of  $^{142}\text{Nd}$  in the solar nebula. *PNAS* **108**, 7693–7697.
- Göpel C., Birck J.-L., Galy A., Barrat J.-A. and Zanda B. (2015) Mn–Cr systematics in primitive meteorites: Insights from mineral separation and partial dissolution. *Geochimica et Cosmochimica Acta* **156**, 1–24.
- Goswami J. N. (1998) Short-lived nuclides in the early solar system. *Proc. Indian Acad. Sci. (Earth Planet Sci.)* **107**, 401–411.
- Gounelle M., Shu F. H., Shang H., Glassgold A. E., Rehm K. E. and Lee T. (2001) Extinct Radioactivities and Protosolar Cosmic Rays: Self-Shielding and Light Elements. *ApJ* **548**, 1051.
- Grady M. M., Graham A. L., Barber D. J., Aylmer D. and Kurat G. (1987) Yamato-82042: an unusual carbonaceous chondrite with CM affinities. *Memoirs of National Institute of Polar Research. Special issue*, 162–178.
- Grossman J. N., Alexander C. M. O., Wang J. and Brearley A. J. (2000) Bleached chondrules: Evidence for widespread aqueous processes on the parent asteroids of ordinary chondrites. *Meteoritics & Planetary Science* **35**, 467–486.
- Grossman J. N. and Brearley A. J. (2005) The onset of metamorphism in ordinary and carbonaceous chondrites. *Meteoritics & Planetary Science* **40**, 87–122.
- Grossman J. N., Clayton R. N. and Mayeda T. K. (1987) Oxygen Isotopes in the Matrix of the Semarkona (LL3.0) Chondrite. *Meteoritics* **22**, 395.
- Halbout J., Javoy M. and Robert F. (1984) Oxygen Isotopes in Type 3 Ordinary Chondrites. **15**, 339–340.
- Halbout J., Mayeda T. K. and Clayton R. N. (1986) Carbon isotopes and light element abundances in carbonaceous chondrites. *Earth and Planetary Science Letters* **80**, 1–18.
- Halliday A. N. and Porcelli D. (2001) In search of lost planets – the paleocosmochemistry of the inner solar system. *Earth and Planetary Science Letters* **192**, 545–559.
- Hartmann L., Ballesteros-Paredes J. and Heitsch F. (2012) Rapid star formation and global gravitational collapse. *Monthly Notices of the Royal Astronomical Society* **420**, 1457–1461.
- Horejsi M. (2012) Ochansk: If it's abundant, it better be good. *Meteorite Times Mag.*

- Hu Y., Chen X.-Y., Xu Y.-K. and Teng F.-Z. (2018) High-precision analysis of potassium isotopes by HR-MC-ICPMS. *Chemical Geology* **493**, 100–108.
- Hu Y., Teng F.-Z., Plank T. and Chauvel C. (2020) Potassium isotopic heterogeneity in subducting oceanic plates. *Sci Adv* **6**, eabb2472.
- Humayun M. and Clayton R. N. (1995) Potassium isotope cosmochemistry: Genetic implications of volatile element depletion. *Geochimica et Cosmochimica Acta* **59**, 2131–2148.
- Ito M., Nagasawa H. and Yurimoto H. (2006) A study of Mg and K isotopes in Allende CAIs: Implications to the time scale for the multiple heating processes. *Meteoritics & Planetary Science* **41**, 1871–1881.
- Jabeen I., Kusakabe M., Nagao K. and Nakamura T. (1998) Oxygen isotope study of Tsukuba chondrite, some HED meteorites and Allende chondrules. *Antarctic Meteorite Research* **11**, 122.
- Jacobsen B., Yin Q., Moynier F., Amelin Y., Krot A. N., Nagashima K., Hutcheon I. D. and Palme H. (2008)  $^{26}\text{Al}$ – $^{26}\text{Mg}$  and  $^{207}\text{Pb}$ – $^{206}\text{Pb}$  systematics of Allende CAIs: Canonical solar initial  $^{26}\text{Al}/^{27}\text{Al}$  ratio reinstated. *Earth and Planetary Science Letters* **272**, 353–364.
- Jacobsen S. B. (2005) The birth of the Solar System in a molecular cloud: Evidence from the isotopic pattern of short-lived Nuclides in the early Solar System. *Chondrites and the Protoplanetary Disk* **341**, 548.
- Jacobsen S. B., Chakrabarti R., Ranen M. C. and Petaev M. I. (2008) High resolution  $^{26}\text{Al}$ – $^{26}\text{Mg}$  chronometry of CAIs from the Allende meteorite. *Lunar and Planetary Science Conference* **39**, 1999.
- Jiang Y., Chen H., Fegley B., Lodders K., Hsu W., Jacobsen S. B. and Wang K. (2019) Implications of K, Cu and Zn isotopes for the formation of tektites. *Geochimica et Cosmochimica Acta* **259**, 170–187.
- Jiang Y., Koefoed P., Pravdivtseva O., Chen H., Li C.-H., Huang F., Qin L.-P., Liu J. and Wang K. (2021) Early solar system aqueous activity: K isotope evidence from Allende. *Meteoritics & Planetary Science* **56**, 61–76.
- Jones R. H. (2012) Petrographic constraints on the diversity of chondrule reservoirs in the protoplanetary disk. *Meteoritics & Planetary Science* **47**, 1176–1190.
- Jörg G., Amelin Y., Kossert K. and Lierse v. Gostomski C. (2012) Precise and direct determination of the half-life of  $^{41}\text{Ca}$ . *Geochimica et Cosmochimica Acta* **88**, 51–65.
- Keller L. P., Thomas K. L., Clayton R. N., Mayeda T. K., DeHart J. M. and McKay D. S. (1994) Aqueous alteration of the Bali CV3 chondrite: Evidence from mineralogy, mineral chemistry, and oxygen isotopic compositions. *Geochimica et Cosmochimica Acta* **58**, 5589–5598.

- Koefoed P., Pravdivtseva O., Chen H., Gerritzen C., Thiemens M. M. and Wang K. (2020) Potassium isotope systematics of the LL4 chondrite Hamlet: Implications for chondrule formation and alteration. *Meteoritics & Planetary Science* **55**.
- Koefoed P., Pravdivtseva O., Chen H., Gerritzen C. and Wang K. (2019) K Isotope Systematics of Individual Chondrules from the LL4 Chondrite Hamlet. *LPSC* **50**, 1672.
- Krot A. N., Libourel G., Goodrich C. A. and Petaev M. I. (2004) Silica-rich igneous rims around magnesian chondrules in CR carbonaceous chondrites: Evidence for condensation origin from fractionated nebular gas. *Meteoritics & Planetary Science* **39**, 1931–1955.
- Krot A. N., Petaev M. I. and Nagashima K. (2021) Infiltration Metasomatism of the Allende Coarse-Grained Calcium-Aluminum-Rich Inclusions. *Progr. Earth Planet. Sci*, accepted.
- Kruijjer T. S., Burkhardt C., Budde G. and Kleine T. (2017) Age of Jupiter inferred from the distinct genetics and formation times of meteorites. *PNAS* **114**, 6712–6716.
- Ku Y. and Jacobsen S. B. (2020) Potassium isotope anomalies in meteorites inherited from the protosolar molecular cloud. *Science Advances* **6**, eabd0511.
- Ku Y. and Jacobsen S. B. (2019) Potassium isotope variations in chondrites. *LPSC* **50**, 1675.
- Ku Y., Petaev M. I., Skripnik A. Y., Ivanova M. A. and Jacobsen S. B. (2021) K isotope variations in chondrules, CAIs, matrix and Bulk Chondrites. *Lunar and Planetary Science Conference*, 2377.
- Kuhnel W. W., Jacobsen S. B., Li Y., Ku Y., Petaev M. I., Huang S., Wu Z. and Wang K. (2021) High-Temperature Inter-Mineral Potassium Isotope Fractionation: Implications for K–Ca–Ar Chronology. *ACS Earth Space Chem.* **5**, 2740–2754.
- Kutschera W., Ahmad I. and Paul M. (1992) Half-Life Determination of  $^{41}\text{Ca}$  and some other radioisotopes. *Radiocarbon* **34**, 436–446.
- Kuwatani T., Yoshida K., Ueki K., Oyanagi R., Uno M. and Akaho S. (2020) Sparse isocon analysis: A data-driven approach for material transfer estimation. *Chemical Geology* **532**, 119345.
- Larsen K. K., Trinquier A., Paton C., Schiller M., Wielandt D., Ivanova M. A., Connelly J. N., Nordlund Å., Krot A. N. and Bizzarro M. (2011) Evidence for magnesium isotope heterogeneity in the solar protoplanetary disk. *ApJL* **735**, L37.
- Lauretta D. S., Nagahara H. and Alexander C. M. O. (2006) *Petrology and origin of ferromagnesian silicate chondrules.*
- Lee T., Shu F. H., Shang H., Glassgold A. E. and Rehm K. E. (1998) Protostellar cosmic rays and extinct radioactivities in meteorites. *ApJ* **506**, 898–912.

- Lewis J. A., Jones R. H. and Garcea S. C. (2018) Chondrule porosity in the L4 chondrite Saratov: Dissolution, chemical transport, and fluid flow. *Geochimica et Cosmochimica Acta* **240**, 293–313.
- Li Y., Wang W., Wu Z. and Huang S. (2019) First-principles investigation of equilibrium K isotope fractionation among K-bearing minerals. *Geochimica et Cosmochimica Acta* **264**, 30–42.
- Libourel G. and Portail M. (2018) Chondrules as direct thermochemical sensors of solar protoplanetary disk gas. *Science Advances* **4**, eaar3321.
- Liu H., Xue Y.-Y., Zhang G., Sun W.-D., Tian Z., Tuller-Ross B. and Wang (王昆) K. (2021) Potassium isotopic composition of low-temperature altered oceanic crust and its impact on the global K cycle. *Geochimica et Cosmochimica Acta* **311**, 59–73.
- Liu M.-C. (2017) The initial  $^{41}\text{Ca}/^{40}\text{Ca}$  ratios in two type A Ca–Al-rich inclusions: Implications for the origin of short-lived  $^{41}\text{Ca}$ . *Geochimica et Cosmochimica Acta* **201**, 123–135.
- Liu M.-C., Chaussidon M., Srinivasan G. and McKeegan K. D. (2012) A Lower Initial Abundance of Short-lived  $^{41}\text{Ca}$  in the Early Solar System and Its Implications for Solar System Formation. *The Astrophysical Journal* **761**, 137.
- Lodders K. (2003) Solar System abundances and condensation temperatures of the elements. *ApJ* **591**, 1220–1247.
- Luck J. M., Othman D. B., Barrat J. A. and Albarède F. (2003) Coupled  $^{63}\text{Cu}$  and  $^{16}\text{O}$  excesses in chondrites. *Geochimica et Cosmochimica Acta* **67**, 143–151.
- Luck J.-M., Othman D. B. and Albarède F. (2005) Zn and Cu isotopic variations in chondrites and iron meteorites: Early solar nebula reservoirs and parent-body processes. *Geochimica et Cosmochimica Acta* **69**, 5351–5363.
- Lugaro M., Heger A., Osrin D., Goriely S., Zuber K., Karakas A. I., Gibson B. K., Doherty C. L., Lattanzio J. C. and Ott U. (2014) Stellar origin of the  $^{182}\text{Hf}$  cosmochronometer and the presolar history of solar system matter. *Science* **345**, 650–653.
- Macke R. (2010) Survey of meteorite physical properties density, porosity and magnetic susceptibility. *Electronic Theses and Dissertations*.
- MacPherson G. J., Bullock E. S., Tenner T. J., Nakashima D., Kita N. T., Ivanova M. A., Krot A. N., Petaev M. I. and Jacobsen S. B. (2017) High precision Al–Mg systematics of forsterite-bearing Type B CAIs from CV3 chondrites. *Geochimica et Cosmochimica Acta* **201**, 65–82.
- MacPherson G. J., Ushikubo T., Kita N. T., Ivanova M. A., Bullock E. S. and Davis A. M. (2013) Petrologic and  $^{26}\text{Al}/^{27}\text{Al}$  Isotopic Studies of Type A CAIs and Documentation of the Fluffy Type A - Compact Type A - Type B CAI Evolutionary Transition. *Lunar and Planetary Science Conference* **44**, 1530.

- Mayeda T. K., Clayton R. N. and Molini-Velsko C. A. (1983) Oxygen and silicon isotopes in ALHA 81005. *Geophysical Research Letters* **10**, 799–800.
- Mayeda T. K., Clayton R. N. and Sodonis A. (1989) Internal Oxygen Isotope Variations in Two Unequilibrated Chondrites. **712**, 153.
- Mayeda T. K., Clayton R. N. and Yanai K. (1987) Oxygen isotopic compositions of several Antarctic meteorites. *Memoirs of National Institute of Polar Research. Special issue*, 144–150.
- Mayeda T. K., Yanai K. and Clayton R. N. (1995) Another Martian Meteorite. *LPSC* **26**.
- McCubbin F. M., Riner M. A., Kaaden K. E. V. and Burkemper L. K. (2012) Is Mercury a volatile-rich planet? *Geophysical Research Letters* **39**.
- McDonough W. F. (2003) Compositional Model for the Earth's Core. *Treatise on Geochemistry* **2**, 568.
- McDonough W. F. and Sun S. -s. (1995) The composition of the Earth. *Chemical Geology* **120**, 223–253.
- Meija J., Coplen T. B., Berglund M., Brand W. A., De Bièvre P., Gröning M., Holden N. E., Irrgeher J., Loss R. D., Walczyk T. and Prohaska T. (2016a) Atomic weights of the elements 2013 (IUPAC Technical Report). *Pure and Applied Chemistry* **88**, 265291.
- Meija J., Coplen T. B., Berglund M., Brand W. A., De Bièvre P., Gröning M., Holden N. E., Irrgeher J., Loss R. D., Walczyk T. and Prohaska T. (2016b) Isotopic compositions of the elements 2013 (IUPAC Technical Report). *Pure and Applied Chemistry* **88**, 293306.
- Meyer B. S. and Clayton D. D. (2000) Short-Lived Radioactivities and the Birth of the sun. *Space Science Reviews* **92**, 133–152.
- Millet M.-A., Dauphas N., Greber N. D., Burton K. W., Dale C. W., Debret B., Macpherson C. G., Nowell G. M. and Williams H. M. (2016) Titanium stable isotope investigation of magmatic processes on the Earth and Moon. *Earth and Planetary Science Letters* **449**, 197–205.
- Moynier F., Beck P., Jourdan F., Yin Q.-Z., Reimold U. and Koeberl C. (2009) Isotopic fractionation of zinc in tektites. *Earth and Planetary Science Letters* **277**, 482–489.
- Moynier F., Hu Y., Wang K., Zhao Y., Gérard Y., Deng Z., Moureau J., Li W., Simon J. I. and Teng F.-Z. (2021) Potassium isotopic composition of various samples using a dual-path collision cell-capable multiple-collector inductively coupled plasma mass spectrometer, Nu instruments Sapphire. *Chemical Geology* **571**, 120144.
- Moynier F., Koeberl C., Beck P., Jourdan F. and Telouk P. (2010) Isotopic fractionation of Cu in tektites. *Geochimica et Cosmochimica Acta* **74**, 799–807.

- Naumenko M. O., Mezger K., Nagler T. F. and Villa I. M. (2013) High precision determination of the terrestrial 40K abundance. *Geochimica et Cosmochimica Acta* **122**, 353–362.
- Nie N. X., Chen X.-Y., Hopp T., Hu J. Y., Zhang Z. J., Teng F.-Z., Shahar A. and Dauphas N. (2021) Imprint of chondrule formation on the K and Rb isotopic compositions of carbonaceous meteorites. *Sci Adv* **7**, eabl3929.
- Onuma N., Ikeda Y., Mayeda T. K., Clayton R. N. and Yanai K. (1983) Oxygen isotopic compositions of petrographically described inclusions from Antarctic unequilibrated ordinary-chondrites. *National Institute Polar Research Memoirs* **30**, 306–314.
- Osadchii V. O., Fedkin M. V. and Osadchii E. G. (2017) Determination of the equilibrium fO<sub>2</sub> in bulk samples of H, L, and LL ordinary chondrites by solid-state electrochemistry. *Meteoritics & Planetary Science* **52**, 2275–2283.
- Petaev M. I. and Jacobsen S. B. (2009) Petrologic study of SJ101, a new forsterite-bearing CAI from the Allende CV3 chondrite. *Geochimica et Cosmochimica Acta* **73**, 5100–5114.
- Pinte C., Price D. J., Menard F., Duchene G., Dent W. R. F., Hill T., Gregorio-Monsalvo I. de, Hales A. and Mentiplay D. (2018) Kinematic Evidence for an Embedded Protoplanet in a Circumstellar Disk. *ApJL* **860**, L13.
- Prantzos N., Doom C., Arnould M. and de Loore C. (1986) Nucleosynthesis and evolution of massive stars with mass loss and overshooting. *The Astrophysical Journal* **304**, 695–712.
- Qin L., Alexander C. M. O., Carlson R. W., Horan M. F. and Yokoyama T. (2010) Contributors to chromium isotope variation of meteorites. *Geochimica et Cosmochimica Acta* **74**, 1122–1145.
- Ramaty R., Kozlovsky B. and Lingenfelter R. E. (1996) Light isotopes, extinct radioisotopes, and Gamma-ray lines from low-energy cosmic-ray interactions. *The Astrophysical Journal* **456**, 525.
- Rankenburg K., Brandon A. D. and Neal C. R. (2006) Neodymium isotope evidence for a chondritic composition of the Moon. *Science* **312**, 1369–1372.
- Recca S. I., Scott E. R. D., Keil K., Clayton R. N., Mayeda T. K., Huss G. I., Jarosewich E., Weeks K. S., Hasan F. A., Sears D. W. G., Wieler R. and Signer P. (1986) Ragland, an L13.4 Chondrite Find from New Mexico. *Meteoritics* **21**, 217–229.
- Regelous M., Elliott T. R. and Coath C. D. (2008) Nickel isotope heterogeneity in the early Solar System. *Earth and Planetary Science Letters* **272**, 330–338.
- Richter F. M., Mendybaev R. A., Christensen J. N., Ebel D. and Gaffney A. (2011) Laboratory experiments bearing on the origin and evolution of olivine-rich chondrules. *Meteoritics & Planetary Science* **46**, 1152–1178.



- Romanek C. S., Perry E. C., Treiman A. H., Socki R. A., Jones J. H. and Gibson E. K. (1998) Oxygen isotopic record of silicate alteration in the Shergotty—Nakhla—Chassigny meteorite Lafayette. *Meteoritics & Planetary Science* **33**, 775–784.
- Rowe M. W., Clayton R. N. and Mayeda T. K. (1994) Oxygen isotopes in separated components of CI and CM meteorites. *Geochimica et Cosmochimica Acta* **58**, 5341–5347.
- Rudnick R. L. and Gao S. (2003) Composition of the Continental Crust. *Treatise on Geochemistry* **3**, 659.
- Ruzicka A., Kring D. A., Hill D. H., Boynton W. V., Clayton R. N. and Mayeda T. K. (1995) Silica-rich orthopyroxenite in the Bovedy chondrite. *Meteoritics* **30**, 57–70.
- Sahijpal S., Goswami J. N. and Davis A. M. (2000) K, Mg, Ti and Ca isotopic compositions and refractory trace element abundances in hibonites from CM and CV meteorites: implications for early solar system processes. *Geochimica et Cosmochimica Acta* **64**, 1989–2005.
- Schiller M., Bizzarro M. and Fernandes V. A. (2018) Isotopic evolution of the protoplanetary disk and the building blocks of Earth and the Moon. *Nature* **555**, 507–510.
- Schiller M., Kooten E. V., Holst J. C., Olsen M. B. and Bizzarro M. (2014) Precise measurement of chromium isotopes by MC-ICPMS. *J. Anal. At. Spectrom.* **29**, 1406–1416.
- Schiller M., Paton C. and Bizzarro M. (2015) Evidence for nucleosynthetic enrichment of the protosolar molecular cloud core by multiple supernova events. *Geochim. Cosmochim. Acta* **149**, 88–102.
- Scott E. R. D. and Krot A. N. (2003) Chondrites and their Components. *Treatise on Geochemistry* **1**, 711.
- Scott E. R. D., Krot T. V., Goldstein J. I. and Wakita S. (2014) Thermal and impact history of the H chondrite parent asteroid during metamorphism: Constraints from metallic Fe-Ni. *Geochimica et Cosmochimica Acta* **136**, 13–37.
- Sears D. W. G., Batchelor J. D., Mason B., Scott E. R. D., Clayton R. N. and Mayeda T. K. (1990) South Australian type 3 chondrites. *Meteoritics* **25**, 407.
- Shukolyukov A. and Lugmair G. W. (2006) Manganese–chromium isotope systematics of carbonaceous chondrites. *Earth and Planetary Science Letters* **250**, 200–213.
- Simon J. I. and DePaolo D. J. (2010) Stable calcium isotopic composition of meteorites and rocky planets. *Earth and Planetary Science Letters* **289**, 457–466.
- Simon S. B., Grossman L., Casanova I., Symes S., Benoit P., Sears D. W. G. and Wacker J. F. (1995) Axtell, a new CV3 chondrite find from Texas. *Meteoritics* **30**, 42–46.

- Spicuzza M. J., Day J. M. D., Taylor L. A. and Valley J. W. (2007) Oxygen isotope constraints on the origin and differentiation of the Moon. *Earth and Planetary Science Letters* **253**, 254–265.
- Sprung P., Kleine T. and Scherer E. E. (2013) Isotopic evidence for chondritic Lu/Hf and Sm/Nd of the Moon. *Earth and Planetary Science Letters* **380**, 77–87.
- Srinivasan G. and Chaussidon M. (2013) Constraints on  $^{10}\text{Be}$  and  $^{41}\text{Ca}$  distribution in the early solar system from  $^{26}\text{Al}$  and  $^{10}\text{Be}$  studies of Efremovka CAIs. *Earth and Planetary Science Letters* **374**, 11–23.
- Srinivasan G., Sahijpal S., Ulyanov A. A. and Goswami J. N. (1996) Ion microprobe studies of Efremovka CAIs: II. Potassium isotope composition and  $^{41}\text{Ca}$  in the early Solar System. *Geochimica et Cosmochimica Acta* **60**, 1823–1835.
- Srinivasan G., Ulyanov A. A. and Goswami J. N. (1994) Ca-41 in the early solar system. *The Astrophysical Journal Letters* **431**, L67–L70.
- Steele R. C. J., Coath C. D., Regelous M., Russell S. and Elliott T. (2012) Neutron-poor Nickel Isotope Anomalies in Meteorites. *The Astrophysical Journal* **758**, 59.
- Stenzel O. J., Hilchenbach M., Merouane S., Paquette J., Varmuza K., Engrand C., Brandstätter F., Koeberl C., Ferrière L., Filzmoser P., Siljeström S., and the COSIMA team (2017) Similarities in element content between comet 67P/Churyumov–Gerasimenko coma dust and selected meteorite samples. *Monthly Notices of the Royal Astronomical Society* **469**, S492–S505.
- Sylvester P. J., Simon S. B. and Grossman L. (1993) Refractory inclusions from the Leoville, Efremovka, and Vigarano c3v chondrites: Major element differences between types A and B, and extraordinary refractory siderophile element compositions. *Geochimica et Cosmochimica Acta* **57**, 3763–3784.
- Tang H. and Dauphas N. (2014)  $^{60}\text{Fe}$ – $^{60}\text{Ni}$  chronology of core formation in Mars. *Earth and Planetary Science Letters* **390**, 264–274.
- Tang H. and Dauphas N. (2012) Abundance, distribution, and origin of  $^{60}\text{Fe}$  in the solar protoplanetary disk. *Earth and Planetary Science Letters* **359–360**, 248–263.
- Taylor G. J. (2013) The bulk composition of Mars. *Geochemistry* **73**, 401–420.
- Teague R., Bae J., Bergin E. A., Birnstiel T. and Foreman-Mackey D. (2018) A Kinematical Detection of Two Embedded Jupiter-mass Planets in HD 163296. *ApJL* **860**, L12.
- Teng F.-Z., Dauphas N. and Watkins J. M. (2017) Non-Traditional Stable Isotopes: Retrospective and Prospective. *Reviews in Mineralogy and Geochemistry* **82**, 1–26.

- Tian Z., Chen H., Fegley B., Lodders K., Barrat J.-A., Day J. M. D. and Wang K. (2019) Potassium isotopic compositions of howardite-eucrite-diogenite meteorites. *Geochimica et Cosmochimica Acta* **266**, 611–632.
- Timmes F. X., Woosley S. E., Hartmann D. H., Hoffman R. D., Weaver T. A. and Matteucci F. (1995)  $^{26}\text{Al}$  and  $^{60}\text{Fe}$  from Supernova Explosions. *The Astrophysical Journal* **449**, 204.
- Trappitsch R., Boehnke P., Stephan T., Telus M., Savina M. R., Pardo O., Davis A. M., Dauphas N., Pellin M. J. and Huss G. R. (2018) New Constraints on the Abundance of  $^{60}\text{Fe}$  in the Early Solar System. *ApJL* **857**, L15.
- Trinquier A., Birck J.-L. and Allegre C. J. (2007) Widespread  $^{54}\text{Cr}$  Heterogeneity in the Inner Solar System. *ApJ* **655**, 1179–1185.
- Trinquier A., Elliott T., Ulfbeck D., Coath C., Krot A. N. and Bizzarro M. (2009) Origin of Nucleosynthetic Isotope Heterogeneity in the Solar Protoplanetary Disk. *Science* **324**, 374–376.
- Van Kooten E. M. M. E., Wielandt D., Schiller M., Nagashima K., Thomen A., Larsen K. K., Olsen M. B., Nordlund Å., Krot A. N. and Bizzarro M. (2016) Isotopic evidence for primordial molecular cloud material in metal-rich carbonaceous chondrites. *Proc Natl Acad Sci U S A* **113**, 2011–2016.
- Verma S. P. (1981) Seawater alteration effects on  $^{87}\text{Sr}/^{86}\text{Sr}$ , K, Rb, Cs, Ba and Sr in oceanic igneous rocks. *Chemical Geology* **34**, 81–89.
- Walsh K. J., Morbidelli A., Raymond S. N., O'Brien D. P. and Mandell A. M. (2011) A low mass for Mars from Jupiter's early gas-driven migration. *Nature* **475**, 206–209.
- Wang K. and Jacobsen S. B. (2016a) An estimate of the Bulk Silicate Earth potassium isotopic composition based on MC-ICPMS measurements of basalts. *Geochimica et Cosmochimica Acta* **178**, 223–232.
- Wang K. and Jacobsen S. B. (2016b) Potassium isotopic evidence for a high-energy giant impact origin of the Moon. *Nature* **538**, 487–490.
- Wasserburg G. J., Busso M., Gallino R. and Nollett K. M. (2006) Short-lived nuclei in the early Solar System: Possible AGB sources. *Nuclear Physics A* **777**, 5–69.
- Weber D., Clayton R. N., Mayeda T. K. and Bischoff A. (1996) Unusual equilibrated carbonaceous chondrites and CO<sub>3</sub> meteorites from the Sahara. *LPSC* **27**.
- Weisberg M. K., McCoy T. J. and Krot A. N. (2006) *Systematics and evaluation of meteorite classification.*
- Weisberg M. K., Prinz M., Clayton R. N. and Mayeda T. K. (1997) CV3 Chondrites: Three Subgroups, Not Two. *Meteoritics and Planetary Science Supplement* **32**.

- Wendt I. and Carl C. (1991) The statistical distribution of the mean squared weighted deviation. *Chemical Geology: Isotope Geoscience section* **86**, 275–285.
- Wiechert U., Halliday A. N., Lee D.-C., Snyder G. A., Taylor L. A. and Rumble D. (2001) Oxygen Isotopes and the Moon-Forming Giant Impact. *Science* **294**, 345–348.
- Williamson J. H. (1968) Least-squares fitting of a straight line. *Canadian Journal of Physics* **46**, 1845.
- Wood B. J., Walter M. J. and Wade J. (2006) Accretion of the Earth and segregation of its core. *Nature* **441**, 825–833.
- Young E. D. (2014) Inheritance of solar short- and long-lived radionuclides from molecular clouds and the unexceptional nature of the solar system. *Earth and Planetary Science Letters* **392**, 16–27.
- Young E. D., Kohl I. E., Warren P. H., Rubie D. C., Jacobson S. A. and Morbidelli A. (2016) Oxygen isotopic evidence for vigorous mixing during the Moon-forming giant impact. *Science* **351**, 493–496.
- Young E. D. and Russell S. S. (1998) Oxygen Reservoirs in the Early Solar Nebula Inferred from an Allende CAI. *Science* **282**, 452–455.
- Yudin I. A. and Smyshlyaev S. I. (1963) Mineragraphic and chemical study of opaque minerals from the Ochansk meteorite. *Meteoritika* **23**, 72–79.
- Zavaritskiy A. N. and Kvasha L. G. (1952) Meteorites from the USSR. *USSR Academy of Science Press. Moscow*, 127–130.
- Zhang J., Dauphas N., Davis A. M., Leya I. and Fedkin A. (2012) The proto-Earth as a significant source of lunar material. *Nature Geoscience* **5**, 251–255.
- Zhang J., Dauphas N., Davis A. M. and Pourmand A. (2011) A new method for MC-ICPMS measurement of titanium isotopic composition: Identification of correlated isotope anomalies in meteorites. *J. Anal. At. Spectrom.* **26**, 2197–2205.
- Zhao C., Lodders K., Bloom H., Chen H., Tian Z., Koefoed P., Petó M. K. and Wang (王昆) K. (2019) Potassium isotopic compositions of enstatite meteorites. *Meteoritics & Planetary Science*.
- Zolensky M. E., Mittlefehldt D. W., Lipschutz M. E., Wang M.-S., Clayton R. N., Mayeda T. K., Grady M. M., Pillinger C. and B D. (1997) CM chondrites exhibit the complete petrologic range from type 2 to 1. *Geochimica et Cosmochimica Acta* **61**, 5099–5115.
- Zolensky M. E., Mittlefehldt D. W., Lipschutz M. E., Xiao X., Clayton R. N., Mayeda T. K., Barrett R. A. and Grady M. M. (1989) The composition and mineralogy of EET 83334. *Meteoritics* **24**, 345.